



VNiVERSiDAD
D SALAMANCA

CAMPUS DE EXCELENCIA INTERNACIONAL

TESIS DOCTORAL

MENCIÓN INTERNACIONAL

Damage evaluation in constructions based on geomatic and dynamic approaches

Luis Javier Sánchez Aparicio

Ávila, 2016

Departamento de Ingeniería Cartográfica y del Terreno
Escuela Politécnica Superior de Ávila
Universidad de Salamanca

AUTOR:

Luis Javier Sánchez Aparicio

SUPERVISORES:

Dr. Diego González Aguilera

Dr. Belén Riveiro Rodríguez

TITULO:

Damage evaluation in constructions based on geomatic and dynamic approaches.

FORMATO

Tesis Doctoral por compendio de artículos, con mención internacional.

PROGRAMA DE DOCTORADO:

Investigación y desarrollo en geotecnologías (R.D. 1393/2007).

Universidad de Salamanca.

Aviso legal:

Se informa al lector que la presente Tesis Doctoral ha sido efectuada según la normativa, impuesta por la Universidad de Salamanca, en el formato de presentación por compendio de publicaciones. Se advierte a todo aquel que quiera disponer, consultar, citar, reproducir o difundir las publicaciones incluidas en la misma. Reservando los derechos a las editoriales de las publicaciones intervinientes.

La presente Tesis Doctoral está compuesta por un total de cuatros artículos científicos que han sido previamente publicados o aceptados para publicación en revistas científicas de impacto internacional:

- **The combination of geomatic approaches and operational modal analysis to improve calibration of finite element models: A case of study in Saint Torcato Church (Guimarães, Portugal).**

Luis Javier Sánchez-Aparicio^a, Belén Riveiro^b, Diego González-Aguilera^a, Luís F. Ramos^c

^aDepartment of Cartographic and Land Engineering, University of Salamanca, Higher Polytechnic School of Avila, Hornos Caleros 50, 05003, Avila, Spain.

^bDepartment of Material Engineering, Applied Mechanics and Construction, School of Industrial Engineering, University of Vigo, Vigo, Spain.

^cISISE, Department of Civil Engineering, University of Minho, Guimarães, Portugal

Construction and Building Materials

DOI: 10.1016/j.conbuildmat.2014.07.106

- **Experimental and numerical approaches for structural assessment in new footbridge designs (SFRSCC-GFPR hybrid structure).**

Luis Javier Sánchez-Aparicio^a, Luís F. Ramos^b, José Sena-Cruz^b, Joaquim O. Barros^b, Belén Riveiro^c

^aDepartment of Cartographic and Land Engineering, University of Salamanca, Higher Polytechnic School of Avila, Hornos Caleros 50, 05003, Avila, Spain.

^bISISE, Department of Civil Engineering, University of Minho, Guimarães, Portugal

^cDepartment of Material Engineering, Applied Mechanics and Construction, School of Industrial Engineering, University of Vigo, Vigo, Spain.

Composite Structures

DOI: 10.1016/j.compstruct.2015.07.041

- **Photogrammetric, geometrical and numerical strategies to evaluate initial and current conditions in historical constructions: a test case in the church of San Lorenzo (Zamora, Spain).**

Luis Javier Sánchez-Aparicio^a, Alberto Villarino-Otero^a, Jesús García-Gago^a, Diego González-Aguilera^a

^aDepartment of Cartographic and Land Engineering, University of Salamanca, Higher Polytechnic School of Avila, Hornos Caleros 50, 05003, Avila, Spain.

Remote Sensing

DOI: 10.3390/rs801006

- **Practical use of multispectral techniques for the detection of pathologies in constructions.**

Luis Javier Sánchez-Aparicio^a, Susana Del Pozo-Aguilera^a, Pablo Rodríguez-Gonzálvez^a, Jesús Herrero-Pascual^a, Ángel Luis Muñoz-Nieto^a, Diego González-Aguilera^a, David Hernández-López^b

a Department of Cartographic and Land Engineering, University of Salamanca, Higher Polytechnic School of Avila, Hornos Caleros 50, 05003, Avila, Spain.

b Institute for Regional Development (IDR), University of Castilla La Mancha, 02071, Albacete, Spain

CRC Press - Taylor & Francis Group

ISBN: 978-1-138-02810-4

INFORME DE LOS SUPERVISORES

La presente Tesis Doctoral, bajo el nombre *Damage evaluation in constructions based on geomatic and dynamic approaches*, y presentada por D. Luis Javier Sánchez Aparicio, queda integrada en la línea de investigación: *Modelling and pathological evaluation of historical buildings of the research unit TIDOP* (<http://tidop.usal.es>), afiliado a la Universidad de Salamanca.

Fruto de la actividad investigadora desarrollada por el Doctorando, durante el periodo de elaboración de la Tesis Doctoral, diversos trabajos científicos han sido publicados en revistas internacionales de prestigio (indexadas en el Journal Citation Reports). Complementario a ello, se ha de reseñar el desarrollo de un software, bajo el título Enhance your Finite Element Model (EyFEM), que aúna las metodologías desarrolladas y empleadas en parte de la publicaciones desarrolladas (ver Anexo I).

En lo que respecta a las publicaciones mostradas en el presente documento, y a fin de corroborar la validez y robustez de los trabajos científicos desarrollados, los artículos fruto de dichos trabajos fueron publicados en revistas científicas de impacto. Dentro de diferentes campos científicos especializados: (i) construcción (*Construction and Building Materials Journal*); (ii) materiales compuestos (*Composite Structures Journal*); (iii) sensor remoto (*Remote Sensing Journal*) e ingeniería & tecnología (*CRC Press-Taylor & Francis Group*). Estas, por orden de publicación, se distribuyen del siguiente modo:

- El artículo científico: *The combination of geomatic approaches and operational modal analysis to improve calibration of finite element models: A case of study in Saint Torcato Church (Guimarães, Portugal)*. Publicado en la revista *Construction and Building Materials Journal*, indexada en el Journal Citation Report y emplazada en el Q1 (primer Decil) de la

categoría *Construction & Building Technology* . Ocupando la doceava posición de ciento veinticuatro revistas indexadas. DOI: 10.1016/j.conbuildmat.2014.07.106.

- La publicación: *Experimental and numerical approaches for structural assessment in new footbridge designs (SFRSCC-GFPR hybrid structure)*. Publicada en la revista *Composite Structures Journal*. Dicha revista, indexada en el primer cuartil, ocupa la tercera posición de veinticuatro revistas. DOI: 10.1016/j.compstruct.2015.07.041.
- El trabajo científico: *Photogrammetric, geometrical and numerical strategies to evaluate initial and current conditions in historical constructions: a test case in the church of San Lorenzo (Zamora, Spain)*. Publicado en la revista científica *Remote Sensing*, indexada y emplazada en el Q1 de sensor remoto. Ocupando la quinta posición de veintiocho revistas. DOI: 10.3390/rs8010060.
- El capítulo del libro: *Practical use of multispectral techniques for the detection of pathologies in constructions (Accepted for publication)*. Ocupando la sexta plaza de sesenta y cinco editoriales (primer Decil) en el campo *Engineering & Technology discipline*. ISBN: 978-1-138-02810-4.

A tenor de los requerimientos para la presentación de la Tesis Doctoral, por compendio de artículos, establecidos por la Universidad de Salamanca. Se considera que los artículos principales, así como los méritos adicionales de la misma, se ajustan de modo óptimo a dichas necesidades, quedando así validadas las metodologías, resultados y conclusiones presentadas en este documento.

Los resultados arrojados durante la elaboración de la Tesis Doctoral han permitido obtener importantes avances en diferentes campos de la ingeniería estrechamente relacionados con la temática desarrollada: (I) el empleo de técnicas geomáticas en la evaluación de daños estructurales presentes en las construcciones; (ii) el uso de técnicas dinámicas basadas en el Análisis Modal Operacional para la calibración y detección de daños estructurales; (iii) el desarrollo de procedimientos para la adaptación de nubes de puntos, bien fotogramétricas o láser escáner, en modelos CAD aptos para análisis numérico y capaces de integrar procesos patológicos de relevancia como grietas o deformaciones; y (iv) el empleo de técnicas de análisis multiespectral en la detección y cuantificación de patologías presentes en construcciones.

Todo ello abre consigo nuevas líneas de investigación y situán a los procedimientos empelados y desarrollados como sólidos cimientos en dicho desarrollo.

La Tesis Doctoral concluye con el correspondiente apartado de conclusiones en el que, de forma precisa y concreta, se especifican las principales aportaciones. De tal forma que puedan ser objeto de crítica y de proyección hacia el desarrollo de futuros trabajos integrados en líneas de investigación.

Lo que firman, a todos los efectos oportunos, en Ávila, a día 5 de Abril de 2016.

Dr. Diego González Aguilera.

Dr. Belén Riveiro Rodríguez

INFORME DE LA ESTANCIA

Luís F. Ramos, Assistant Professor from the Civil Engineering Department at University of Minho, Portugal, certifies that Luis Javier Sánchez Aparicio, PhD Student of the Geotechnologies Research and Development doctorate, has undergone a short stay at University of Minho during his pre-doctoral period, with the duration of 3 months at the University of Minho (Portugal), within the Department of Civil Engineering. During his entire stay he has been followed and tutored by me.

During this period of time, the student has carried out research tasks within the field of pathologic analysis of civil constructions, summarized as follow:

- Full geometric characterization of Saint Torcato church in Guimarães, Portugal, through laser scanner and photogrammetry. CAD model creation and adjustment for its analysis using the finite element method. Definition of a methodology to fully calibrate and afterwards analyze the model.
- Static and dynamic analysis using finite elements of a hybrid footbridge (*GFRP-SFRSCC*) that suffered from cracking. Ensuring robust calibration of the model, as well as its preparation for a possible damage identification analysis.
- Geometric characterization using laser scanner and dynamic test on the main Tower of Guimarães' Castle (Guimarães, Portugal).
- Geometric characterization using laser scanner, in order to carry out a Tube Jack test on an irregular masonry Wall. Preparation of the procedure that should be followed to analyze the deformations through the Digital Image Correlation (*DIC*).

In conclusion, I express my high appreciation of Luis Javier Sánchez Aparicio's professional qualities, his commitment and capacity to carry out high quality and independent research work, besides his ability to fruitfully collaborate with different people and other fields of knowledge, and his high communication skills.

University of Minho, July 30, 2014.

Dr. Luís F. Ramos.

AGRADECIMIENTOS

Quizás sea de los que crean que nada surge de la nada, *Ex nihilo nihil fit*, y por ende, la consecuente finalización de la presente Tesis Doctoral no ha sido más que un suceso de causas que estaban predestinadas a existir. Por ello, agradecer a todas aquellas personas que alguna vez influyeron en la consecuencia de esas causas se convertiría en una ardua tarea. Sin embargo, dentro de ese amplio número, surge un grupo más selecto que sin duda ha contribuido fuertemente a la consecución de la Tesis Doctoral y los cuales merecen mis más sinceros agradecimientos.

En primer lugar quiero dirigir dichos agradecimientos a mis padres, pues sin su incesante ímpetu y sacrificio por proporcionarnos a mí y a mi hermana una completa formación académica, aún en tiempos difíciles, no hubiera sido posible. Del mismo quiero agradecer a mi hermana María y a Paloma su apoyo constante durante toda la etapa. Enfatizándose en aquellos momentos complicados, permitiéndome así seguir escalando hasta la consecución final de la Tesis Doctoral.

A los Doctores Diego González-Aguilera y Belén Riveiro Rodríguez, mis supervisores, por su constante e incondicional apoyo, paciencia y dedicación. Al Doctor Luís F. Ramos, mi tutor de estancia en la Universidad de Minho (Portugal), por su espíritu, dedicación e interés. Sin olvidar las intensas y productivas conversaciones científicas que entablaron conmigo.

A mis compañeros del grupo TIDOP de la Universidad de Salamanca, por la oportunidad brindada de intercambiar experiencias, conocimientos y la posibilidad de trabajar con ellos.

RESUMEN

Resulta inevitable corroborar el constante avance y perfeccionamiento en el uso de materiales y técnicas constructivas en el campo de la ingeniería civil. Desde el empleo de rocas y ladrillos en mamposterías, hasta hormigones autocompactantes reforzados con fibras de acero o polímeros extruidos. Sin embargo no ha de olvidarse, que al igual que ocurre durante el transcurso vital de cualquier ser vivo, todas estas soluciones constructivas no quedan exentas de procesos patológicos. Que si bien, adquieren importancias diferentes según el tipo de proceso y material afectado, no han de pasarse por alto, condicionando consigo la vida útil de las propias construcciones.

Motivado por ello, la presente Tesis Doctoral centra sus esfuerzos en el desarrollo de metodologías y soluciones, capaces de localizar, evaluar, materializar e incluso predecir aquellas afecciones patológicas que degraden la capacidad portante de las construcciones. Abogando consigo por metodologías globales de detección y cuantificación de daños basadas en las disciplinas de la geomática (a través del empleo de sistemas láser escáner y fotogramétricos) y la dinámica de estructuras (mediante el método de Análisis Modal Operacional).

Con el fin de corroborar la aplicabilidad de los procedimientos desarrollados, estos son empleados en diferentes tipos de construcciones: desde construcciones históricas y vernáculas, en fase experimental hasta construcciones “modernas” erigidas en hormigón armado.

A raíz de los resultados arrojados se concluye que los sensores empleados, así como las técnicas y metodologías desarrolladas, adquieren un protagonismo esencial en el conocimiento estructural de las construcciones civiles. Por un lado, los sistemas láser escáner y fotogramétricos son capaces de suministrar productos “ricos” en cualidades geométricas y radiométricas. Sin embargo, requieren de metodologías complementarias para materializar mecánicamente (a excepción de los resultados

provistos por las estrategias basadas en Correlación Digital de Imágenes) posibles afecciones patológicas. La respuesta a dicha necesidad puede ser encontrada en el empleo de las técnicas basadas en la dinámica de estructuras, más concretamente en el Análisis Modal Operacional, y el Método de los Elementos Finitos. El empleo de ambas técnicas ofrece por ende un amplio espectro de posibilidades sobre el cual cuantificar y caracterizar los daños presentes en las construcciones.

Nature, to be commanded, must be obeyed.

Francis Bacon (1605)

INDICE

Introducción.....	1
Objetivos de la Tesis.....	15
Capítulo I : The combination of geomatic approaches and operational modal analysis to improve the calibration of finite element models: a case of study in saint torcato church (guimarães, Portugal). 17	
Capítulo II: Experimental and numerical approaches for structural assessment in new footbridge designs (SFRSCC-GFPR hybrid structure).....	31
Capítulo III: Photogrammetric, geometrical and numerical strategies to evaluate initial and current conditions in historical constructions: a test case in the church of San Lorenzo (Zamora, Spain).....	45
Capítulo IV: Practical use of multispectral techniques for the detection of pathologies in constructions.....	67
Capítulo V: Conclusiones y Futuras investigaciones.....	89
Anexo I: Enhance your Finite Element Models software.....	103
Anexo II: Descriptores de calidad de los artículos publicados.....	109

INTRODUCCIÓN

Resulta irrefutable basar el éxito de las construcciones, especialmente en lo referente a su vida útil, en el constante avance experimentado en el uso de materiales y técnicas de construcción. Desde soluciones altamente arraigadas en la sociedad basadas en el empleo de muros, arcos y dinteles erigidos en fábricas de mampostería pétreo o adobe hasta sistemas estructurales novedosos que incluyen el uso de polímeros o fibras como materiales resistentes en tableros de hormigón autocompactante.

Sin embargo, es bien conocido que las cargas de servicio, las acciones ambientales o accidentales pueden causar daños en dichos sistemas estructurales, disminuyendo consigo su capacidad prestacional. Derivado de ello, es posible definir el daño como aquella debilidad no deseada presente en la construcción, que pone en riesgo la seguridad y el comportamiento de esta (Stubbs, 1985). Dicha debilidad, comúnmente conocida como proceso patológico, pueden manifestarse a través de diferentes síntomas como grietas, delaminaciones o corrosiones, según el tipo de construcción considerada (Watt, 1999).

En términos de escala, el daño comienza a nivel material, sin implicar necesariamente una pérdida total de la funcionalidad del sistema estructural. Pero provocando que dicho sistema no opere en sus condiciones óptimas. Si dicho daño no es correctamente tratado, este puede crecer a diferentes niveles (crecimiento espacial o temporal) (Farrar & Worden, 2007). Afectando así a la estructura hasta un punto no aceptable: el fallo estructural. Motivado por ello, resulta indispensable desarrollar sistemas capaces de detectar y diagnosticar los daños presentes en las estructuras, con objeto de diseñar de forma

adecuada planes de mantenimiento y sistemas de restauración que protejan la vida útil de la construcción.

En dentro de estos sistemas, donde los procesos enfocados en la evaluación de las condiciones estructurales adquieren un valor importante. Dichos procedimientos, comúnmente conocidos como procesos de monitorización de la salud estructural (Worden & Barton, 2004), asumen que el daño presente en la construcción esta intimamente ligado a un factor temporal. Afectando así de forma negativa a la vida útil de dichas estructuras (Liang & Yuan, 2015; Lorenzoni et al., 2013; Luís F. Ramos et al., 2010). Es por ello, que la definición de daño puede ligarse a una variación de las propiedades materiales y/o geométricas de la estructura considerada. Incluyendo, cambios en las condiciones de contorno o en las conexiones, que afecten de forma negativa al comportamiento actual del sistema estructural (Farrar & Worden, 2007).

En una primera instancia, es posible clasificar los procedimientos de monitoreo de la salud estructural en sistemas locales y globales (Housner et al., 1997). Por un lado, los métodos locales (e.j. rayos x o métodos acústicos) se caracterizan por actuar sobre áreas locales de la estructura, con una mayor sensibilidad que los métodos globales. Por otro lado, los métodos globales (de menor diversidad que los locales), son capaces de caracterizar los daños que influyen en el comportamiento global de la estructura (Haque et al., 2012).

Sin embargo, dicho sistema de clasificación local/global tiene un enfoque meramente “espacial”. Requiriendo de sistemas adicionales capaces de evaluar y caracterizar los daños presentes. Bajo dicha premisa, la clasificación inicialmente definida por (Rytter, 1993) y posteriormente modificada por (Worden & Dulieu-Barton, 2004) y (Yan et al., 2007) provee un catálogo válido sobre el cual analizar el comportamiento de las metodologías aplicadas. Dicho sistema de clasificación queda definido de la siguiente forma:

- Nivel 1 o Detección: incluye las metodologías capaces de proveer información cualitativa del daño presente.

- Nivel 2 o Localización: comprende aquellas estrategias capaces de proveer información sobre la probable localización del daño.
- Nivel 3 o Clasificación: incluye aquellos procedimientos capaces de reconocer los diferentes procesos patológicos.
- Nivel 4 o Evaluación: encapsula las metodologías que permiten estimar el área afectada por el daño.
- Nivel 5 o Predicción: considera aquellos procedimientos que ofrecen información sobre las condiciones de estabilidad estructural, y por tanto, estima la vida útil residual de la construcción.

Ha de destacarse, la existencia de una interconexión jerárquica entre los diferentes niveles definidos. Esto hace, por ejemplo, que el nivel de información 3 lleve intrínseco los niveles 1 y 2.

Diversos son los test no destructivos que permiten la identificación de daños en sistemas estructurales. La mayoría de dichos procedimientos, sin embargo, solo pueden ser aplicados cuando la estructura no está en uso. Restringiendo así el número de técnicas adecuadas para la monitorización de la salud estructural del sistema. Dentro de dicho campo selecto, las técnicas dinámicas han adquirido un interés especial, en comparación con los sistemas quasi-estáticos, los cuales presentan una menor sensibilidad al daño. Ello posiciona a las técnicas basadas en la dinámica de estructuras como las preferentes en este campo, posibilitando la evaluación de la estructura bajo condiciones operacionales, la determinación de daños y su monitorización (Peeters & De-Roeck, 2001; Ramos, 2007).

De forma complementaria a los métodos de clasificación de daños definidos anteriormente, un tercer sistema de clasificación ha de ser definido: las estrategias basadas y no basadas en modelos. Por un lado, las estrategias no basadas en modelos, basan su éxito en la comparación de dos estados, uno dañado y otro de referencia,

empleando además detectores (los cuales expresan las desviaciones de determinados parámetros) tales como el análisis wavelet, los cambios en los parámetros modales o los cambios en las derivadas de los parámetros modales (Ramos, 2007). Por otro lado, los sistemas basados en modelos, comparan la respuesta proporcionada por una simulación numérica, generalmente una simulación por Elementos Finitos. Estas últimas estrategias permite una evaluación de daños superior al nivel 3 (acorde a la clasificación de Rytter). Entrando así en concordancia con otro pilar básico en la caracterización de daños: la prognosis. La prognosis permite estimar la vida útil remanente de un sistema (Farrar et al., 2003) basándose en los resultados arrojados por un modelo predictivo del estado actual del sistema estructural, y para el cual las variables y el daño presente deben de estar correctamente determinados.

En los últimos años, los modelos numéricos por Elementos Finitos (Zienkiewicz & Taylor, 1994) han copado gran parte del interés científico (Saloustros et al., 2015; Adewole & Bull, 2013). En contraposición con métodos más clásicos, como la estática gráfica (Huerta, 2008) o el análisis límite (Heyman, 1997), dichos sistemas de simulación numérica se han posicionados como potenciales soluciones a las diferentes necesidades ingenieriles existentes. Permitiendo la evaluación estructural bajo condiciones específicas, tales como las simulaciones dinámicas (Ramos et al., 2013), sísmicas (Milani & Valente, 2015) o estáticas (Gonilha et al., 2014). En contraste a dicha flexibilidad, los sistemas de simulación numérica por Elementos Finitos requieren de un conocimiento extenso de las variables intervinientes, en particular, de las condiciones de contorno o de las variables mecánicas que rigen el comportamiento de los materiales intervinientes. Es en este punto, donde la dinámica de estructuras y en especial el Análisis Modal Operacional se han posicionado como las técnicas preferidas para complementarlas (Osmancikli et al. 2015; Türker & Bayraktar, 2014; Ramos et al., 2013). Sin embargo, este no es el único requerimiento para obtener una simulación numérica adecuada de los sistemas estructurales. La calibración de su respuesta estructural (variables, condiciones de contorno, etc.) y su correcta definición geométrica son aspectos críticos ha considerar Mottershead & Friswell, 1993). Para los cuales las disciplinas de la geomática y la calibración de modelos numéricos pueden

proveer la solución adecuada.

Por un lado, las técnicas de calibración de modelos numéricos, enfocadas en el ajuste de la respuesta del sistema estructural frente a variables desconocidas o aproximadas (Simoen et al., 2015), tratan de minimizar las discrepancias entre el modelo experimental y el modelo numérico. Dentro de dicha disciplina amplio es el número de técnicas empeladas, desde enfoques basados en el método de (Douglas & Reid, 1982) hasta técnicas de mayor complejidad como las definidas por (Simoen et al., 2015). Sin embargo, y de forma independiente a la técnica empelada, varios son los aspectos en común: (i) el empleo de una función objetiva a minimizar; (ii) el empleo de variables acotadas; y (iii) la necesidad de un proceso de optimización.

Por otro lado, la disciplina de la geomática centra sus esfuerzos en la definición geométrica de la construcción. Dicho aspecto, particularmente atractivo en las construcciones históricas, es de gran interés para la Comunidad Científica Internacional. Posicionando a los sensores geomáticos (principalmente los sistemas láser escáner y los sensores fotogramétricos) como la técnica no-destructiva más adecuada para la caracterización geométrica (Conde et al., 2015; Villarino et al., 2014; Riveiro et al., 2011). Dicho conjunto de sensores son capaces de proveer de un producto tridimensional, denso y preciso de la construcción: la nube de puntos. Sin embargo dicha nube de puntos, compuesta por millones de puntos distribuidos en el espacio, carece de sentido alguno para las simulaciones numéricas por Elementos Finitos. Requiriendo de un sistema de transición hacia modelos CAD aptos para dichas simulaciones. Dicha transformación no adquiere un carácter trivial. No aprovechando así la potencialidad ofrecida por la nube de puntos, siendo únicamente empleada como base para la construcción manual de modelos CAD, a través de dos metodologías básicas (Tognaccini, 2009): (i) metodologías que empelan vistas ortogonales para dibujar contornos sobre la nube de puntos; o (ii) secciones aplicadas sobre las direcciones principales de la malla. De forma paralela de dichos enfoques, que no ofrecen una solución óptima para aprovechar las potencialidades geométricas de la nube de puntos, otras soluciones emergen con fuerza. Estas soluciones alternativas tratan de

aprovechar los conceptos de las superficies paramétricas (e.j. planos, cilindros, etc.) (Cabaleiro et al., 2014; Varady, 2008), los sistemas basados en B-splines Racionales No Uniformes (NURBs) (Piegl & Tiller, 2012) y las estrategias de voxelización (Castellazzi et al., 2015). Tras dicho productos (nube de puntos o imágenes), eminentemente geométricos y proporcionado por los sistemas láser escáner o fotogramétricos, se esconde un componente radiométrico también de gran potencialidad para la detección y cuantificación de daños.

Una de las principales aplicaciones de los sensores remotos puede ser encontrada en la clasificación de terrenos y cultivos a través del análisis de las imágenes capturadas (Del Pozo et al., 2015; Moody et al., 2014; Pope & Rees, 2014). Dicho enfoque, comúnmente conocido como clasificación multiespectral, clasifica los píxeles (entendiendo como tales a las unidades básicas de una imagen) en clases según su respuesta radiométrica. Dicha clasificación, emplea diversas bandas espectrales y sensores (que actúan en diferentes espectros) a fin de robustecer la detección de clases informacionales de la superficie analizada. Probando ser de gran interés en la detección de patologías en construcciones (Armesto et al., 2010). Detrás de dicha capacidad, la flexibilidad a la hora de adquirir imágenes y la posibilidad de comparar estados temporales diferentes permiten emplazar al enfoque basado en la clasificación multiespectral de imágenes como una solución potencial en la detección global de daños. Permitiendo la identificación de daños y pudiéndose emplear como sistemas alternativos a la monitorización de la salud estructural de la construcción.

Sin embargo, el concepto de clasificación multiespectral no adquiere toda su potencialidad en la detección y monitorización de patologías sin la presencia de los denominados algoritmos de clasificación. Dentro de este campo, dos son los enfoques principales (Li et al., 2014): (i) las estrategias de clasificación supervisada; y (ii) los métodos de clasificación no-supervisados. Mientras que los sistemas de clasificación supervisada requieren de la interacción del usuario, a través de la definición de las áreas de entrenamiento, los sistemas no supervisados únicamente requieren como input las diferentes bandas

espectrales consideradas.

Parece por tanto lógico, y atendiendo a los clasificadores y las descripciones anteriormente expuestos, que una completa caracterización del daño presente en las construcciones requiere de un proceso multidisciplinar. Dicho proceso no ha de ser solo capaz de localizar y cuantificar el daño, sino también de disponer de la suficiente capacidad para predecir el comportamiento futuro de la estructura (prognosis). Atendiendo a ello, la presente Tesis Doctoral aboga por el empleo de técnicas propias de las disciplinas de la geomática (láser escáner y fotogrametría) y la dinámica de estructuras (a través del Análisis Modal Operacional), al igual que los procedimientos basados en el clasificación multispectral de imágenes como herramientas para la caracterización de daños a nivel global. Todo ello, complementado por estrategias numéricas avanzadas por Elementos Finitos y metodologías de calibración numérica (métodos basados en modelos) que permitan llegar a predecir el comportamiento futuro de las construcciones evaluadas.

Considerando dichos pilares como la estructura básica de los procedimientos de detección de daño a nivel global, los Capítulos del I al IV describirán la actividad de investigación llevada a cabo en los diferentes campos descritos a continuación: (i) Capítulo I: caracterización geométrica, identificación dinámica y calibración numérica; (ii) Capítulo II: identificación dinámica y calibración numérica; (iii) Capítulo III: caracterización geométrica y calibración numérica; y (iv) Capítulo IV: análisis multispectral de imágenes.

Definidos los diferentes campos de actuación para una correcta definición del daño a nivel global, resulta necesario establecer un marco general sobre el cual integrar los diferentes enfoques considerados y que permita una mejor trazabilidad y futura mejora en la metodología. Eco de ello, el **Capítulo I** (correspondiente a la primera publicación), desarrolla dicha integración (a excepción del análisis multispectral) bajo un marco común de actuación: el análisis de una construcción histórica con daños estructurales, considerando como nexo de unión la simulación numérica de esta.

Sin duda alguna, los sistemas láser escáner y fotogramétricos (a través del enfoque

Structure from Motion) han ganado una gran relevancia en la caracterización geométrica de construcciones (Conde et al., 2015, Villarino et al., 2014, Barazzetti et al., 2010). Sin embargo, ambos sistemas terrestres presentan como principal desventaja la imposibilidad de adquirir datos en zonas inaccesibles de la construcción (e.j. tejados, cúpulas o torres). Requiriendo el uso de tecnologías adicionales que sean capaces de suplir dicha limitación. Es, dentro del campo de la fotogrametría, donde las cámaras digitales (cámaras RGB, multiespectrales, etc.) embarcadas en plataformas VANT (Vehículo Aéreo No Tripulado) pueden posicionarse como la solución ideal (Del Pozo et al., 2014; Scaioni et al., 2009).

En otras palabras, la combinación de los sistemas láser escáner y Structure from Motion (en su versión terrestre y aérea) parecen ser las soluciones óptimas para la completa caracterización geométrica de la construcción. Sin embargo, la necesidad de emplear múltiples estaciones, y por ello diferentes nubes de puntos, requieren del correcto registro de estas dentro de un sistema común. Es en este campo, donde algoritmos como el Iterative Closest Points (Besl & McKay, 1992) o el algoritmo Least Square Surface Matching (Acka & Gruen, 2007) pueden ser empujados. Sin embargo, el registro de varias nubes de puntos lleva consigo una acumulación de errores que requiere de ser compensada, y donde algoritmos como el Generalized Procrustes Analysis (Toldo et al., 2010) pueden solventar el problema.

Tal y como se mencionó con anterioridad, el paso de la nube de puntos a un modelo CAD no es una tarea trivial en la actualidad. Las prácticas comunes están básicamente enfocadas en el empleo de secciones, vistas ortogonales o segmentaciones manuales de la nube de puntos. No explotando las ventajas ofrecidas por dichos productos. De forma paralela a estos sistemas de segmentación manual, emergen nuevos enfoques que pueden emplazarse como posibles soluciones a la conversión CAD, tales como la Descomposición Funcional (Varady, 2008) o los sistemas NURBs basados en la cuadrilaterización de la malla (Branch et al., 2008).

Una vez el modelo geométrico es definido (y adaptado para el correspondiente análisis

numérico) y su daño localizado. Es requisito disponer de una correcta interpretación de los resultados. Es aquí, donde los procedimientos basados en el Análisis Modal Operacional y la calibración de modelos numéricos se sitúan como piezas indispensables.

Dentro del diferente abanico de posibilidades que brindan los ensayos in-situ, la identificación modal se emplaza como una de las soluciones de mayor potencialidad. De forma más específica el Análisis Modal Operacional, también conocido como identificación modal ambiental, trata de extraer los parámetros modales de la estructura (tales como las frecuencias, los modos de vibración o los coeficientes de amortiguamiento) considerando como fuentes de excitación las ambientales. Dicha técnica puede ser empleada a través de diferentes metodologías, encargadas de extraer los parámetros modales (Ramos, 2007): (i) técnicas en el dominio de la frecuencia como la Descomposición Mejorada en el Dominio de la Frecuencia; y (ii) los métodos en el dominio temporal como los Sistemas de Identificación Estocásticos. Dicha técnica puede aumentar su potencialidad a través del empleo de las técnicas de calibración numérica, que toman como objetivo básico la minimización de las discrepancias existentes entre los modelos numéricos y los datos experimentales.

Ampliamente extendido, el método de Douglas-Reid (Douglas & Reid, 1982) permite calibrar modelos numéricos por Elementos Finitos (et al., 2014; Gentile & Saisi, 2007). Dicha metodología minimiza las discrepancias existentes entre las simulaciones numéricas y los resultados obtenidos en las diferentes campañas experimentales. Requiriendo únicamente la resolución de un sistema no lineal de ecuaciones y la minimización de la función objetiva considerada.

Ha de considerarse también, que el presente capítulo trata de abordar el daño presente a través de un enfoque discreto. Considerando para ello el agrietamiento como una discontinuidad en la estructura, y requiriendo por tanto una definición específica de la grieta dentro del modelo numérico. De ello resulta la necesidad de disponer de estrategias de caracterización de daños basadas en enfoques difusos (De Borst et al., 2004). Capaces

de detectar y cuantificar el daño presente sin necesidad de materializar físicamente las patologías existentes (enfoque discreto).

Complementario a ello, cabe remarcar el sistema de calibración empleado, basado en el enfoque “*simplista*” propuesto por (Douglas & Reid, 1982), y cuyas variables de calibración únicamente pueden restringirse al ámbito de la dinámica. Es por tanto necesario, mudar hacia estrategias de calibración robustas capaces de integrar en las funciones objetivas componentes de carácter estático como las deformaciones.

En respuesta a dichas necesidades, el segundo artículo presentado en la presente Tesis Doctoral, y materializado en el **Capítulo II**, desarrolla un sistema de calibración robusta de modelos numéricos capaz de integrar los datos procedentes de campañas experimentales estáticas y dinámicas dentro de un enfoque Determinista. Dicho enfoque, considera la estructura como un conjunto de propiedades conocidas o asumidas que presentan una relación con el comportamiento arrojado por esta (Simoen et al., 2015). Bajo dicha hipótesis de trabajo, los enfoques Deterministas calibran la respuesta de los modelos numéricos a través de la determinación del valor óptimo de las variables consideradas. Minimizando las discrepancias entre los datos experimentales y numéricos. Dicho “*set*” de variables ha de estar acotado entre unos valores coherentes.

Definido el concepto general que rige los enfoques Deterministas, parece lógico asumir la posibilidad de integrar los daños presentes en la estructura como variaciones de las propiedades mecánicas de los elementos que la constituyen. En acordancia con la definición previa de daño: “*Derivado de ello es posible definir el daño como aquella debilidad no deseada presente en la construcción que pone en riesgo la seguridad y comportamiento de esta*”. Ajustar la respuesta mecánica de los elementos intervinientes en una simulación numérica puede resultar en un amplio número de variables a optimizar, y por ende en un sistema mal condicionado. Donde la matriz Hessiana se vuelve singular y difícil de invertir de forma precisa. Dicha situación no garantiza una solución única y estable (frente a cambios pequeños de las variables), requiriendo de una resolución

complementaria a través de los denominados procedimientos de regularización (Titurus & Friswell, 2008). Sin embargo, y aunque dicho procedimiento puede ser implementado en el enfoque Determinista considerado, dos inconvenientes han de ser tenidos en cuenta: (i) la evaluación de grandes matrices de sensibilidad y altos tiempos de computación y; (ii) la consideración del daño como un fenómeno no continuo en la estructura. Considerando dichas premisas, el **Capítulo II** emplea el concepto de función de daño, inicialmente desarrollado por (Teughels & De Roeck, 2003), como punto de partida. Bajo dicha metodología es desarrollado un sistema híbrido de detección de daño basado en la combinación de funciones de daños discretas y sistemas de subestructuración.

A día de hoy, resulta inevitable destacar la importancia adquirida por los sistemas de identificación dinámica en la evaluación de la salud en las construcciones. Dicha relevancia estriba en la habilidad que presentan estas técnicas en la detección y monitoreo de daños (Ramos et al., 2013; Teughels & De Roeck, 2003). Dando lugar a un amplio número de metodologías (Rainieri & Fabbrocino, 2014) e indicadores (Dong et al., 1994; Stubbs et al., 1992; Pandey et al., 1991), parte de los cuales pueden operar conjuntamente con las simulaciones por Elementos Finitos y ofrecer un resultado robusto del comportamiento estructural del sistema evaluado (Zordan et al., 2014).

Sin embargo, y de forma paralela a los desarrollos mencionados en el campo de la dinámica, emerge la necesidad de desarrollar indicadores geométricos capaces de proveer valores equitativos en el campo de la estática. A día de hoy, son varios estudios que emplean indicadores estáticos en la calibración de modelos numéricos (a destacar el procedimiento mostrado en el Capítulo 2), los cuales adquieren un carácter meramente local al derivar de datos puntuales de la estructura (Solis et al., 2013).

Inspirado por dicha necesidad, el **Capítulo III** introduce dos nuevos parámetros de calidad geométrica. Dichos indicadores, denominados Global Metric Hausdorff (GHm_s) y Local Metric Hausdorff (Ghm_s), y basados en el concepto de distancia simétrica Hausdorff (Hausdorff, 2008), son capaces de aprovechar la gran densidad de datos geométricos

provistos por los sensores geomáticos con la finalidad de calibrar la respuesta de los modelos numéricos.

De forma paralela a lo anteriormente mencionado, y considerando la importancia que adquiere la geometría de la construcción en la correcta simulación numérica de la misma, el **Capítulo VIII** trata de mejorar el enfoque geométrico desarrollado en el primer capítulo, basado en el empleo de la teoría de Morse (Varady, 2008) para la segmentación de entidades topológicas, el ajuste de formas paramétricas y uso auxiliar de procedimientos comunes en ingeniería inversa. Dicha mejora irá enfocada en la incorporación de superficies NURBs (Piegl & Tiller, 2012). Consideradas como superficies no paramétricas de alto nivel, las NURBs se caracterizan por su amplia versatilidad y habilidad de representar complejas superficies. Sin embargo, dichas representaciones requieren del empleo de técnicas complementarias tales como la cuadrilateración de la malla triangular. Bajo dicho contexto, los enfoques basados en la teoría de Morse y el Análisis Espectral de mallas parecen responder a dichas necesidades (Branch et al., 2008). Acorde a lo anteriormente expuesto, el **Capítulo III** parte de la base desarrollada por (Branch et al., 2008) e incorpora dentro de su estructura operacional algoritmos de generación de mallas manifold (Attene, 2010) y los diferentes procesos patológicos presentes (agrietamientos, falta de material, etc.).

Llegados a este punto, es posible obtener una evaluación de los procesos patológicos ampliamente relacionados con aspectos geométricos de la construcción (tales como agrietamientos o falta de material). Sin embargo, no hemos de olvidar la existencia de determinadas patologías con un peso importante en la vida útil de la construcción, tales como: (i) la existencia de procesos de alteración biológica (algas, hongos, mohos, etc.); (ii) hitos geológicos que condicionan la composición mineral y las propiedades de los materiales; o (iii) la presencia de humedades que pueden derivar en procesos de corrosión en hormigones armados. Con objeto de ampliar el abanico de patologías detectadas, y por ende, la potencialidad de los sensores empelados en la detección de daños, el **Capítulo IV** aboga por el empleo de las técnicas multispectrales como la solución más óptima para

ello. Sin embargo, y aunque tradicionalmente el concepto de clasificación multiespectral ha estado ligado intimamente a las imágenes captuadas por un único sensor (generalmente una cámara multiespectral) (Campbell, 2002). La presente Tesis Doctoral presente la clasificación multiespectral de imágenes como un proceso de registro de sensores que trabajan en diferentes longitudes de onda (e.j. Cámara RGB, cámara infrarroja o sistemas láser escáner). Complementario a ello, son empleados diversos indicadores, tales como la matriz de confusión o el coeficiente Kappa de Cohen (Armesto et al., 2010), con objeto de evaluar la robustez y calidad de las clasificaciones efectuadas. El empleo conjunto de los conceptos anteriormente definidos permiten obtener un resultado válido en la detección de determinadas patologías. Como resultado el **Capítulo IV** muestra la aplicación práctica de los enfoques de clasificación multiespectral en la evaluación y monitorización patológica de estructuras. Dicho enfoque es empelado en un total de tres construcciones, donde proceso patológicos tales como humedades o acciones biológicas son latentes: (i) probable corrosión y eflorescencia en estructura de hormigón armado; (ii) actividad biológica (algas, líquenes, etc.) en construcciones históricas; y (iii) caracterización del granito Abulense, como un caso especial de facie alterada granítica cuyas propiedades mecánicas (resistencia a heladas, resistencia a flexión o compresión) es inferior al granito no alterado (García-Talegón et al., 1993).

OBJETIVOS DE LA TESIS

Definidos los pilares básicos, descritos en la Introducción, para una correcta identificación de los daños estructurales a nivel global. La presente Tesis Doctoral ha sido construida bajo los siguientes objetivos:

- I. Evaluación de la aplicabilidad de los sensores geomáticos (sistemas láser escáner terrestre y cámara digitales) en construcciones con daños estructurales.
- II. Desarrollo de estrategias de modelización y construcción de modelos CAD en estructuras con procesos patológicos con un claro componente geométrico (deformaciones y grietas), aptos para posteriores simulaciones numéricas.
- III. Evaluación de los procedimientos de dinámica de estructuras basados en el enfoque del Análisis Modal Operacional en la evaluación de daños.
- IV. Aplicación y desarrollo de metodologías robustas para la calibración de modelos numéricos. Capaces de localizar e interpretar los daños presentes en las construcciones.
- V. Aplicación del análisis multiespectral de imágenes en la detección de patologías con un componente eminentemente radiométrico (e.j. Caracterización de materiales, humedad en hormigones, acciones biológicas, etc.) y con una estrecha relación con la estabilidad y la vida útil de la construcción.

En términos más prácticos y en lo concerniente a la investigación llevada a cabo, los sensores empelados así como las metodologías desarrolladas han sido evaluadas sobre diferentes tipos de construcciones: desde construcciones históricas y vernaculas, hasta construcciones en hormigón armado o soluciones estructurales en fase experimental.

THE COMBINATION OF GEOMATIC APPROACHES AND OPERATIONAL MODAL ANALYSIS TO IMPROVE THE CALIBRATION OF FINITE ELEMENT MODELS: A CASE OF STUDY IN SAINT TORCATO CHURCH (GUIMARÃES, PORTUGAL).

RESUMEN: Definidos los pilares básicos de actuación para una correcta definición a nivel global de los daños (atendiendo a la introducción previamente expuesta). El presente capítulo tratara de aunar dos disciplinas independientes bajo un mismo marco operacional: la geomática y el análisis dinámico de estructuras. Dicha hibridación permitirá además, la disposición de unos sólidos cimientos sobre los cuales mejorar los procedimientos que serán desarrollados en capítulos posteriores.

A fin de corroborar la viabilidad de los procedimientos empelados (sistemas láser escáner, fotogramétricos y el Análisis Modal Operacional), estos serán aplicados a una construcción histórica con problemas estructurales: la iglesia de San Torcato en Portugal. De forma resumida, el procedimiento desarrollado y empleado en el presente capítulo incluye: adquisición de datos dinámicos y geomáticos, el registro de sensores, el desarrollo de un sistema de segmentación y modelización CAD y por último la calibración del modelo numérico resultante.

Los resultados arrojados por la simulación numérica (con valores bajos de discrepancia entre frecuencias y altos valores MAC, considerando la complejidad de la edificación), sugieren que la consideración e integración adecuada de procesos patológicos como los agrietamientos son aspectos críticos en la correcta definición de los modelos numéricos.

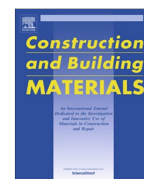
Palabras clave: Structure from Motion; Sistema láser escáner; Modelado por Elementos Finitos; Calibración modal; Estructuras de mampostería; Ortoimagen; Inspección de daños; Modelado CAD.



ELSEVIER

Contents lists available at ScienceDirect

Construction and Building Materials

journal homepage: www.elsevier.com/locate/conbuildmat

The combination of geomatic approaches and operational modal analysis to improve calibration of finite element models: A case of study in Saint Torcato Church (Guimarães, Portugal)



CrossMark

Luis Javier Sánchez-Aparicio^{a,*}, Belén Riveiro^{b,2}, Diego González-Aguilera^{a,1}, Luís F. Ramos^{c,3}^a Department of Land and Cartographic Engineering, University of Salamanca, High Polytechnic School of Avila, Hornos Caleros 50, 05003 Avila, Spain^b Department of Material Engineering, Applied Mechanics and Construction, School of Industrial Engineering, University of Vigo, Vigo, Spain^c ISE, Department of Civil Engineering, University of Minho, Guimarães, Portugal

HIGHLIGHTS

- Numerical study applied to historical building with non-intrusive sensors.
- Structure from Motion, allows generating realistic and complete 3D models.
- The methodology presented transforms the data from geotechnologies into CAD models.
- Operational modal analysis for finite element model calibration.
- Modelled features from Structure from Motion can improve the dynamical response.

ARTICLE INFO

Article history:

Received 4 April 2014

Received in revised form 27 June 2014

Accepted 23 July 2014

Available online 20 August 2014

Keywords:

Structure from Motion
Laser scanner surveying
Finite element model
Modal updating
Masonry structures
Orthoimage
Damage survey
CAD modeling

ABSTRACT

This paper present a set of procedures based on laser scanning, photogrammetry (Structure from Motion) and operational modal analysis in order to obtain accurate numeric models which allows identifying architectural complications that arise in historical buildings. In addition, the method includes tools that facilitate building-damage monitoring tasks. All of these aimed to obtain robust basis for numerical analysis of the actual behavior and monitoring task.

This case study seeks to validate said methodologies, using as an example the case of Saint Torcato Church, located in Guimarães, Portugal.

© 2014 Elsevier Ltd. All rights reserved.

1. Introduction

The conservation of historic buildings requires understanding their structural behavior, and consequently: (i) their boundary conditions, (ii) the characteristics of the constitutive materials (iii) the

origin of the damage that the building suffers and (iv) their vulnerability [1]. Therefore the creation of accurate numerical models is imperative in order to obtain adequate restoration systems.

Masonry walls are very common in the vast majority of existing monuments. Cracked elements, associated with different events (settlements and/or excessive displacement loadings) are a common problem that reduces the service life of these structures [2]. The fracture phenomena (cracks) are caused by the masonry's high brittleness to tensile stresses. Furthermore, the structural behavior is highly dependent of the structural geometry. This is why four conditions are required to carried out proper analysis: (i) having a complete and accurate geometric characterization of the structure; (ii) knowing the material's mechanical properties (iii) characterizing all the loads acting in the structure; and (iv) providing

Abbreviations: UAV, Unmanned Aerial Vehicle; SfM, Structure from Motion; PW, Photogrammetry Workbench; MAC, Modal Assurance Criterion; DR, Douglas-Reid Method; ICP, Iterative Closest Point; NURBS, Non-Uniform Rational B-Splines.

* Corresponding author. Tel.: +34 920353500; fax: +34 920353501.

E-mail addresses: luisj@usal.es (L.J. Sánchez-Aparicio), lramos@civil.uminho.pt (L.F. Ramos).

¹ Tel.: +34 920353500; fax: +34 920353501.

² Tel.: +34 986 813 661; fax: +34 986 811 924.

³ Tel.: +351 253510200; fax: +351 253510217.

<http://dx.doi.org/10.1016/j.conbuildmat.2014.07.106>
0950-0618/© 2014 Elsevier Ltd. All rights reserved.

numerical models that correctly simulate the characteristic behavior of the structure (non-linear material behavior, ground settlement, contact between bricks, etc.).

Modern restoration techniques for built heritage are characterized by minimal intervention, compatibility, durability and reversibility [3]. Identifying and monitoring the pathological condition of the building plays a key role in understanding the current behavior of the structure and the choice of restoration methods to be accomplished [4].

Traditional measuring methods often had a significant dependence of the worker's skills and they normally have associated high time cost. These methods were replaced by direct interpretations done over the building plans (design models) [5–7]. The constant progress of the numeric method of finite elements and computer processing allows the generation of increasingly complex geometric models; that is why it is more and more imperative the necessity of relying on sensors capable to provide massive detailed data and features for the model. Is in this field where geomatic sensors like terrestrial laser scanner [8,9] or digital camera [10] have acquired important roles, due to the capacity of acquire accurate geometrical information needed by the numerical models.

In the present paper, the proposed methodology for data acquisition combines and enhances the laser scanning and digital camera system providing, beside the characteristics defined above, the versatility of adaptation to different infrastructures. All of this within a single application, a hybrid point-cloud, which greatly eases the preparation of geometrically precise numerical models that also serve as a basis for the monitoring of the structure through the analysis of, either the point-cloud or by the analysis of the obtained orthoimages.

The paper relies on the application of the proposed methodology on a case study, St. Torcato Church, close to the city of Guimarães, Portugal [1]. This historical construction has moderate to severe damage and needs to be strengthened. The methodology has been carried out to upgrade and calibrate the finite element model using a global dynamic identification, including crack and geometric improvement, in order to complement with the static and dynamic monitoring system and a future numerical analysis. All this will be made in order to obtain the current stress state of the building and asses the effectiveness of subsequent restoration mechanism that aims at stabilizing the damage.

Within this context, this article attempts to demonstrate a methodology for data acquisition and processing and it is organized in the following way: Section 1 is the introduction; Section 2 presents the instruments for data acquisition which are the laser scanner and the set formed by the UAV and digital camera; Section 3 wherein the methodology for obtaining the hybrid point-cloud and the calibration of the model is shown; Section 4 the data obtained by the laser scanner and the digital camera sensors is analyzed separately, for the presented case study and for the potential of the hybrid point-cloud (this applies not only to the numerical finite-element analysis but also to damage analysis monitoring); and finally in Section 5, the conclusions are drawn.

2. Materials and methods

As described in Section 1, the aim of this methodology is to generate precise finite-element numerical models for subsequent structural analysis. These must be precise, in terms of geometry accuracy and they must contain the necessary data to monitor and track the evolution of damages in the structure. All this within an accurate georeferenced framework and with non-intrusive sensors as the main source.

2.1. Laser scanner system: the terrestrial laser scanner

Currently the terrestrial laser scanning system has acquired great relevance by offering a wide range of advantages; one of the greatest one is the acquisition of non-contact three-dimensional geometry of the analyzed surface, preventing any

disruption and allows to accurately capture geometry, providing a high density of data (millions of points) [11]. This feature includes that it does no dependency on specific lighting conditions [12]. It is therefore the combination of accuracy, speed and range of measures that has placed the system as the most powerful tool for three-dimensional modeling and reconstruction of monuments [13,14].

In order to establish a valid methodology to make more accurate finite element models, two different laser scanning systems have been analyzed based on different measurement principles (Table 1): (i) Riegl LMS-Z390i based on time of flight principle (ii) Faro Focus 3D based on the phase shift principle. For details on these measurement principles, refer to [15].

2.2. Imaging system: UAV and "Structure from Motion"

While the laser scanning system allows fast capture and processing of data, it has some drawbacks such as the difficulty for transport and the restriction of stationing in certain elevated places inside historic buildings, these places often are critical. Therefore, it is necessary to use additional platforms and sensors capable of providing accurate data from any position; for this the onboard digital camera on an Unmanned Aerial Vehicle (UAV) platform is used (Fig. 1).

The chosen photogrammetric platform was designed by Roca et al. [16]. It is made of aluminum and carbon fiber, and comprises a total of eight MK-3638 SLOW-FLY APC propeller motors controlled by a central 12×3.8 Brushless Control V2.0 that can manage separately the rotational speed of each of the motors. All of this provides the system with great stability and robustness against failure in flight.

In addition to this platform, a low-cost sensor, a Canon EOS 450D digital camera that had been previously geometrically calibrated (Table 2), and a Canon EF 20 mm wide-angle lens were assembled. The wide-angle lens is meant to minimize the amount of images taken.

In recent years photogrammetric data processing systems (SfM) have taken a great relevance; they are able to include into their structure the advantages of computer vision (automation and flexibility) and those of photogrammetry (accuracy and reliability) [17] in order to obtain dense three-dimensional models (point clouds) that can compete in accuracy with the laser scanner system [18]. Within this field highlights the Photogrammetry Workbench (PW) software, which implements the "Structure from Motion" system, ensuring automation (in the transformation of 2-D images to 3-D point clouds), flexibility (by allowing work with any type of camera, calibrated and non-calibrated) and quality (to ensure precision and quite acceptable resolutions).

3. Methodology

3.1. Generating the CAD model and its integration with finite elements

The early stage in the laser scanning and the Structure from Motion (SfM) data processing, have been omitted in this article, since our main interest is focused on establishing a robust methodology that serves as a template for subsequent restoration actions. This template will be based on the hybrid point cloud, which comes from the combination of data obtained from laser scanning, the SfM and the analysis of the products that are obtained from them. For more details about SfM flow see either [19].

Also is imperative to building an accurate CAD model which allows us to evaluate the actual behavior of the construction as a basis for the numerical analysis. However, at an early stage, the point cloud provided by the laser scanning and the SfM present superabundant information in different coordinate systems. As a result, this data is not suitable for CAD model building. Following a semi-automatic method that allows adapting the point cloud to an accurate and suitable CAD model for numerical analysis is presented (Fig. 2).

This methodology requires a multi-phase post-processing that involves three main steps: (i) data fusion at the same coordinate system through registration algorithms; (ii) point cloud resampling and (iii) point cloud simplification (removing certain architectural details without relevance) and parameterization for CAD model conversion.

3.1.1. Hybrid point cloud registration

A complete documentation of historical buildings requires the use of multiple point cloud data set. Is a requirement therefore to place all of these point clouds in the same coordinate system in order to be processed together.

Table 1
Comparison of technical specifications between laser scanner system Riegl LMS Z-390i and Faro Focus 3D.

	Riegl LMS Z-390i	Faro Focus 3D
Measurement principle	Time of flight	Phase shift
Wavelength	1550 nm	905 nm
Measurement range	1–400 m	0.6–120 m
Accuracy nominal value	6 mm a 50 m in specific lighting and reflectance conditions	2 mm a 25 m in specific lighting and reflectance conditions
Field of view	360° Horizontal 80° Vertical	360° Horizontal 305° Vertical
Capture rate	11,000 points/s	122,000/976,000 points/s
Beam divergence	0.3 m rad	0.19 m rad



Fig. 1. Image of the UAV platform and the digital camera (left). Image taken during the data collection of the point cloud SfM (right).

Table 2
Canon EOS 450D digital camera geometric calibration settings.

Parameter	Value
Sensor size	$W = 22.2425$ mm $H = 14.8336$ mm
Principal point	$X_p = 10.8716$ mm $Y_p = 7.4449$ mm
Focal length	$f = 20.4222$ mm
Radial distortion	$K_1 = 2.157e-004$ mm $K_2 = -4.189e-007$ mm $K_3 = 0$ mm
Tangential distortion	$P_1 = 4.321e-005$ mm $P_2 = -1.003e-005$ mm

The proposed methodology is based on a registration system coarse to fine. In an initial stage a point cloud pair-wise registration is carried out. This step takes as a base the ICP (Iterative Closest Point) algorithm [20], that minimize the difference between two points clouds, requiring a total of $n - 1$ alignments, where n is the number of point clouds.

Using pair-wise registration causes an error propagation along the registration of all the point cloud scans. In order to minimize this error accumulation a global registration, based on Generalized Procrustes Analysis [21], was used considering the pair-wise registration, previously made, as the rough registration needed.

3.1.2. Hybrid point cloud resampling and CAD conversion

Traditionally the step procedure from the raw point cloud to the CAD model could be made through three different approaches [22]: (i) orthogonal views; (ii) sections applied along directions and over the mesh and (iii) Non-Uniform Rational B-Splines (NURBS) generated from the mesh. The two first approaches require a high manual work made by the user, whereas the NURBS approach demands high computational cost.

In this article an alternative and semi-automatic approach is presented, which combines NURBS and parametric shapes approximations with the addition of a segmentation process described

below, in order to build a suitable CAD model for structural applications. While NURBS-based method was used for complex shapes like (vault or domes), the parametric-based method was used for the rest of the structure.

Once the registration procedure has been completed, the resulting point cloud needs to be resampled (due to the high amount of data) in order to generate a suitable CAD model for the numerical analysis. In this case several methodologies could be applied based on [23]: (i) Principal Component Analysis; (ii) Quadric-Based Polygonal Surface Simplification; (iii) Clustering methodologies and (iv) Radial Based Function. For the proposed methodology a resampling based on curvature has been applied, in order to decimate flat surfaces without losing detail in features areas. This curvature based resampling follows the next steps: (i) creating a local neighborhood of the analysis point; (ii) local surface based on quadratic approximation and (iii) extraction of the normal and principal curvatures.

After that, the resulting point cloud is meshed, since the majority of segmentation procedures are also performed over meshes. The segmentation process is performed by Functionally Decomposed Surface Models [24]. Once the segmentation is done, the different surfaces created are approximate to NURBS and parametric shapes. As a result a manageable CAD model is generated and could be imported and used for a FEM package.

Additionally to the mentioned above, some relevant features like cracks, can be included into the CAD model that defines more realistically the building's behavior. It is sufficient to extract the area of interest from the point cloud, either SfM or laser, to mesh that area and to incorporate it into the CAD model (Fig. 3).

3.2. Crack recognition and characterization

Digital image analysis is a tool of great potential in the field of pathological characterization of buildings. Several authors demonstrate the feasibility of this analysis to characterize either from the terrestrial laser scanner [25,26] or from the image captured by a digital camera [27,28].

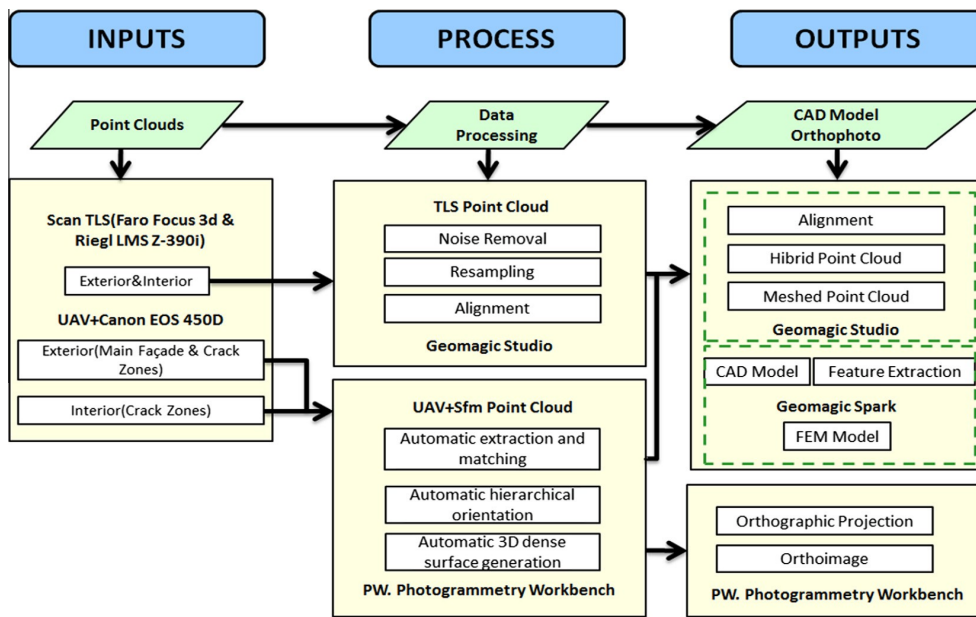


Fig. 2. Workflow for the proposed methodology.

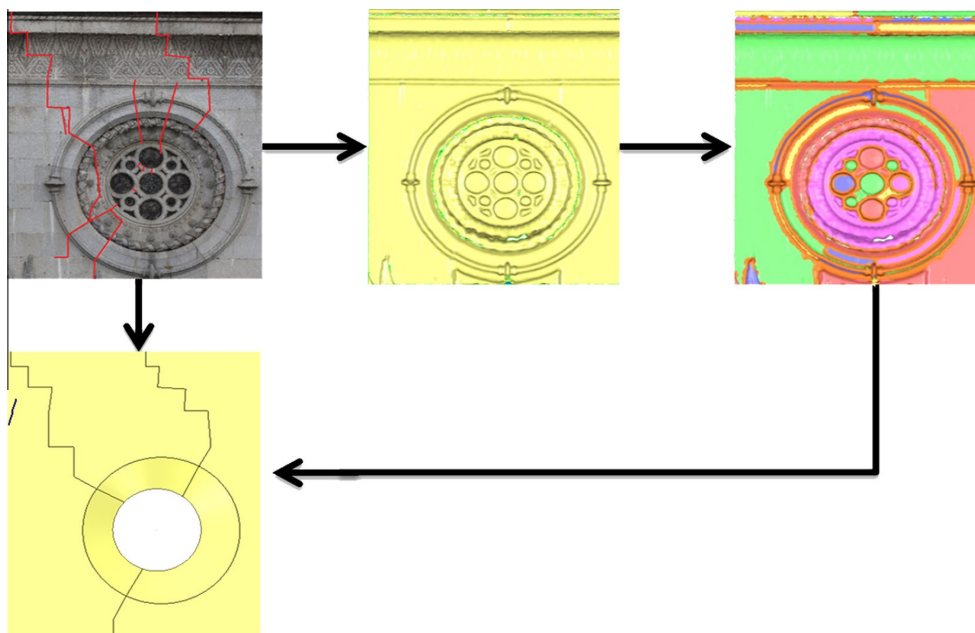


Fig. 3. Graphical description of the proposed methodology. From left to right: point cloud, mesh model, segmentation model, CAD model with major cracks.

Besides offering robust tools for generating three-dimensional models from two-dimensional data (digital image), PW can also obtain orthoimages on specific areas and specific levels, providing the user with precise documentation from anywhere in the building.

Given the high density of points gathered during the three-dimensional reconstruction, the production of orthoimages will

require only two points to provide adequate scale, taken from the laser point cloud and a reference plane, in order to run an orthographic projection. The pixel size of this projection is calculated according to the density of the cloud of points, close to the resolution of the initial images [29].

Given the fact that the obtained orthoimage stands as a product without geometric distortions and in real scale, it is sufficient to

directly measure on it and so obtaining crack characterization (length and opening).

3.3. Finite element numerical model

The geometric accuracy and high level of detail provided by the laser scanning systems and Structure from Motion, provide complex CAD models. In order to solve this geometric complexity, for the discretization elements it is required: (i) high flexibility to adapt themselves to the geometry and (ii) great compatibility with automatic meshing algorithms [7]. All this makes the tetrahedral discretization elements with an isoparametric formulation the most suitable for the meshing of complex CAD models.

3.4. Calibration of the finite element numerical model

The analytical results obtained from the calculation model are sensitive to material properties and boundary conditions [30] thus making necessary to gather experimental data to optimize the numerical model.

Among the different possibilities available today for the implementation of in-situ tests on historic buildings, experimental modal identification is the most popular method [1]. This technique is a non-intrusive system with the capability to identify the global properties of the structure. It allows to obtain vibration frequencies, damping coefficients and mode shape of historic buildings, which may be related to various physical properties (Young modulus, density, stiffness of connections between parts, etc.) which makes possible to validate the analytical models [31].

This publication builds on the data obtained from the accelerometers configuration adopted in 2009. The campaign counted a total of 35 measuring points with 9 sets spread throughout the Church, for more details see [1] (Fig. 4).

The basic objective of these methods is to improve the correlation between the experimental data and those obtained from finite element model, through small changes in a group of model parameters [32]. The criterion often used to assess the correlation is the

MAC (Modal Assurance Criterion), this being defined from the following formula (1) [33]:

$$MAC_{u,d} = \frac{[(\varphi_i^u)^T(\varphi_i^d)]^2}{(\varphi_i^u)^T(\varphi_i^u)(\varphi_i^d)^T(\varphi_i^d)} \quad (1)$$

where φ_i^u y φ_i^d correspond to the mode shape vector on experimental and numerical model respectively for a vibration mode i .

As noted above, the goal is to minimize the existing differences between the experimental behavior and numerical model, considering the experimental values as references. Used in 2007 for the calibration of the numerical model for the Monza Cathedral bell tower [34], the methodology proposed by Douglas-Reid [35] (DR) can be used for calibration of finite element numerical models. This method tries to minimize the difference between theoretical and experimental parameters through the natural frequencies, or another modal parameter, using the following approach:

$$R_i^{FE}(X_1, X_2, \dots, X_n) = \sum_{k=1}^N [A_{ik}X_k + B_{ik}X_k^2] + C_i \quad (2)$$

To solve these equations, a total of $2n + 1$ values are required to be calculated, taking into account initial values, as well as lower and upper bounds for all updating parameters.

Using the methodology followed by [34], the next step consists of determining the modal frequencies and minimize their difference according to the following objective functions (3) and (4):

$$J = \sum_{i=1}^m w\varepsilon \quad (3)$$

$$\varepsilon = f_i^{EXP} - f_i^{FE}(X_1, X_2, \dots, X_n) \quad (4)$$

where J is the objective function to be minimized, w are the weights considered through engineering criterion and ε represents the error function (difference between the frequency obtained by operational modal analysis f_i^{OMA} and numerical analysis f_i^{FE}).

The main drawback of this methodology lies in the consideration of a unique modal parameter; frequency. To obtain more

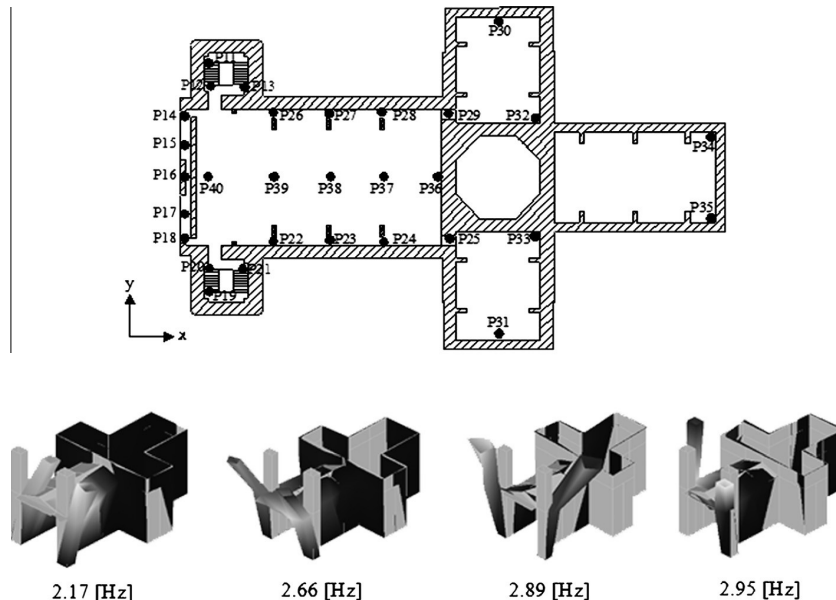


Fig. 4. Scheme of the arrangement of the 35 accelerometers on the Church (above). Mode shape obtained from operational modal analysis (bellow).

accurate results the objective function must be modified, including the MAC values (5):

$$J = 1/2 \left[W_f \sum_{i=1}^m \left(\frac{f_{i,FEM}^2 - f_{i,EXP}^2}{f_{i,EXP}^2} \right)^2 + W_m \sum_{i=1}^m (1 - MAC_{i,FEM})^2 \right] \quad (5)$$

where J is the objective function to be minimized, W_f and W_m are the weights considered for the frequency and vibration modes, f is the frequency and MAC the Modal Assurance Criterion values, both values corresponding to the vibration mode i .

4. Experimental result and discussion

Located in the village of St. Torcato, within the municipality of Guimarães (northern Portugal), the Church of St. Torcato is a clear example of historic building built in stone material, showing moderate-severe structural damage made evident mostly by cracks in its main façade. Starting at the entrance arch keystone, it extends through the rosette to the coronation, splitting this element in two macroblocks [1] (Fig. 5).

Such crack increases the width along its development up to the roof. The movement in opposite directions of the main façade towers due to the settlement suffered by the building is remarkable, as well as some “chruising” type cracks caused by the compressive stress concentration resulting from eccentric loads originating in the towers.

Built in style “Neo-Manuelinio” the Church of Saint Torcato mix Classics, Gothic, Renaissance and Romanesque elements in its extension [6]. This gives it a special and complex aesthetic that along its length, with a height of about 50 m in the towers, prevents effective tridimensional data capture with laser scanner, topographic techniques or manual measurements [36]. The binomial Structure from Motion and laser scanning is the ideal solution allowing abundant and accurate three-dimensional data capture anywhere in the building.

The results obtained are hereby analyzed independently, according to the source sensor (laser scanner or digital camera) and the resulting numerical model of the combination of these and the calibration using operational modal analysis.

4.1. Terrestrial laser scanner

For the study we have considered the two most popular measuring systems for survey of buildings and civil infrastructures: the laser time of flight and phase difference [25].

Multiple tests have been carried out in the exterior as well as in the interior of the Church. Since the point-cloud is defined by density of points, the acquisition rate and range, the laser scanner LMS Z-390i Riegl (based on time of flight) is considered to be the most suitable for data capture in the exterior. Besides, it has a larger range compared to the Faro Focus 3D laser. Indoors, the data acquisition speed of the Faro Focus 3D scanner (122,000 points/s) compared to the speed of the Riegl LMS laser Z-390i (11,000 points/s), together with its portability proved to be the most important advantages for gathering the data in the interior of the Church.

While in both cases the laser system provides a sufficient and suitable density of points to accurately monitor deformations [37], the amount of data and distinctive features provided might be insufficient of the extraction and monitoring of cracks (for example, it does not record texture) (Fig. 6).

The final model had a total of 29 scans and 267,601,626 points: (i) 14 scans were done of the outside with the Riegl LMS laser Z-390i, (ii) 3 interior shots were taken with the Riegl LMS laser Z-390i and (iii) 12 interior scans were made with the Faro Focus 3D laser. However, the top of the towers and the rooftop of the Church could not be modelled because no suitable location was found for the laser to reach those areas. In addition, the data collection was hampered by additional conditions: the excessive laser beam skew angle on the ledge, top of the towers and the openings between the chapels preventing a complete and accurate characterization of the building and of the critical areas. Thus requiring a complementary technique capable of solving such weaknesses, UAV and SfM.

4.2. UAV and Structure from Motion

The point-clouds collected by laser scanning do not provide a sufficient amount of data for a full geometric characterization of the outer shell: either the distance from scanner to object the range is too large, the point of view is insufficient or the laser system cannot be placed in a certain location, such as in the upper region of the façade beyond the central cornice.

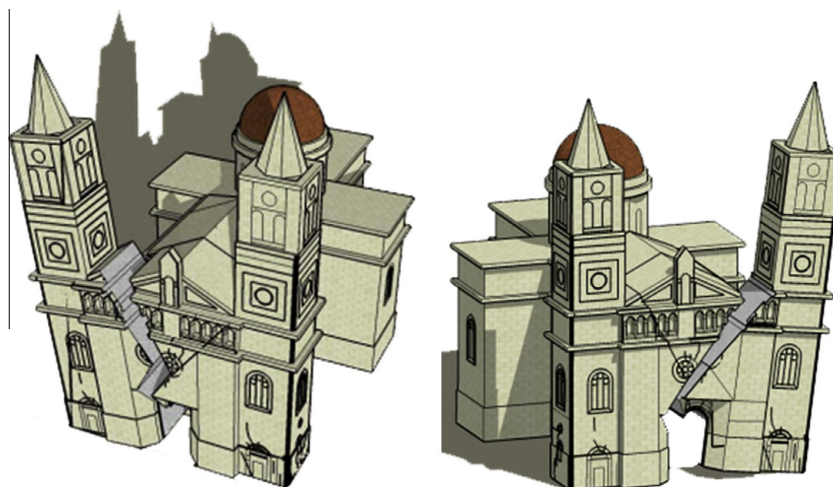


Fig. 5. Representation of the possible structural failure collapse mechanisms of the Church of Saint Torcato. It is possible to observe the formation of two macro-blocks.

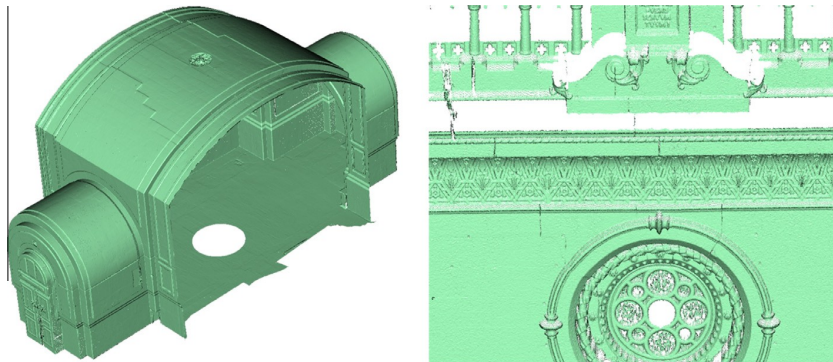


Fig. 6. Settlement of the entrance vault detail (left). Settlement of the entrance vault detail (right).

In addition to the aforementioned, the obliqueness phenomenon must be considered. As shown by authors such as [38,39], this phenomenon is highly correlated with the value of uncertainty in obtaining a point's spatial coordinates. This phenomenon is of great importance in obtaining accurate products and it is highlighted by this case study, where it is critical in certain areas, such as in the inclination of the towers or in the cracking of the central façade.

All this requires a supplementary technology to the laser scanning, this is UAV + SfM; a non-intrusive way of solving the problems described above through its great portability and ability to collect data. Besides, it gathers an extra supply of analyzable features, which makes it possible to get complete point-cloud models, which form the foundation for accurate and thorough CAD models. These models profit from the features obtained from the hybrid point-cloud, such as cracks (Fig. 7).

This model, generated through the described technique, is comprised of a total of 398 photographs taken by UAV platform: (i) 273

photos of the main façade divided in 3 vertical strips (1 for each tower and one for the main façade) and (ii) 125 photos of the cracks on chapels, also divided in 3 vertical strips. Alongside these photographs, 117 additional shots were taken without UAV platform (terrestrial photogrammetry): (i) 85 photos of the arches of the chapels of the main nave and (ii) 32 photos at the level of the Church choir.

Both techniques, terrestrial laser scanner and SfM, complement to each other, and their combination is the ideal solution for restoring built heritage. While the laser scanner provides the system a set of precise, dense and fast capture data with which it is possible to monitor structural movement and generate a CAD model suitable for numerical analysis, the UAV + SfM system combines with it perfectly supplying the geometric data of the areas that were unreachable through the previous system. In addition, it characterizes completely the structure's pathological conditions by obtaining direct and georeferenced data.



Fig. 7. Front elevation of the point cloud obtained through SfM technique and PW software (left). Detailed comparison between the laser scanner point cloud and the one obtained in PW software (right).

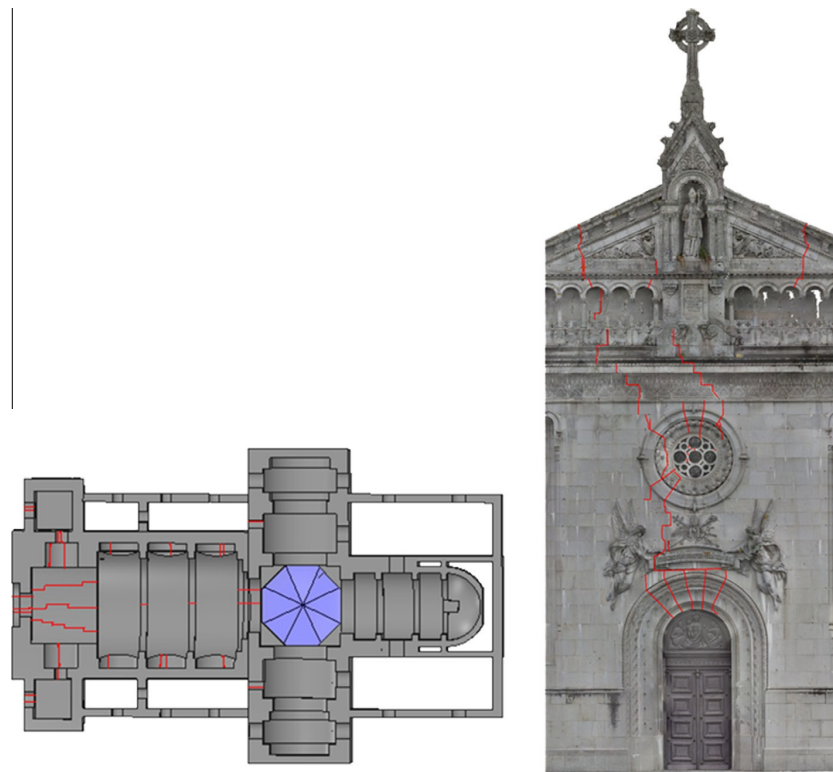


Fig. 8. Results of the inspection for damages: plan view at ground level (left). Main façade orthoimage inspection for damages (central part) (right).

However, the resulting data of both sensor show different coordinate system but the high redundancy allows the creation of a single model applying the methodology explained in Section 3, that finally is converted into a valid CAD model of the building for the subsequent analysis. An average value of 0.0125 with a standard deviation of 0.0065 was found in the coarse registration process. Later, in the fine registration process this values down to 0.0035 with a standard deviation of 0.0011. The final hybrid point cloud had a total of 40,359,060 points (that represents a 10% of the original set).

4.3. Characterization of structural pathologies

The characterization of cracks plays a fundamental role in structure monitoring in terms of stability and safety. Traditionally such monitoring was conducted with graduated cards, mechanical or electronic gauges, or LVDT (linear variable differential transformer). However, this equipment has significant drawbacks [27]: (i) firstly, there is a need for permanent plates, that may become damaged or can be lost, (ii) they provide data only from certain points and certain directions, (iii) the cracking is not directly measured; it is assumed that its activity is correctly defined by the variation of the reference points. In addition to this, some of these methods strongly rely on temperature (this is the case of electronic gauges).

Thanks to the combined use of the shown spatial-data capture techniques, it is possible not only to obtain high density point-clouds and photorealistic textures (this is the case of UAV + SfM system) but also high quality orthoimages in any position and on determined surfaces, thus solving the problems described above. All supplemented with direct product georeferencing, which

makes perfectly viable to monitor the movement of the structure and the evolution of damage that may arise.

The aforementioned methods combined with an accurate numerical model will comprise all the necessary tools for sizing and evaluating the restoration system of the building.

The first damage inspection of the monument [6] was carried out in 1998. The inspection indicated that the façade suffered structural damages, made evident by cracks running from its bottom, in the keystone to the coronation. In addition, pathologies are observed in the entrance dome keystone under the choir, in the arcs are that make up different bays of the main nave and in cracks on the side of the building.

It is on the main facade where the building shows a greater amount of these pathological conditions, spread along as cracking and displacement on elements of arches and vaults (Fig. 8). Fig. 8 results of the inspection for damages: plan view at ground level (left). Main façade orthoimage inspection for damages (right).

4.4. Geometrical CAD model

Made by the proposed methodology, the Saint Torcato CAD model has greater geometric complexity than the one exposed by Lourenço and Ramos [6]. Within this geometric improvement is remarkable a better characterization of the main façade and towers, including architectural details over the balcony and along the towers.

Since most of the façade shows structural pathological conditions, it is therefore expected that the dynamic response of the structure will be influenced in part by such cracking. The high correlation between the CAD model and the actual photogrammetric point cloud allows to incorporate these characteristics into the

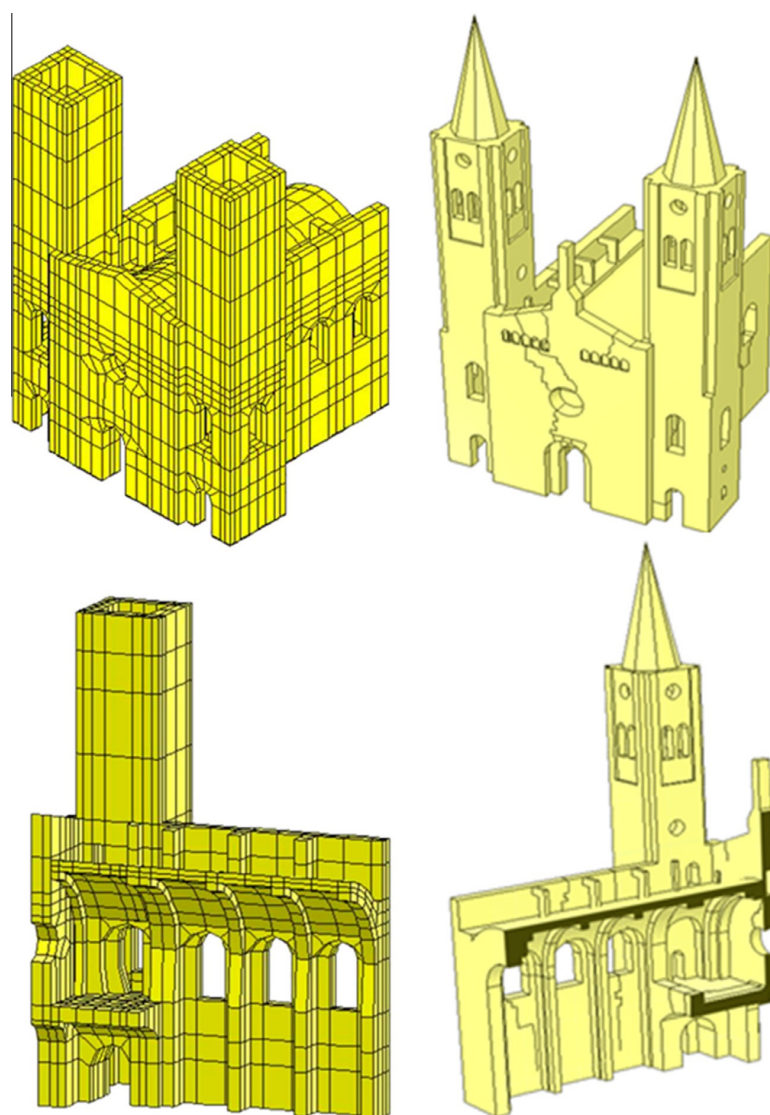


Fig. 9. Isometrics views of the initial geometric model (left) and the one generated by the proposed methodology (right).

CAD model directly, only requiring the meshing of the area under study. Also this model, presents different wall thickness, increasing the model realism (Fig. 9).

4.5. Definition of the numerical calculation model

While the geometric aspect has been completely improved by the methodology presented, the material characterization (homogeneous and isotropic), since at the time no experimental test were carried out, the input loads and boundary conditions remain the same than the initial one. For the loads have been consider: (i) gravitational loads; (ii) truss self-weight and (iii) roof self-weight.

Complementary to this loads conditions, it is necessary to correctly simulate the elastic behavior (Winkler model) of the ground in which the structure stands and also a proper simulation of the behavior of the transept. Such behavior has been emulated through CONTACT173/TARGET170 elements [40].

The discretization of the model has been carried out considering a 4-node isoparametric tetrahedral element (SOLID65) with a maximum size of 0.60 m. In order to increase the robustness of the tetrahedral mesh, element softening has been carried out using Laplace algorithm [40].

All this results in a total of 218,244 discrete elements into the numerical model (212537 SOLID65, 5707 CONTACT173/TARGET170) (Fig. 10).

4.6. Modal analysis, calibration of the numerical model

The next step required to obtain an accurate finite element model is to calibrate their elastic parameters and thus adapt the dynamic behavior of the numerical model to the real one. In order to accurately calibrate the numerical model it is necessary to follow a three-step procedure: (i) initial hypothesis, (ii) manual calibration and (iii) robust calibration. The initial hypothesis considered were: the elastic properties of masonry, the major

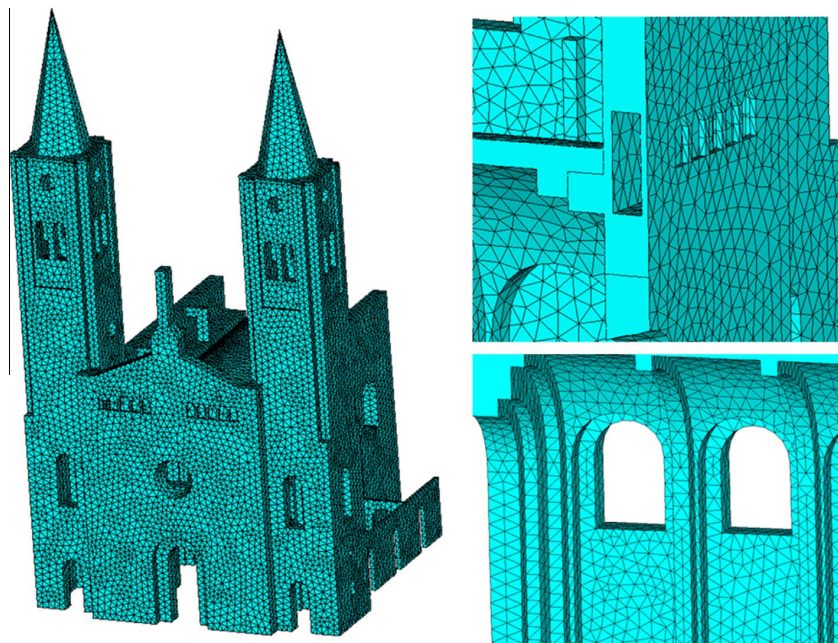


Fig. 10. Isometric view of the mesh model (left). Mesh detail of the balcony and chapels (right).

Table 3
Summary of the adopted values for the calibration of the numerical model.

	Initial values	Lower bound	Upper bound	Updated value
$E_{MASONRY}$ (GPa)	10	5	15	9.19
$\delta_{MASONRY}$ (kg/m ³)	2500	2400	2700	2600
$K_{NFAÇADE}$ (GPa/m)	0.0001	0.00005	0.01	0.0004
$K_{TFAÇADE}$ (GPa/m)	0.1	0.05	1	0.53
$K_{NFIRSTCAP}$ (GPa/m)	1	0.05	5	0.40
K_{NSOIL} (GPa/m)	0.585	0.0585	5.85	0.627
$K_{NTRANSEPT}$ (GPa/m)	0.1	0.005	1	0.29
$K_{TRANSEPT}$ (GPa/m)	0.0001	0.00001	0.01	0.00002

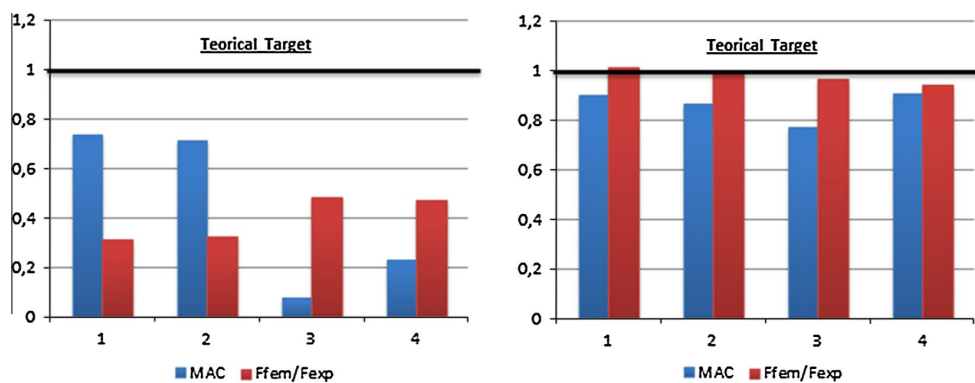


Fig. 11. Comparison between representative values of dynamic response (frequencies and MAC): value ratio of the initial model proposed by Lourenço (left). Ratios obtained with the hereby proposed methodology (right).

cracks on the main façade and the main nave, the elastic behavior of the soil, and the simulation of the connection between the nave and the transept.

Within the manual calibration stage, numerous tests have been required, evaluating separately each of the considered elastic vari-

ables and rejecting those that did not bring improvements to the numerical model. Finally, have been chosen a total of eight parameters, namely: Young modulu's of the masonry ($E_{MASONRY}$) and its density ($\delta_{MASONRY}$), the normal ($K_{NFAÇADE}$) and shear ($K_{TFAÇADE}$) stiffness of the major cracks on the main façade, the normal ($K_{NFIRSTCAP}$)

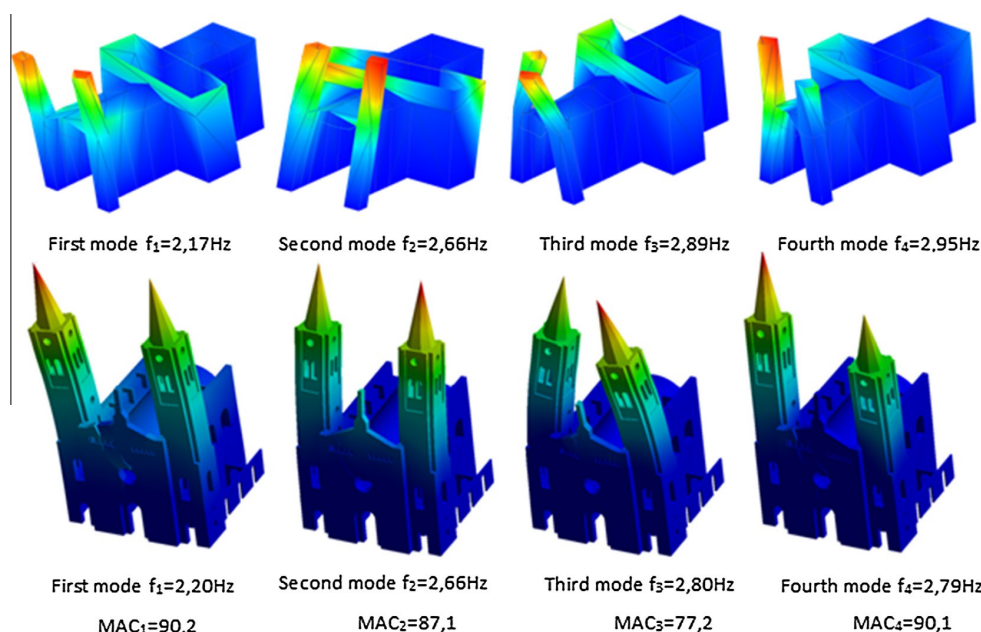


Fig. 12. Comparison between the vibrational model from the OMA and those from the hereby presented finite element numerical model.

stiffness of the major cracks on the main nave, the soil's normal stiffness (K_{NSOIL}), as well as the simulation of the connection between the main nave and the transept through a normal stiffness ($K_{NTRANSEPT}$) and a shear one ($K_{TTRANSEPT}$). During the last step, the accurate calibration of the previously discretized parameters through DR methodology (described above) was required, providing the results presented below (Table 3).

The now calibrated elastic properties of the masonry show a globally damaged material. The high elasticity obtained in the simulation of the transept confirmed that the building, as it progressed, suffered settlements and cracking. However, the rise in rigidity of the elastic properties in comparison to the initially calculated in [6], denote soil compaction. As shown in (Fig. 11) (Fig. 12), the relative ratios between the experimental and numerical frequencies, with a value close to one for the standard MAC indexes denote a high correlation between the experimental dynamic behavior of the building and the numerical one. Through the simulation of the cracks, it was possible to correctly simulate the dynamic behavior and the high existing elasticity in the central area of the building.

5. Conclusions

The methodology presented aims to compile the information from different sensors in order to establish a complete geometric characterization of historic buildings. The combined method for data acquisition solves most common problems encountered today like the preparation of accurate CAD models and the analysis of structure characteristics (displacements and cracking).

Using the laser scanner alone would not solve some of the problems that arise today, i.e. the lack of data in areas that are not accessible to the system or the difficulty of cracking identification. That is why it is essential to incorporate a complementary data capture system able to meet solving problems. The perfect complement for an accurate, quick and complete data capture is the Image Structure from Motion System on UAV platform. Other advantages provided by this second capture system, lies in the potential that

digital image analysis gives to the graphical product. This digital image analysis makes possible to completely characterize cracking (length and opening).

The binomial SfM-laser scanner is a reliable foundation from which to analyze appropriate restoration actions, following the procedure: (i) analysis of the causes through the numerical model (ii) displacement and stress state along the structure (iii) analysis of the effectiveness of the system (analysis of the numerical model including restoration activities, analysis of cracks and collapses systems).

The methodology presented can be applied to other infrastructures, such as tunnels or bridges, given the high versatility of the sensors described and the wide range of possibilities that they offer. All this is complemented by a global dynamic analysis of the structure that allows a reliable calibration of the numerical model through the elastic system variables.

The Saint Torcato Church (Guimarães, Portugal) represents an ideal case study for evaluating the potential of the method developed. Based on the geometric characterization performed through the presented methodology, several research works are taking place, in order to improve the characterization of the different materials by Ground Penetration Radar and Boroscopic Camera, for further FEM analysis.

References

- [1] Ramos LF, Aguiar R, Lourenço PB, Moreira S. Dynamic structural health monitoring of Saint Torcato church. *Mech Syst Signal Process* 2013;35(1–2):1–15.
- [2] Grimm CT. Masonry cracks: a review of the literature 1988:257–80.
- [3] ICOMOS. Recommendations for the analysis, conservation and structural restoration of architectural heritage. In: *International scientific committee for analysis and restoration of structures of architectural heritage*; 2003.
- [4] Vercher J, Gil E, Mas A, Lerma C. Diagnosis/intervention criteria in damaged slabs by severe corrosion of prestressed joists. *J Perform Constr Facil* 2013;45:45.
- [5] Betti M, Vignoli A. Assessment of seismic resistance of a basilica-type church under earthquake loading: modelling and analysis. *Adv Eng Softw* 2008;39(4):258–83.
- [6] Lourenço PB, Ramos LF. Investigaç o sobre as Patologias do Santu rio de S o Torcato. Final Report. University of Minho 1999;99-DEC/E-5.

- [7] Taliercio A, Binda L. The Basilica of San Vitale in Ravenna: investigation on the current structural faults and their mid-term evolution. *J Cult Heritage* 2007;8(2):99–118.
- [8] Armesto J, Roca-Pardiñas J, Lorenzo H, Arias P. Modelling masonry arches shape using terrestrial laser scanning data and nonparametric methods. *Eng Struct* 2010;32(2):607–15.
- [9] Pieraccini M, Dei D, Betti M, Bartoli G, Tucci G, Guardini N. Dynamic identification of historic masonry towers through an expeditious and non-contact approach: application to the “Torre del Mangia” in Siena [Italy]. *J Cult Heritage* 2014;15(3):275–82.
- [10] Riveiro B, Solla M, de Arteaga I, Arias P, Morer P. A novel approach to evaluate masonry arch stability on the basis of limit analysis theory and non-destructive geometric characterization. *Automat Constr* 2013;31:140–8.
- [11] Lubowiecka I, Armesto J, Arias P, Lorenzo H. Historic bridge modelling using laser scanning, ground penetrating radar and finite element methods in the context of structural dynamics. *Eng Struct* 2009;31(11):2667–76.
- [12] Park HS, Lee HM, Adeli H, Lee I. A new approach for health monitoring of structures: terrestrial laser scanning. *Comput-Aided Civ Infrastruct Eng* 2007;22(1):19–30.
- [13] Guidi G, Frischer B, Russo M, Spinetti A, Carosso L, Micoli LL. Three-dimensional acquisition of large and detailed cultural heritage objects. *Mach Vision Appl* 2006;17(6):349–60.
- [14] Yastikli N. Documentation of cultural heritage using digital photogrammetry and laser scanning. *J Cult Heritage* 2007;8(4):423–7.
- [15] Pfeifer N, Briese C. Laser scanning: principles and applications summary. In: *Third international exhibition and scientific congress on geodesy, mapping, geology, geophysics, Novosibirsk, Russia; 2007*.
- [16] Roca D, Lagüela S, Díaz-Vilarifo L, Armesto J, Arias P. Low-cost aerial unit for outdoor inspection of building façades. *Automat Constr* 2013;36:128–35.
- [17] Barazzetti L, Binda L, Scaioni M, Taranto P. Photogrammetric survey of complex geometries with low-cost software: application to the ‘G1’ temple in Myson, Vietnam. *J Cult Heritage* 2011;12(3):253–62.
- [18] TAPEnADE. Case study: Maya bass-relief. Copan (Honduras); 2012.
- [19] Westoby MJ, Brasington J, Glasser NF, Hambrey MJ, Reynolds JM. ‘Structure-from-Motion’ photogrammetry: a low-cost, effective tool for geoscience applications. *Geomorphology* 2012;179:300–14.
- [20] Besl PJ, McKay ND. A method for registration of 3-D shapes. *IEEE Trans Pattern Anal Mach Intell* 1992;14(2):239–56.
- [21] Toldo R, Beinat A, Crosilla F. Global registration of multiple point clouds embedding the generalized procrustes analysis into an ICP framework. *3DPVT 2010 Conference*; 2010.
- [22] Tognaccini R. La Chiesa di Santa Maria del Mar a Barcelona-Dal Rilievo Tridimensionale all’Analisi Strutturale. Pisa, Italy: University of Pisa; 2009.
- [23] Nguyen V-S, Bac A, Daniel M. Simplification of 3D point clouds sampled from elevation surfaces; 2013.
- [24] Varady T. Automatic procedures to create CAD models from measured data. *Comput-Aided Des Appl* 2008;5(5):577–88.
- [25] González-Jorge H, González-Aguilera D, Rodríguez-Gonzálvez P, Arias P. Monitoring biological crusts in civil engineering structures using intensity data from terrestrial laser scanners. *Constr Build Mater* 2012;31:119–28.
- [26] Armesto-González J, Riveiro-Rodríguez B, González-Aguilera D, Rivas-Brea MT. Terrestrial laser scanning intensity data applied to damage detection for historical buildings. *J Archaeol Sci* 2010;37(12):3037–47.
- [27] Barazzetti L, Scaioni M. Crack measurement: development, testing and applications of an automatic image-based algorithm. *ISPRS J Photogramm Remote Sens* 2009;64(3):285–96.
- [28] Lubowiecka I, Arias P, Riveiro B, Solla M. Multidisciplinary approach to the assessment of historic structures based on the case of a masonry bridge in Galicia [Spain]. *Comput Struct* 2011;89(17–18):1615–27.
- [29] Deseignigny MP, DeLuca L, Remondino F. Automated image-based procedures for accurate artifacts 3D modeling and orthoimage generation. *Icomos* 2012;113.
- [30] Friswell MI, Mottershead JE, Ahmadian H. Finite-element model updating using experimental test data: parametrization and regularization. *Philos Trans R Soc Lond Ser A: Math, Phys Eng Sci* 2009;359(1778):169–86.
- [31] Ramos LF, De Roeck G, Lourenço PB, Campos-Costa A. Damage identification on arched masonry structures using ambient and random impact vibrations. *Eng Struct* 2010;32(1):146–62.
- [32] Mottershead JE, Friswell MI. Model updating in structural dynamics: a survey. *J Sound Vib* 1993;167(2):347–75.
- [33] Allemang RJ, Brown DL. A correlation coefficient for modal vector analysis; 1982.
- [34] Gentile C, Saisi A. Ambient vibration testing of historic masonry towers for structural identification and damage assessment. *Constr Build Mater* 2007;21(6):1311–21.
- [35] Douglas BM, Reid WH. Dynamic test and system identification of bridges. *J Struct Div* 1982;108(10):2295–312.
- [36] Scaioni M, Barazzetti L, Brumana R, Cuca B, Fassi F, Prandi F. Rc-Heli and Structure from Motion techniques for the 3-D reconstruction of a Milan dome spire. *ISPRS* 2009. XXXVIII-5/W1.
- [37] Gordon S, Lichti D, Stewart M, Franke J. Structural deformation measurement using terrestrial laser scanners. In: *11th FIG symposium on deformation measurements*. Santorini, Greece; 2003.
- [38] Lichti D, Gordon S. Error propagation in directly georeferenced terrestrial laser scanner points clouds for cultural heritage recording. Athens (Greece): FIG Working Week; 2004.
- [39] Schaefer P, Skaloud J, Landtwing S, Legat K. Accuracy estimation for laser point cloud including scanning geometry. In: *5th International symposium on mobile mapping technology*. Padova (Italy); 2007.
- [40] ANSYS. ANSYS manual sets. USA; 2012.

CAPÍTULO II

EXPERIMENTAL AND NUMERICAL APPROACHES FOR STRUCTURAL ASSESSMENT IN NEW FOOTBRIDGE DESIGNS (SFRSCC-GFPR HYBRID STRUCTURE).

RESUMEN: Dentro del campo de la ingeniería civil, el empleo de métodos numéricos por Elementos Finitos ha adquirido una importancia significativa. Al permitir el uso de dichas simulaciones en la evaluación de estructuras bajo diferentes solicitaciones y condiciones. Sin embargo, dichas simulaciones numéricas requieren de un conocimiento extenso de las propiedades mecánicas de los materiales, daños presentes, uniones y condiciones de contorno actuantes. Por ello, complementario al requisito de ejecutar campañas experimentales que permitan obtener dichas propiedades mecánicas, es necesario disponer de metodologías de calibración capaces de explotar dichos datos.

El presente capítulo, centrará sus esfuerzos en el desarrollo y aplicación de un sistema de calibración Determinístico sobre una pasarela peatonal (constituida por perfiles extruidos de material polímero reforzado con fibra de vidrio y un tablero de hormigón autocompactante reforzado con fibra de acero), la cual presenta daños a lo largo de su tablero. Combinando para ello campañas experimentales (estáticas y dinámicas). La evaluación de los daños presentes fue materializada mediante un procedimiento híbrido, que emplea funciones de daño discretas y un sistema de subestructuración, compuesto por un sistema de funciones lineales de daños.

A raíz de los resultados arrojados, es posible concluir la potencialidad ofrecida por las funciones de daño definidas. Aún en situaciones desfavorables donde la ausencia de un modelo sin daños imposibilita el análisis de daños por ciertos índices (ausencia de un modelo base o de referencia).

Los resultados arrojados por la calibración mixta (estática y dinámica) del modelo muestran una buena precisión en los resultados numéricos, sin olvidar la correcta localización de los daños presentes en el tablero.

Palabras clave: Perfiles extruidos GFPR; Campaña experimental; Análisis Operacional Modal; Calibración de modelos por Elementos Finitos, Identificación de daños; Estructuras civiles.



ELSEVIER

Contents lists available at ScienceDirect

Composite Structures

journal homepage: www.elsevier.com/locate/compstruct

Experimental and numerical approaches for structural assessment in new footbridge designs (SFRSCC–GFRP hybrid structure)



Luis Javier Sánchez-Aparicio^{a,*}, Luís F. Ramos^{b,1}, José Sena-Cruz^{b,1}, Joaquim O. Barros^{b,1}, Belén Riveiro^{c,2}

^a Department of Land and Cartographic Engineering, University of Salamanca, High Polytechnic School of Avila, Hornos Caleros, 50, 05003 Avila, Spain

^b ISESE, Department of Civil Engineering, University of Minho, Guimarães, Portugal

^c Department of Material Engineering, Applied Mechanics and Construction, School of Industrial Engineering, University of Vigo, Vigo, Spain

ARTICLE INFO

Article history:

Available online 20 July 2015

Keywords:

GFRP pultruded profiles
Experimental tests
Operational Modal Analysis
Finite Element Model Updating
Damage identification
Civil structures

ABSTRACT

Within the civil engineering field, the use of the Finite Element Method has acquired a significant importance, since numerical simulations have been employed in a broad field, which encloses the design, analysis and prediction of the structural behaviour of constructions and infrastructures. Nevertheless, these mathematical simulations can only be useful if all the mechanical properties of the materials, boundary conditions and damages are properly modelled. Therefore, it is required not only experimental data (static and/or dynamic tests) to provide references parameters, but also robust calibration methods able to model damage or other special structural conditions. The present paper addresses the model calibration of a footbridge bridge tested with static loads and ambient vibrations. Damage assessment was also carried out based on a hybrid numerical procedure, which combines discrete damage functions with sets of piecewise linear damage functions. Results from the model calibration shows that the model reproduces with good accuracy the experimental behaviour of the bridge.

© 2015 Elsevier Ltd. All rights reserved.

1. Introduction

In the last few years, new civil engineering designs have emerged in the field of the construction of footbridges, considering new materials [1,2] and constructive [3–5] solutions. Within these new materials, have received special attention the use of fiber reinforced polymer (FRP) and glass fiber reinforced polymer (GFRP), offering better resistance to environmental agents and the advantages of high stiffness-to-weight and strength-to-weight ratios when compared to conventional construction materials [6,7]. They also can be combined with traditional materials, like concrete or steel, offering particularly effective flexural properties [8–10]. These hybrid structures are particularly suitable for footbridge structures thanks to the possibility of an easy and quick erection.

However, several characteristics restrict the use of this type of materials: (i) high deformability (low elastic and shear modulus); (ii) brittle failure; (iii) behaviour at elevated temperatures; and (iv) lack of specific design codes [11]. Due to the small service loads, these structures usually are light and slender. For these reason the interaction with pedestrians or wind can arise some structural problems [12,13]. Considering the mentioned above, several tests are needed in order to assess the structural behaviour of these structures in different scenarios. The diversity of materials and the interaction between them makes the Finite Element Methods (FEM) as the most feasible solution to evaluate and simulate these structures.

In contrast with the potentialities that the FEM can offer, some choices (mechanical properties of the materials or structural conditions) may give erroneous numerical results. Within this context, this paper attempts to demonstrate a methodology to evaluate, through experimental tests and robust numerical calibration strategies, the structural behaviour of a pedestrian bridge prototype. The bridge was experimentally tested with several static and dynamic tests and with the main results, a model calibration was performed to tune the mechanical parameters.

In order to obtain a robust finite element model, which represent accurately the structural behaviour of the footbridge a

Abbreviations: GFRP, Glass Fibre Reinforced Polymer; SFRSCC, Steel Fibre Reinforced Self-Compacting Concrete; FEM, Finite Element Method; FEMU, Finite Element Model Updating; MAC, Modal Assurance Criterion.

* Corresponding author. Tel.: +34 920353500; fax: +34 920353501.

E-mail addresses: luisj@usa.es (L.J. Sánchez-Aparicio), ramos@civil.uminho.pt (L.F. Ramos), jsena@civil.uminho.pt (J. Sena-Cruz), barros@civil.uminho.pt (J.O. Barros), belenriveiro@uvigo.es (B. Riveiro).

¹ Tel.: +351 253510200; fax: +351 253510217.

² Tel.: +34 1 986814052; fax: +34 986811924.

<http://dx.doi.org/10.1016/j.compstruct.2015.07.041>
0263-8223/© 2015 Elsevier Ltd. All rights reserved.

damage assessment was carried out, based on a hybrid numerical procedure, which combines discrete damage functions with sets of piecewise linear functions to evaluate the damage present at the structure. Special attention was paid to the influence of the supports, the interaction between structural components and the damage response of the SFRSCC deck.

This paper is organized as follows: Section 1 is the introduction; Section 2 a general structural description of the hybrid footbridge is presented; Section 3 presents the static and dynamic tests performed on the footbridge; Section 4 a robust dynamical-static calibration process is carried out; and finally in the Section 5 the conclusion are drawn.

2. GFRP–SFRSCC hybrid footbridge

2.1. Description of the structure

The studied prototype at full scale was developed in the framework of research project PONTALUMIS – Development of a prototype of a pedestrian bridge in GFRP-ECC, involving ICIST/Instituto Superior Técnico, ISISE/University of Minho and company ALTO – Perfis Pultrudidos, Lda. The footbridge design was carried out considering the main potentialities of the used materials. Therefore, the composite Steel Fiber Reinforced Self-Compacting Concrete (SFRSCC) material was placed in zones where compressive stresses exist, whereas GFRP girders were used to carry the tensile stresses. The cross section of the bridge is characterized by the following: (i) a SFRSCC deck; (ii) SFRSCC jackets placed in the vicinity of the supports; and (iii) GFRP girders (Fig. 1).

The connection between the structural components (SFRSCC deck and GFRP pultruded girders) was made through two different solutions: (i) for the contact areas located above the jackets an epoxy resin layer with 2 mm of thickness was used; and (ii) for the remaining contact zones the same adhesive solution was used in combination with a redundant mechanical connection based on M10 stainless steel bolts, with 300 mm of spacing (two per main girder's flange), in order to extend the bridge life time due to rheological effects, vandalism and accidental loads.

Complementary to the previous structure, a group of secondary girders were placed between the main ones. This solution prevents any distortion caused by eccentric loads. Positioned at the support, quarterspan and midspan sections, this profiles were constituted by I-shaped ($200 \times 100 \text{ mm}^2$) GFRP pultruded profiles and connected to the main girders by means of equal length angle GFRP ($60 \times 8 \text{ mm}^2$) profiles and stainless steel bolts (M10) threaded rods and nuts.

The footbridge structure presents a total length of 11.00 m on two pairs of supports (two pinned and two sliding), as show (Fig. 2). More details can be found elsewhere [11].

2.2. Mechanical properties of the footbridge components

Made by E-glass fiber rovings and mats embedded in a isophthalic polyester, the main and secondary pultruded profiles have been characterized by the following tests [11]: (i) tension (EN ISO 527) [14]; (ii) compression (ASTM D 695) [15]; and (iii) shear test (10° off-axis tension test), according to the recommendations of Hodgkinson [16]. Allowing the evaluation of several material mechanical properties, namely: (i) longitudinal elasticity modulus in tension ($E_{L,t}$); (ii) transverse elasticity modulus in compression ($E_{T,c}$); (iii) in-plane shear modulus (G_{LT}); (iv) longitudinal tensile strength ($f_{tu,L}$); and (v) in-plane shear strength ($T_{u,LT}$). These properties are summarized in Table 1.

For the SFRSCC material, a specific mixture composition was used (details about the mix design are available in [17]: (i) cement;

(ii) limestone filler; (iii) water; (iv) superplasticizer; (v) fine sand; (vi) river sand; (vii) crushed stone; and (viii) fibers. The compressive strength and flexural properties of the SFRSCC were assessed according to standards NP EN 12390-3 [18] and RILEM TC 162-TDF, respectively [19], providing the following mechanical information: (i) Young's modulus; (ii) compressive strength (f_{cm}); (iii) cracking strength in flexure ($f_{cr,L}$); (iv) equivalent flexural tensile strengths ($f_{eq,2}$ and $f_{eq,3}$); and (v) residual flexural tensile strengths ($f_{R,1}$ to $f_{R,4}$) (see Table 2).

The epoxy adhesive used to bond the main girders to the SFRSCC deck has an elasticity modulus in tension of $E_a = 8.8 \text{ GPa}$ and a tensile strength of $f_{au} = 17.3 \text{ MPa}$ [20]. The redundant mechanical connection into the span between jackets was materialized by stainless steel anchors (M10 \times 55). This solution present a bearing capacity of $f_{bk} = 700 \text{ MPa}$ (according to the manufacturer). For the present study case, three different types of connections had been considered: (i) epoxy layer; (ii) epoxy layer and bolt; and (iii) bolt L-union between secondary and main girders. This connection were materialized through interface elements, considering the mechanical properties obtained in the different experimental program carried out (Table 3).

3. Experimental programs

3.1. Static test

In order to ensure the correct erection, disposition and performance of the different structural elements in the footbridge several static tests were performed [11]. These experimental tests were mainly focused on the characterization of the bending response of the footbridge, as well as the deformation recovery after unloading. For this purpose, the footbridge was loaded with multiple close-spaced water reservoirs, with a total weight of 8.8 kN/m^2 . These reservoirs were placed in different uniformly and distributed configurations (load case A–C, see Table 4). All the loading and unloading operations were performed as fast as possible in order to minimize creep effects on the concrete. As a result, three load configuration (A–C) were evaluated: (i) load distributed on the entire span with a width of 1.20 m; (ii) load in the central part of the span with a length of about 2.70 m and a small gap of 0.30 m in the vicinity of midspan; and (iii) load in the central part of the span with a length of 5.10 m and a small gap of 0.30 m in the vicinity. In order to evaluate the different load setups, different sensors were placed along the footbridge: (i) electrical transducers (with a precision of 0.01 mm); and (ii) axial strains electric strain gauges (Fig. 3).

As results of the static tests (see Table 4 and Fig. 3), the acquired data was distributed into five groups, namely: (i) midspan deflection ($\delta_{ms,Avg}$); (ii) axial strains on the SFRSCC deck ($\varepsilon_{c,Avg}$); (iii) axial strains on the web of the main girders ($\varepsilon_{w,Avg}$); (iv) axial strains on the bottom flanges of the main girders ($\varepsilon_{c,Avg}$); and (v) curvature at midspan (ζ).

3.2. Dynamical identification test

A dynamical identification campaign, based on the Operational Modal Analysis (OMA) approach, was performed with the aim of identifying the modal properties of the structure. With a sensitivity of 10 V/g , range of $\pm 0.5 \text{ g}$, and $8 \mu\text{g rms}$ broadband resolution, a total of eighteen uniaxial piezoelectric accelerometers were place on different locations on the vertical direction (Fig. 4).

By using Enhanced Frequency Domain Decomposition (EFDD) technique [22] each mode is estimated as a decomposition of the system's response spectral densities into several single degree of freedom systems.

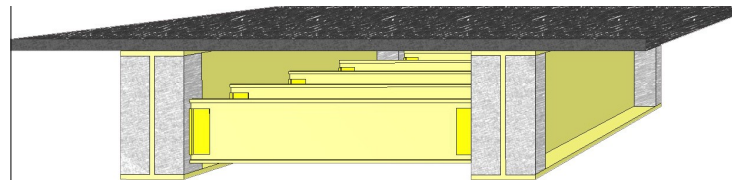


Fig. 1. Isometric view of the footbridge (in dark-grey the SFRSCC concrete, in light-grey the SFRSCC jackets and in yellow the GFRP profiles). (For interpretation of the references to colour in this figure legend, the reader is referred to the web version of this article.)

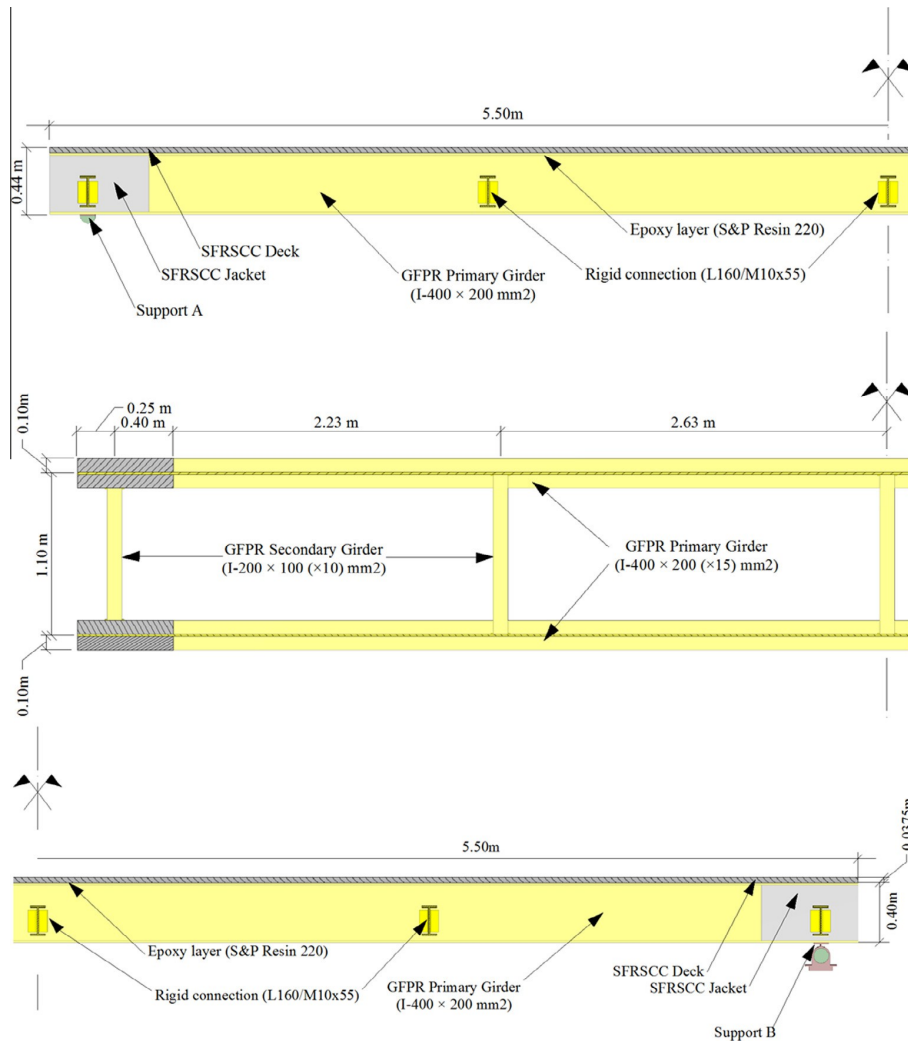


Fig. 2. Section views of the SFRSCC–GFRP footbridge (units in meters). Longitudinal sections (above and middle). Transversal view (below).

Table 1
Mechanical properties of the GFRP pultruded profiles [11].

Part	E_{Lc} (GPa)	E_{Tc} (GPa)	G_{LT} (GPa)	f_{uL} (MPa)	T_{uLT} (MPa)	p (kN/m ³)
GFRP web	23.98 ± 1.61	4.55 ± 0.52	3.49 ± 0.43	278.90 ± 23.78	20.42 ± 1.15	18.00
GFRP flange	35.71 ± 1.83	3.57 ± 0.36	–	336.94 ± 37.51	–	18.00

Table 2
Mechanical properties of the SFRSCC material used [11].

$E_{c,28}$ (GPa)	f_{cm} (MPa)	$f_{ct,L}$ (MPa)	$f_{eq,2}$ (MPa)	$f_{eq,3}$ (MPa)	$f_{R,1}$ (MPa)	$f_{R,2}$ (MPa)	$f_{R,3}$ (MPa)	p (kg/m ³)
37.75 ± 1.3	75.95 ± 10.0	6.21 ± 1.2	10.42 ± 2.4	10.56 ± 2.4	10.17 ± 2.1	10.27 ± 2.34	9.71 ± 2.34	2325.78

Table 3
Mechanical properties obtained in the experimental program [21].

Variable	Epoxy layer	Epoxy layer and bolts	Bolt union
K (N/m ³) × 10 ⁶	288.55 ± 59.75	300.57 ± 71.79	140.02 ± 9.63

A total of 16 vibration modes were identified. It is noted that, in this modal identification, several modal shapes present an asymmetric behaviour. This phenomenon can be attributed to the presence of damage in the structure especially in the first and fourth quarterspan (Fig. 5).

Following this antisymmetric behaviour in the different vibration modes, a visual inspection was carried out. Some micro-cracks on the SFRSCC deck were detected, the average value of the crack width being about 0.06 mm, in the vicinity of the quarterspans and an isolate crack in the midspan, with an average value of 1.5 mm (Fig. 6).

4. Finite element updating strategy

4.1. Numerical model of the footbridge

In order to simulate the structural (static and dynamic) behaviour of the footbridge a tridimensional FE model was built using the commercial software TNO Diana [23]. With a total of 24,334 elements high-order elements (CHX60) [23], with 10 cm as the maximum dimension (Fig. 7). For the epoxy connections (main girder-deck and secondary girder-primary girder) interfaces elements were chosen, avoiding the use of highly distorted solid elements, since the width of these connections are about 2 mm. As a result, 3,240 interface elements (Q24IF) were used.

The numerical model includes the following structural components: (i) GFRP main girders; (ii) GFRP secondary girders; (iii) bolted connections with a GFRP L union; (iv) SFRSCC deck; (v) SFRSCC jackets; (vi) epoxy-bolt layer; and (vii) epoxy layer. All the structure is supported by two groups of pinned supports (in the left side) and other two groups of sliding supports (right side). Both supports are modelled by 88 spring elements in the main directions (SP2TR).

Finally, the material properties (mean and deviation values) obtained by the different tests carried out (see Tables 1–3), were consider for the FE model. Also a perfect normal bond was assumed at the GFRP-epoxy and SFRSCC-epoxy interfaces, consider only the interface stiffness [1].

4.2. Cost function and optimization algorithm

Finite Element Model Updating (FEMU) strategy can be employed in a wide range of applications [24–26]: (i) design; (ii) simulation; (iii) prediction; and (iv) damage identification. In this

Table 4
Static test results for the three different load configurations [11].

Setup	$\delta_{ms,Avg}$ (mm)	$\epsilon_{c,Avg}$ (µm/m)	$\epsilon_{w,Avg}$ (µm/m)	$\epsilon_{f,Avg}$ (µm/m)	ζ (10 ⁴ m ⁻¹)
A (along the entire span)	38.07	–190	320	1102	30.6
B (central part of the span)	23.27	–145	220	712	20.3
C (central part of the span)	43.28	–252	392	1208	34.6

context, several approaches can be carried out [27]: (i) Deterministic approaches; (ii) Bayesian finite element strategies; and (iii) Fuzzy approaches.

For the present study case, a deterministic strategy was followed. The success of this approach is based on minimizing the residual vector (r) of the objective function (J), considering the data derived from the experimental campaigns, defined by the Eq. (1).

$$r = \frac{1}{2} \left\| \begin{matrix} J^{sta} \\ J^{din} \end{matrix} \right\|^2 \quad (1)$$

where $\|\bullet\|$ denotes the Euclidean norm, r is the residual vector of J^{sta} and J^{din} (static and dynamic residuals, respectively). The objective function terms ($J = J^{sta} + J^{din}$) are given by:

$$J^{sta} = \frac{1}{2} W_\delta \sum_{j=1}^m \left(\frac{\delta_j^{num} - \delta_j^{exp}}{\delta_j^{exp}} \right)^2 \quad (2)$$

$$J^{din} = \frac{1}{2} \left[W_f \sum_{i=1}^m \left(\frac{f_i^{num} - f_i^{exp}}{f_i^{exp}} \right)^2 + W_\phi \sum_{i=1}^m \left(\phi_i^{num} - \frac{\phi_i^{exp}}{|\phi_{ref}^{exp}|} \right)^2 \right] \quad (3)$$

where W_f , W_ϕ , and W_δ are the weights considered for the frequency, vibration modes and static displacements, respectively, f is the frequency, ϕ the modal displacements, δ the static displacements, and ϕ_{ref} is a scaling factor (normalization) that enable a comparison between the experimental and numerical modes displacements. For the dynamic functions (J^{din}) the i index indicates the mode shape and for the static one (J^{sta}) the j index indicates the load case.

Generally, the residuals values (r) of the objective function (J) to be minimized shows a non-linear relation with the unknowns. For these purpose a non-linear least squares function was used to solve the problem. Inside this non-linear least squares framework the Trust Region Reflective iterative algorithm was employed. In each iteration, the search area is reduced to a zone known as "trust region" [28]. Finally, the objective function (J) was approximated to a quadratic minimizer by the truncated Taylor series.

As exposed in [27], the gradient-based optimizations method, in our case the Gauss–Newton approach with the Trust Region Reflective algorithm, requires the computation of the Jacobian (or sensitivity matrix) and Hessian matrix. Both matrix can be solved following a special structure integrated into the least squares problem Eqs. (4) and (5).

$$\nabla J(\theta) = \sum_{i=1}^m r_i(\theta) \nabla r_i(\theta) = Jacob(\theta)^T r(\theta) \quad (4)$$

$$\begin{aligned} \nabla^2 J(\theta) &= Jacob(\theta)^T Jacob(\theta) + \sum_{i=1}^m r_i(\theta) \nabla^2 r_i(\theta) \\ &\cong Jacob(\theta)^T Jacob(\theta) \end{aligned} \quad (5)$$

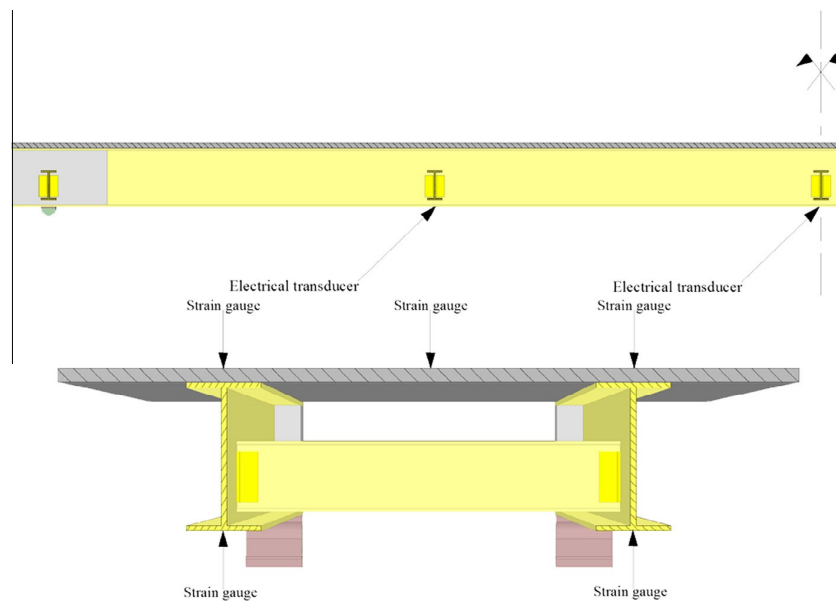


Fig. 3. Cross-section of the footbridge: Longitudinal cross-section, with the electrical transducers (above). Transversal cross-section, at mid-span, with the strain gauges sensors (below).

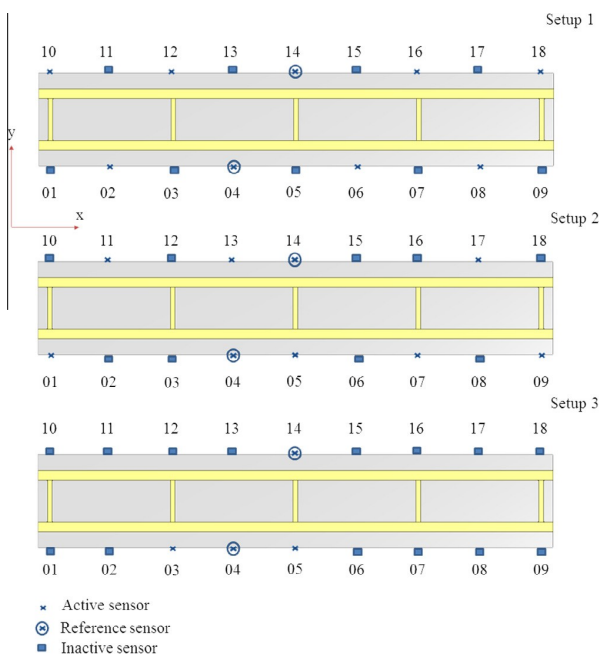


Fig. 4. Modal identification test: accelerometers positions and test setups.

where $Jacob$ is the Jacobian matrix, r the vector which contains the residuals, θ the different variables that will be optimized, ∇J is the first derivative of the objective function and $\nabla^2 J$ the second one. The index n indicates the number of unknowns consider during the optimization.

Aiming at avoiding unrealistic results, boundary constraints were applied to the updating parameters, based on the deviation values obtained in the different mechanical test (see Tables 1–3) and other values provided in literature [13,20,21]. With respect

to the model updating, only the first six vibration modes were considered (see Table 5).

4.3. Robust model updating

Given the complexity of the structure, several calibration stages were considered, namely: (i) initial model updating; (ii) support stiffness model updating; and (iii) damaged model updating. As model robustness indicators for results quality check, the following quantities were used: (i) relative error between frequencies; (ii) modal assurance criterion [29]; and (iii) relative error between displacements for the different load cases.

In the first stage, on the initial model updating only the Young's modulus of the main materials (SFRSCC deck, pultruded profiles flanges and webs) and the stiffness of the different epoxy solutions (with and without bolt redundancies, see Section 2.2) were calibrated (see Table 6). It should be stressed that, for the pultruded profile material and given its orthotropic behaviour, in order to reduce the number of updating variables a constant relation between longitudinal and transversal Young's modulus was

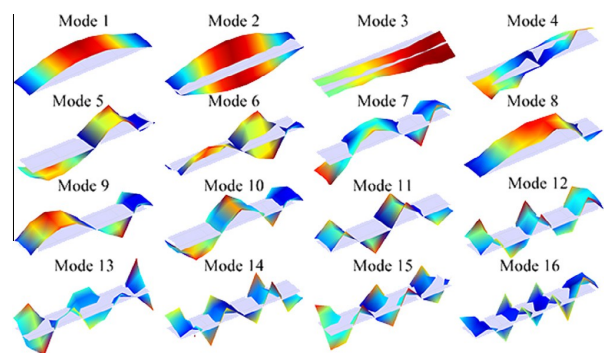


Fig. 5. Results of the 16 modes obtained from the Operational Modal Analysis campaign (the x axis was consider along the longitudinal direction, the y along the transversal and z along the orthogonal direction) [11].

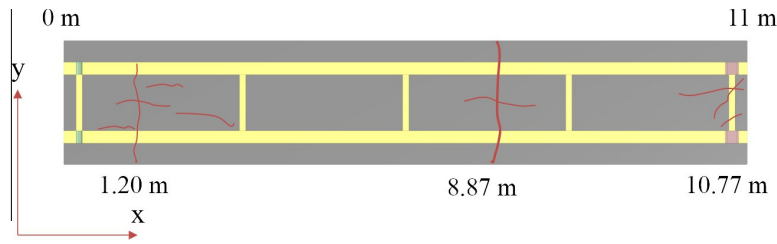


Fig. 6. Damage inspection on the footbridge (cracks are in red color). (For interpretation of the references to colour in this figure legend, the reader is referred to the web version of this article.)

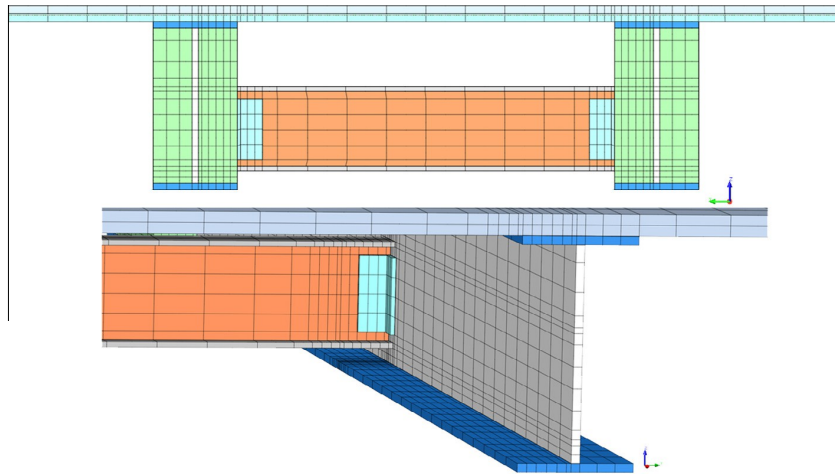


Fig. 7. Front view of the mesh model (above). Mesh detail of the inner part (below).

Table 5
Results values from the Enhanced Frequency Domain Decomposition.

Mode shape	Frequency		Damping ratio		Description
	Mean value (Hz)	CoV (%)	Mean value (Hz)	CoV (%)	
1	6.40	0.28	1.89	18.69	1st Vertical bending mode
2	8.16	0.01	1.26	11.77	1st Lateral Torsional mode
3	12.13	0.63	1.96	16.28	1st Lateral bending mode
4	20.78	12.28	1.57	62.08	2nd Torsional mode
5	22.16	6.14	0.92	20.59	2nd Vertical bending mode
6	23.74	0.09	0.76	11.65	3rd Torsional mode

Table 6
Results of the initial model robust calibration.

	Initial values	Lower bound	Upper bound	Updated values
E_{SPRSCC} (GPa)	37.75	33.82	41.68	39.90
$E_{GFPR-FLAN}$ (GPa)	35.71	30.22	41.20	41.12
$E_{GFPR-WEB}$ (GPa)	23.98	19.15	28.81	28.80
K_{EPOXY} (N/m ³)	14.43×10^{10}	5.53×10^{10}	23.33×10^{10}	17.3×10^{10}
$K_{EPOXY-BOLT}$ (N/m ³)	15.03×10^{10}	4.27×10^{10}	25.79×10^{10}	25.2×10^{10}

established ($E_{L,t}/E_{t,c}$): (i) 5.27 for the GFPR webs; and (ii) 10.00 for the GFPR flanges. This relation was considered in the different calibration procedures.

Following the results obtained in Table 4 with above considerations, the model has high static and dynamic deviations with an average error in frequencies and displacement of 33.06% and 55.04%, respectively (see Tables 7 and 8). Also, the third mode shape was not identified numerically.

Taking into account the previously results, it follows that the structural consideration of the initial model do not fit with the real behaviour of the footbridge (high structural stiffness). As a subsequent calibration, the footbridge supports were modelled with a different approach. Elastic springs in the main directions of both supports were considered, and subsequently a sensitivity analysis was performed, taking into account the initial values proposed by [13]. The results obtained in this analysis shows that the elastic springs are extremely sensitive, especially in the x and y direction. The same initial values and bounds have been considered for the elastic modulus, obtaining the presented in Table 9.

Analyzing the results obtained in terms of quality index (Figs. 8 and 9), an average relative error of 3.5% (relative error between frequencies) was obtained. Additionally, an average MAC value of

Table 7
Summary of the dynamical results obtained with the initial considerations, in terms of relative error in frequencies and MAC values.

Vibration mode	f_{exp} (Hz)	f_{num} (Hz)	Error (%)	MAC (%)
1	6.40	10.69	67.05	98
2	8.16	10.80	32.39	99
3	12.13	-	-	-
4	20.79	20.04	-3.59	82
5	22.16	25.86	16.70	89
6	23.74	27.09	14.10	88

Table 8

Summary of the results obtained in the initial model, through the static correlation values considered (relative error in displacement).

Load case	$disp_{exp}$ (mm)	$disp_{num}$ (mm)	Error (%)
A	-38.07	-16.08	-57.77
B	-23.27	-11.29	-51.50
C	-43.28	-19.10	-55.86

Table 9

Results obtained in the robust calibration of the spring model.

	Initial values	Lower bound	Upper bound	Update values
E_{SPRSCC} (GPa)	37.75	33.82	41.68	34.10
$E_{CFRP-FLAN}$ (GPa)	35.71	30.22	41.20	38.94
$E_{CFRP-WEB}$ (GPa)	23.98	19.15	28.81	28.81
E_{EPOXY} (N/mm ²)	14.43×10^{10}	5.53×10^{10}	23.33×10^{10}	9.72×10^{10}
$E_{EPOXY-BOLT}$ (N/m ²)	15.03×10^{10}	4.27×10^{10}	25.79×10^{10}	21.52×10^{10}
K_{Ax} (N/m)	10.00×10^6	10.00×10^5	10.00×10^7	4.37×10^6
K_{Ay} (N/m)	10.00×10^5	10.00×10^4	10.00×10^6	8.78×10^5
K_{Bx} (N/m)	10.00×10^3	10.00×10^2	10.00×10^5	1.69×10^4
K_{Bz} (N/m)	10.00×10^5	10.00×10^4	10.00×10^6	4.24×10^5

92.0% (with a minimum value of 86% in the sixth mode) was obtained and an average displacement relative error of 5.0%. Therefore, it can be stressed that the results obtained by the second model are more accurate compared with the previous one. But from the obtained results (the different modal shapes and error in frequencies) it is observable that the different modes considered

have negative and positive frequencies errors. Said phenomena indicates a wrong relation between stiffness of the different structural parts, and also burden the model calibration (Fig. 8).

Evaluating more in depth the different measurement points through the COMAC index (Co-ordinate Modal Assurance Criterion) [30] as a damage indicator (see Fig. 9), large discrepancies can be observed at different points (2, 9, 11 and 18), whose origin can be attributed to the structural damage (Fig. 6).

Considering the exposed above, it is expected that trough appropriate damage identification and quantification the results will improve. From the damage inspection previously showed (Fig. 6), it is possible to conclude that mainly three areas can be improved with the damage calibration (the vicinity of first and fourth quarter-spans with a generalize damage) and the third quarter-span (due to the presence of an isolate crack).

4.4. Damage function

Based on the classification defined by [31], four levels of damage assessment can be established: (i) level 1 or Detection; (ii) level 2 or Localization; (iii) level 3 or Assessment; and (iv) level 4 or Prediction of the remaining service life. The FEMU strategy allows a damage assessment up to level 3. This implies that this model-based approach is able of detecting, locating and quantifying the damage acting on the structure. Such potential is related to the understanding of damage in the structure. When the structure suffers damage it implies a degradation of the mechanical properties which can be simulated by the decrease of stiffness of the surrounding elements in the said area. The calibration of this structure, as well as the damage identification and extension, can

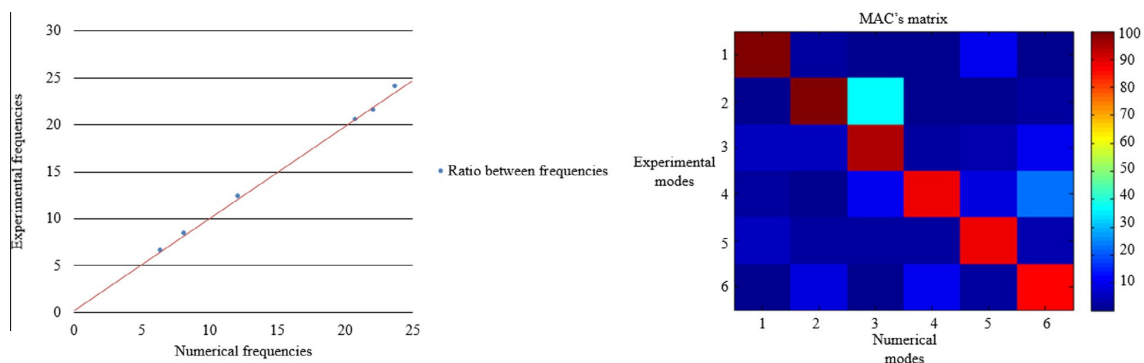


Fig. 8. Frequency pair between spring model updated and OMA (left). MAC matrix with the first six modes (right).

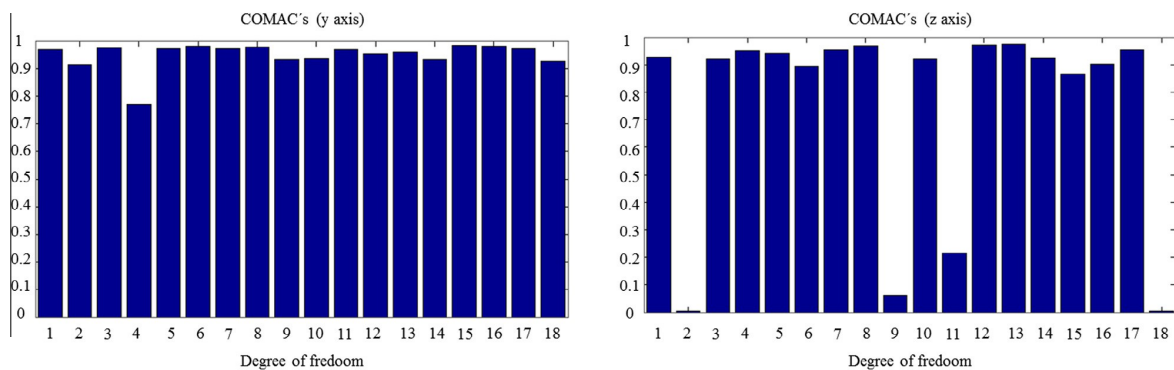


Fig. 9. COMAC values obtained in the spring model updating: COMAC values in y direction (left) and COMAC values in z direction (right).

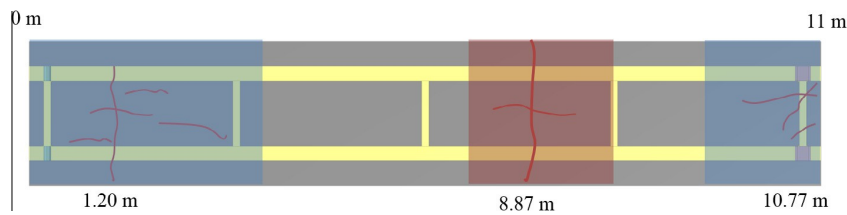


Fig. 10. Schematic representation of the damage identification strategies employed during the robust model updating. In blue the areas with substructure damage functions and in red the area with a discrete damage function. (For interpretation of the references to colour in this figure legend, the reader is referred to the web version of this article.)

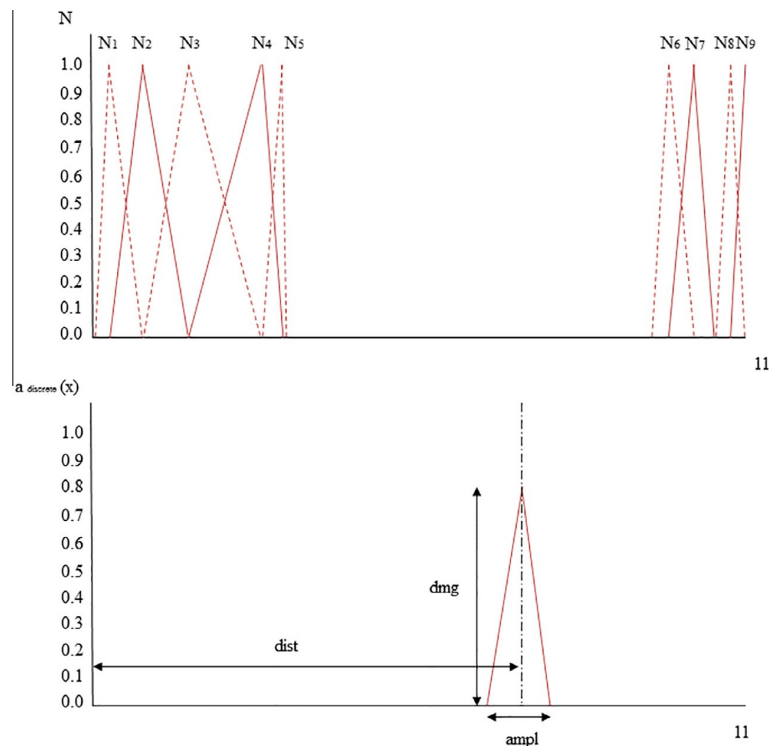


Fig. 11. Different shape functions used during the robust model updating. Substructure damage functions (above). Discrete damage function (below).

be made through the adjustment of the mechanical properties of the different elements affected by this damage.

However, adjusting the stiffness of all elements results in a large number of variables to be tuned, leading to an ill-conditioned problem that can be minimized through different approaches. One approach is the regularization technique [32]. Nevertheless, two drawbacks must be considered. On the one hand, as exposed above, evaluate the function sensitivity implies assessing the sensitivity of each variable, which results in a time consuming solution. On the other hand, less “real” results obtained by the updating of each element (non-continuous damage assumption) are obtained.

In order to solve these drawbacks, the damage quantification can be made through three different approaches: (i) discrete approach that considers the crack as a macroblock splitter through interface elements [33]; (ii) diffused approach that considers a degradation zone [25] on the surroundings of the damage area; and (iii) sub-structuring the model and applying damage functions [24,27].

Generally, the third approach could be applied successfully in different structures [32], but in contrast with the procedure showed in this updating analysis, a reference undamaged model is not available.

For these purpose, a twofold methodology was applied: (i) sensitivity analysis, maintaining the variables previously obtained, of the different damage areas through different FE bands along the damage quarter-spans; and (ii) applying a damage strategy, with different damage functions assumptions, to materialize the damage present in the structure (Fig. 10).

For the present case of study and considering the damage inspection (see Fig. 6), and the COMAC’s values (see Fig. 9), an adaptation of the second and third approach was used (Fig. 10): sub-structuring technique with piecewise linear functions show in Eq. (6) for the first and fourth quarter spans (with a general damage), and a discrete damage shape function for the isolate crack shown in Eq. (7) (see Fig. 11).

Table 10
Summary of the updated variables (without consider the damage variables) obtained in the damage model calibration.

	Initial values	Lower bound	Upper bound	Update values
E_{SPRSCC} (GPa)	37.75	33.82	41.68	39.66
$E_{GFRP-FLAN}$ (GPa)	35.71	30.22	41.20	39.29
$E_{GFRP-WEB}$ (GPa)	23.98	19.15	28.81	28.81
E_{EPOXY} (N/m ²)	14.43×10^{10}	5.53×10^{10}	23.33×10^{10}	9.49×10^{10}
$E_{EPOXY-BOLT}$ (N/m ²)	15.03×10^{10}	4.27×10^{10}	25.79×10^{10}	13.13×10^{10}
K_{Ax} (N/m)	10×10^6	10×10^5	10×10^7	4.77×10^6
K_{Ay} (N/m)	10×10^5	10×10^4	10×10^6	8.98×10^5
K_{Bx} (N/m)	10×10^5	10×10^2	10×10^5	1.44×10^4
K_{By} (N/m)	10×10^5	10×10^4	10×10^6	4.77×10^5

$$N_{substructure,i} = \begin{cases} \frac{x-x_{i-1}}{x_i-x_{i-1}} & x \in [x_{i-1}, x_i] \\ \frac{x_{i+1}-x}{x_{i+1}-x_i} & x \in [x_i, x_{i+1}] \\ 0 & otherwise \end{cases} \quad (6)$$

$$a_{discrete}(dmg, dist, ampl) = \begin{cases} dmg \left(\frac{x_i-x_{dist}-ampl}{x_{dist}-x_{dist}-ampl} \right) & x \in [x_{dist}-ampl, x_{dist}] \\ dmg \left(\frac{x_{dist+ampl}-x}{x_{dist+ampl}-x_{dist}} \right) & x \in [x_{dist}, x_{dist+ampl}] \\ 0 & otherwise \end{cases} \quad (7)$$

where $N_{substructure}$ indicates the shape function for the substructure approach, x the centroid of the damage elements, x_i the border centroid between substructures, $a_{discrete}$ the damage function for the discrete approach, dmg the damage value of the function (between 0 and 1), $dist$ the distance from the origin to the point (into the discrete damage function), and $ampl$ the discrete damage aperture.

After defining the different shape functions, the damage can be applied following Eqs. (8) and (9),

$$K_{damage,i} = N_i(1 - a_i) \quad (8)$$

$$a_i = p * N_i \quad (9)$$

where $K_{damage,i}$ is the stiffness matrix which contains the damage values of the different elements affected by the damage for the

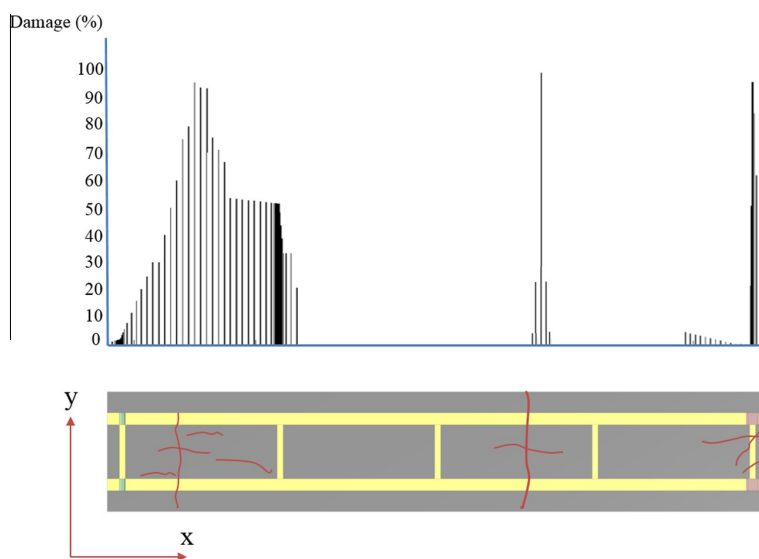


Fig. 12. Graphical comparison between the numerical and experimental damage obtained by the proposed methodology.

Table 11
Summary of the results, for the damage model, through the dynamical correlation values considered (relative error in frequencies, MAC values).

Vibration mode	f_{exp} (Hz)	f_{num} (Hz)	Error (%)	MAC (%)
1	6.40	6.61	3.28	100
2	8.16	8.33	2.08	100
3	12.13	12.33	1.65	96
4	20.79	20.51	-1.35	90
5	22.16	21.52	-2.89	89
6	23.74	24.09	1.47	86

Table 12
Summary of the results obtained in the damage model, through the static correlation values considered (relative error in displacement).

Load case	$disp_{exp}$ (mm)	$disp_{num}$ (mm)	Error (%)
A	-38.07	-39.15	2.82
B	-23.27	-23.80	2.27
C	-43.28	-43.71	0.98

shape function N_i , a_i is the damage coefficient and p is the design variables to be minimized. As a result the different values of the affected elements can ben obtained. Finally, once the different damage strategies were correctly defined, the Jacobian matrix $Jacob$ needs to be re-formulated with the following considerations, Eq. (10):

$$Jacob_{\theta} = \begin{cases} \frac{\partial J}{\partial \theta} \rightarrow \text{if } \theta \text{ is an undamage variable} \\ \frac{\partial J}{\partial \theta} = \frac{\partial J}{\partial a_{sub}} N_{sub}(\theta) \rightarrow \text{if } \theta \text{ is an substructure variable} \\ \frac{\partial J}{\partial \theta} = \frac{\partial J}{\partial a_{dis}} \left[\frac{\partial N_{dis}(\theta)}{\partial dmg} \quad \frac{\partial N_{dis}(\theta)}{\partial x_{dist}} \quad \frac{\partial N_{dis}(\theta)}{\partial ampl} \right] \rightarrow \text{if } \theta \text{ is an discrete variable} \end{cases} \quad (10)$$

where J is the objective function, θ variable to be updated, a and N (with the index sub for substructure and dis for discrete) the damage and shape functions and dmg , x_{dist} , $ampl$ the different variables of the discrete damage function. For the resolution of the derivatives, a finite difference approach was consider.

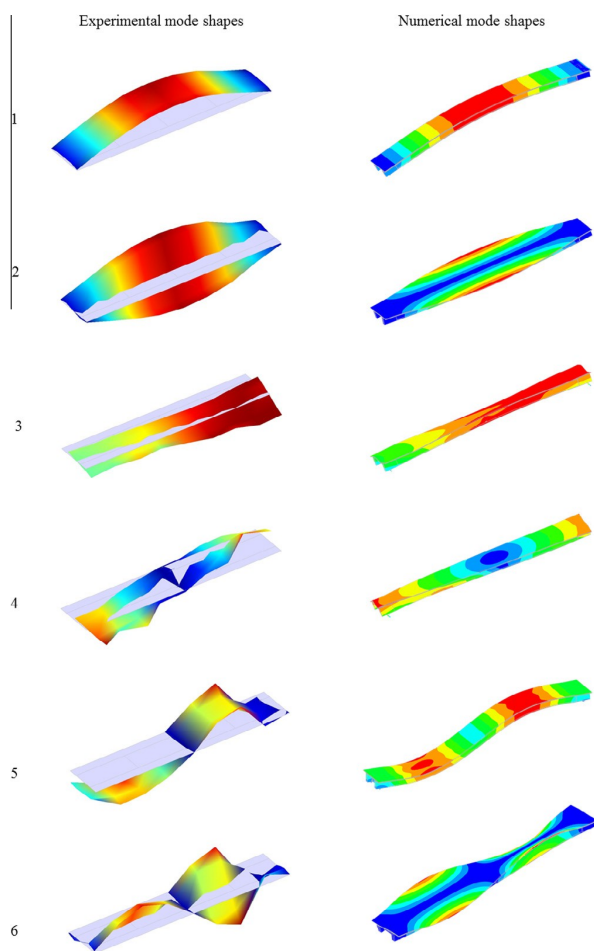


Fig. 13. Experimental and numerical mode shapes of the first six modes.

4.5. Robust calibration with damages functions

The damage presented by the footbridge can only be observed only in the intrados of the footbridge's deck. Considering this, only the lower elements of the footbridge's deck has been updated (by the proposed damage identification). As a result of the robust calibration a new model of the footbridge has been obtained (Table 10). This model presents a damage along its deck as show (Fig. 12).

Regarding the damages of the first and fourth quarterspans, as it was expected, a general damage was obtained with higher values next to the more damage areas, according with the visual inspection (Fig. 6). Also, through the discrete function, it was possible to identify the isolate crack, which is in the third quarterspan, at a distance of the deck origin equal to 7.60 m (in contrast to 7.37 m obtained in the visual inspection), originate by the presence of a transversal crack.

As a result, the final model shows a better similarity with the experimental results (see Tables 11 and 12). In terms of updating results, an average error in frequencies of 2.12% and an average MAC value of 93.50%. Considering the static behaviour, it was also observed an improvement in the results with an average error equal to 2.02%.

Finally (Fig. 13) presents a comparison between the different mode shapes identified experimentally and tuned numerically.

5. Conclusions

Nowadays, the evaluation of new constructive solutions and therefore the evaluation of new infrastructures implies a multidisciplinary task. Such analysis must involve: (i) mechanical tests of the different components; (ii) experimental programs to understand the global behaviour of the structure; and (iii) accurate numerical simulations to design, evaluate and predict its structural behaviour. Nevertheless, the interaction between different components (joints), boundary conditions and damage, are unavoidable considerations within a numerical simulation. In order to solve this, in the present paper it was shown a robust calibration method based on a non-linear least-squares method complemented by a hybrid strategy to detect and quantify the damage. The proposed methodology was validated with a high innovative structure: a hybrid footbridge based on a SFRSCC deck and GFRP pultruded profiles. The model updating analysis was carried out with results from experimental data (static and dynamic tests). It considers the stiffness of the different joints (L-union and GFRP main girders-deck union), non-perfect supports and damage as a set of linear damage functions.

Finally, an accurate damage identification analysis was performed, arising in an accurate model. However, there are always further needs of investigations in order to improve results, mainly the MAC's values for the fifth mode shape and to consider the cracks direction in the damage functions as a design variable to better improve their effects.

References

- [1] Mendes P, Barros J, Sena-Cruz J, Teheri M. Influence of fatigue and aggressive exposure on GFRP girder to SFRSCC deck all-adhesive connection. *Compos Struct* 2014;110:152–62.
- [2] Nguyen H, Mutsuyoshi H, Zatar W. Hybrid FRP-UHPFRC composite girders: part 1 – experimental and numerical approach. *Compos Struct* 2015;125: 631–52.
- [3] Bel Hadj Ali N, Rhode-Barbarigos L, Pascual Albi AA, Smith IFC. Design optimization and dynamic analysis of a tensegrity-based footbridge. *Eng Struct* 2010;32:3650–9.
- [4] Yeh F-Y, Chang K-C, Sung Y-C, Hung H-H, Chou C-C. A novel composite bridge for emergency disaster relief: concept and verification. *Compos Struct* 2015;127:199–210.
- [5] Chen Z, Cao H, Zhu H, Hu J, Li S. A simplified structural mechanics model for cable-truss footbridges and its implications for preliminary design. *Eng Struct* 2014;68:121–33.
- [6] Cabral-Fonseca S, Correia JR, Rodrigues MP, Branco FA. Artificial accelerated ageing of GFRP pultruded profiles made of polyester and vinylester resins: characterisation of physical-chemical and mechanical damage. *Strain* 2012;48:162–73.
- [7] Liao K, Schultheisz CR, Hunston DL. Effects of environmental aging on the properties of pultruded GFRP. *Compos Part B Eng* 1999;30:485–93.
- [8] Gonilha JA, Correia JR, Branco FA. Creep response of GFRP-concrete hybrid structures: application to a footbridge prototype. *Compos Part B Eng* 2013;53:193–206.
- [9] Keller T, Schaumann E, Vallée T. Flexural behavior of a hybrid FRP and lightweight concrete sandwich bridge deck. *Compos Part A Appl Sci Manuf* 2007;38:879–89.
- [10] Deskovic N, Triantafyllou TC, Meier U. Innovative design of FRP combined with concrete: short-term behavior. *J Struct Eng* 1995;121:1069–78.
- [11] Gonilha J, Barros J, Correia J, Sena-Cruz J, Branco F, Ramos L, et al. Static, dynamic and creep behaviour of a full-scale GFRP-SFRSCC hybrid footbridge. *Compos Struct* 2014;118:496–509.
- [12] Thambiratnam DP, Perera NJ, Abeysinghe CM, Huang M-H, De Silva SS. Human activity-induced vibration in slender structural systems. *Struct Eng Int* 2012;22:238–45.
- [13] Gonilha JA, Correia JR, Branco FA. Dynamic response under pedestrian load of a GFRP-SFRSCC hybrid footbridge prototype: experimental tests and numerical simulation. *Compos Struct* 2013;95:453–63.
- [14] ISO. ISO 527-1:2012. Plastics-determination of tensile properties. Genève. 2012.
- [15] ASTM. ASTM D 695. Standard test method for compressive properties of rigid plastics. West Conshohocken, Pennsylvania. 2002.
- [16] Hodgkinson JM. Mechanical testing of advanced fibre composites. Elsevier; 2000.
- [17] Barros J, Pereira E, Santos S. Lightweight panels of steel fiber-reinforced self-compacting concrete. *J Mater Civil Eng* 2007;19:295–304.

- [18] IPQ IplQ, NP EN 12390-3:2011. Testing hardened concrete part 3: compressive strength of test specimens, Caparica; 2011.
- [19] RILEM. International RILEM workshop on test and design methods for steel fibre reinforced concrete-background and experiences; 2003.
- [20] Firmo JP, Correia JR, França P. Fire behaviour of reinforced concrete beams strengthened with CFRP laminates: protection systems with insulation of the anchorage zones. *Compos Part B Eng* 2012;43:1545–56.
- [21] Gonilha J, Aquino A, Correia J, Branco F. Experimental evaluation of the GFRP/ECC connection–shear connection tests: phase 1. ICIST internal project report A. 5; 2010.
- [22] Gade S, Møller N, Herlufsen H, Konstatin-Hansesn H. Frequency domain techniques for operational modal analysis. 1st IOMAC Conference; 2005.
- [23] Diana T. Finite element analysis user's manual-release 9.4. 4. TNO DIANA; 2011.
- [24] Teughels A, De Roeck G. Damage assessment of the Z24 bridge by FE model updating. *Key engineering materials*. Trans Tech Publ; 2003 [p. 19–26].
- [25] Ramos LF, Marques L, Lourenço PB, De Roeck G, Campos-Costa A, Roque J. Monitoring historical masonry structures with operational modal analysis: two case studies. *Mech Syst Signal Processing* 2010;24:1291–305.
- [26] Mishra AK, Chakraborty S. Development of a finite element model updating technique for estimation of constituent level elastic parameters of FRP plates. *Appl Math Comput* 2015;258:84–94.
- [27] Simoen E, De Roeck G, Lombaert G. Dealing with uncertainty in model updating for damage assessment: a review. *Mech Syst Signal Processing* 2015;56–57:123–49.
- [28] Coleman TF, Li Y. An interior trust region approach for nonlinear minimization subject to bounds. *SIAM J Optim* 1996;6:418–45.
- [29] Allemang RJ, Brown DL. A correlation coefficient for modal vector analysis. *Proceedings of the 1st international modal analysis conference*. SEM, Orlando; 1982. p. 110–6.
- [30] Foti D. Dynamic identification techniques to numerically detect the structural damage. *Open Constr Build Tech J* 2013;7:43–50.
- [31] Rytter A. *Vibrational based inspection of civil engineering structures: unknown*; 1993.
- [32] Titurus B, Friswell M. Regularization in model updating. *Int J Numer Meth Eng* 2008;75:440–78.
- [33] Sánchez-Aparicio LJ, Riveiro B, González-Aguilera D, Ramos LF. The combination of geomatic approaches and operational modal analysis to improve calibration of finite element models: a case of study in Saint Torcato Church (Guimarães, Portugal). *Constr Build Mater* 2014;70:118–29.

CAPÍTULO III

PHOTOGRAMMETRIC, GEOMETRICAL AND NUMERICAL STRATEGIES TO EVALUATE INITIAL AND CURRENT CONDITIONS IN HISTORICAL CONSTRUCTIONS: A TEST CASE IN THE CHURCH OF SAN LORENZO (ZAMORA, SPAIN).

RESUMEN: Bajo el nombre de *Photogrammetric, geometrical and numerical strategies to evaluate initial and current conditions in historical constructions: A test case in the church of San Lorenzo (Zamora, Spain)*. El Capítulo III trata de abordar una doble vertiente en el campo de la geomática.

Por un lado, mejora la metodología de segmentación y paso a modelos CAD desarrollada en el Capítulo I a través del empleo de superficies no paramétricas NURBs y procedimientos complementarios de cuadrilaterización de la malla (teoría de Morse y análisis Espectral). Por otro lado, desarrolla índices de calidad geométrica basados en el concepto de distancia simétrica Hausdorff que permiten calibrar y evaluar la bondad de las simulaciones numéricas.

A fin de evaluar las metodologías e índices propuestos se dispone como caso de estudio una cúpula de ladrillo y arquitectura vernácula con severos daños estructurales. Entre dichos daños caben destacar unas grandes deformaciones de 20 cm, la formación de dos rótulas plásticas y la pérdida de material.

Resultado de dichos estudios, se puede concluir la validez a priori de los índices geométricos propuestos así como de las metodologías de modelado geométrico empelado. En lo que respecta a la construcción evaluada, los resultados no parecen concluyentes requiriendo de ensayos

complementarios que permitan conocer mejor las propiedades mecánicas de la estructura.

Palabras clave: Correlación Digital de Imágenes; Structure from Motion; Métrica Global Hausdorff, Métrica Local Hausdorff, B-Splines Racionales No-Uniformes; Modelado por Elementos Finitos, Arquitectura vernácula; Construcciones históricas.



Article

Photogrammetric, Geometrical, and Numerical Strategies to Evaluate Initial and Current Conditions in Historical Constructions: A Test Case in the Church of San Lorenzo (Zamora, Spain)

Luis Javier Sánchez-Aparicio *, Alberto Villarino, Jesús García-Gago and Diego González-Aguilera

Received: 16 September 2015; Accepted: 8 January 2016; Published: 13 January 2016

Academic Editors: Fabio Remondino, Parth Sarathi Roy, Randolph H. Wynne and Prasad Thenkabail

Department of Land and Cartographic Engineering, University of Salamanca, High Polytechnic School of Avila, Hornos Caleros, 50, 05003 Avila, Spain; avillarino@usal.es (A.V.); jesusmkg@usal.es (J.G.-G.); daguilera@usal.es (D.G.-A.)

* Correspondence: luisj@usal.es; Tel.: +34-920-353-500; Fax: +34-920-353-501

Abstract: Identifying and quantifying the potential causes of damages to a construction and evaluating its current stability have become an imperative task in today's world. However, the existence of variables, unknown conditions and a complex geometry hinder such work, by hampering the numerical results that simulate its behavior. Of the mentioned variables, the following can be highlighted: (i) the lack of historical information; (ii) the mechanical properties of the material; (iii) the initial geometry and (iv) the interaction with other structures. Within the field of remote sensors, the laser scanner and photogrammetric systems have become especially valuable for construction analysis. Such sensors are capable of providing highly accurate and dense geometrical data with which to assess a building's condition. It is also remarkable, that the latter provide valuable radiometric data with which to identify the properties of the materials, and also evaluate and monitor crack patterns. Motivated by this, the present article investigates the potential offered by the combined use of photogrammetric techniques (DIC and SfM), as well as geometrical (NURBs and Hausdorff distance) and numerical strategies (FEM) to assess the origin of the damage (through an estimation of the initial conditions) and give an evaluation of the current stability (considering the deformation and the damage).

Keywords: digital image correlation; structure from motion; global metric Hausdorff; local metric Hausdorff; non-uniform rational B-Splines; finite element modelling; vernacular architecture; historical construction

1. Introduction

The conservation of built heritage is today considered a fundamental aspect of modern society. Their artistic, cultural, and intrinsic value make these constructions extremely important. Complementary to this, the lack of the building's own mechanical values and the characteristic behavior of its masonry, the complex interaction between components, and the lack of documentation, make the analysis of such constructions remarkably difficult. Currently, and derived from these considerations, numerous regulations propose the integration of different approaches among which are [1]: (i) the study of the construction's history; (ii) inspection; (iii) monitoring; and (iv) structural analysis.

Regarding the numerical calculations, the static graphic [2] and limit analyses [3] traditionally provided the necessary tools to study the stability and bearing capacity of historical structures [4]. However, such numerical strategies have among their drawbacks the difficulty to evaluate damages [1].

In contrast with these models, the Finite Element Method (FEM) has been widely used for the evaluation of historical buildings at different levels; from complex and large constructions through macromodelling techniques [5], to the use of micromodelling strategies [6], where the units are independently discretized, or homogenized [7]. However, the large number of involved variables, as well as interaction with other structures, conditions the results.

It is in the field of built constructions where remote sensors and especially photogrammetric and laser scanner systems have proven great worth for their analysis [3,8–10]. These sensors are able to provide accurate and dense geometric and radiometric values with which to assess these buildings, as well as obtaining the data through non-intrusive means. Despite this, the data they provide (in form of dense and accurate point clouds) is largely untapped, since it is only used for the construction of simplified CAD models [10].

On one hand, the present article introduces two novel robustness parameters (based on geometrical components) in order to increase their applicability, obtained from the symmetrical Hausdorff distance [11]. These parameters, called Global Hausdorff metric (GHm_s) and Local Hausdorff metric (LHm_s), help ascertain whether the variables or simulated conditions improve or worsen the numerical results, in comparison with the real deformation provided by the photogrammetric and laser scanner systems.

On the other hand, the article introduces a methodology based on a Non-Uniform Rational B-Splines (NURBs) modelling strategy, with the purpose of providing an accurate geometrical model (with the current deformation and damage) for the evaluation of the current stability of the construction. This strategy is able to take advantage of the properties provided by the Structure from Motion products: (i) density; (ii) accuracy; and (iii) photorealistic texture, within a numerical environment.

In order to confirm the feasibility of the proposed geometrical strategies (GHm_s , LHm_s and NURBs modelling), they are applied to a case study: the dome of the church of San Lorenzo in Sejas de Aliste (Zamora, Spain). This construction, built in brick masonry, has suffered severe structural damages, shown through significant deformation, cracking and plastic hinges that reduce its bearing capacity. It seems necessary to perform a structural evaluation in order to design efficient restoration actions.

The article is organized as follows: Section 1 consists of an introduction and brief state of the art, Section 2 describes the different image-based techniques that were employed; Section 3 is made up of the description of the construction, the current deformation, damage, and the numerical aspect through the FEM; Section 4 describes two robustness indices based on geometrical discrepancies, a manual calibration of the model and a complementary strategy to evaluate the current stability of the construction (considering the complex geometry and the presented cracking); and finally, Section 5 shows the conclusions.

2. Image Based Approaches: Digital Image Correlation and Structure from Motion

The great diversity of approaches today, along with their flexibility, place image-based procedures as a suitable solution for the analysis of constructions [3,9,12], materials [13,14], and pathologies [8].

The different methodologies that comprise this approach, particularly in the field of numerical evaluation of constructions, highlight: (i) Digital Image Correlation (DIC); and (ii) image-based modelling procedures. While the former provides mechanical data of materials and constructive solutions (in the form of displacement and strains), the latter allows the definition of a dense, accurate, and photorealistic geometrical model of the construction. Their combination provides relevant information for the numerical analysis of the structure.

2.1. 2D Digital Image Correlation

A wide variety of methodologies has been developed and used to study material and union behavior. Some of these are [14,15]: (i) Moiré interferometry; (ii) Holography interferometry; (iii) Shearography; and (iv) Digital Image Correlation.

These methodologies prove to have important advantages, compared to traditional methods based on strain gauges or LVDT's (Linear Variable Differential Transformer) such as their non-invasiveness and their full-field data information. In comparison, traditional methods provide only local information and require direct contact with the tested material. Within this wide range of techniques, the use of Digital Image Correlation (DIC) stands out.

To characterize the materials used in the dome, various compression tests were performed separately on each material (three in each material) during the experimental campaign that was carried out. Considering the procedure defined by [16], an extra specification, such as the mortar joint material (made by gypsum mortar), was considered.

In order to verify the flexibility and accuracy of the shown method, one standard sensor was used for both the DIC and the SfM: a digital reflex camera Canon 500D. However, in contrast to the image-based modelling strategy, DIC requires the preparation of the analyzed specimen, following the approach defined by [16]: (i) MIG (Mean Intensity Gradient) evaluation [17] of the speckle pattern; (ii) camera pose estimation [18]; and (iv) camera calibration [19].

Once the specimen has been correctly pre-processed, different images were captured during the test (Figure 1). Also, concerning the test setup, a large focal distance and working distance were used in order to minimize the geometrical distortion, out of plane displacements (approximation to a telecentric lens system) [20], depth of field, and light conditions.

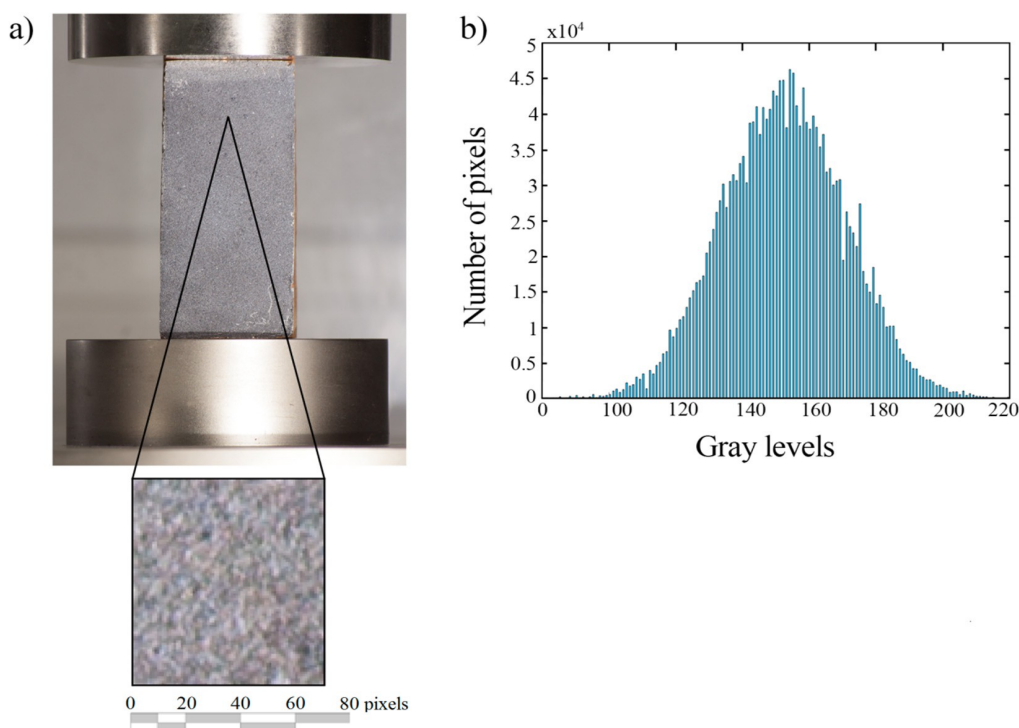


Figure 1. (a) Detail view of the brick and speckle pattern applied during the Digital Image Correlation (DIC) test; (b) Histogram of the speckle pattern.

The basic principle of DIC is the tracking (or matching) of the different areas of the images which were captured during the test (before and after deformation occurs), called subsets. As an initial approximation of this tracking, a correlation coefficient (generally the Zero Normalized Cross Correlation) [20] is used. Later, this initial approximation is optimized by the use of a non-linear

strategy (such as the Inverse Compositional Gauss Newton method) [20] which allows the evaluation of the displacement suffered by the subset along the different captured images (Figure 2) [16].

Complemented to this optimization process an interpolation process (based on splines) is used with the aim of obtain sub-pixel accuracy [20]. Considering multiple subsets in the image, their analysis can provide a full-field displacement. Later, the strains suffered by the specimen during the test, which allow the evaluation of its mechanical properties, can be obtained by a direct relationship between the obtained displacement on the measurement point and the initial length of the virtual extensometers [16]. A total of three virtual extensometers were placed on the ROI: (i) A-A' and B-B' in the longitudinal direction; and (ii) C-C' in the transversal direction.

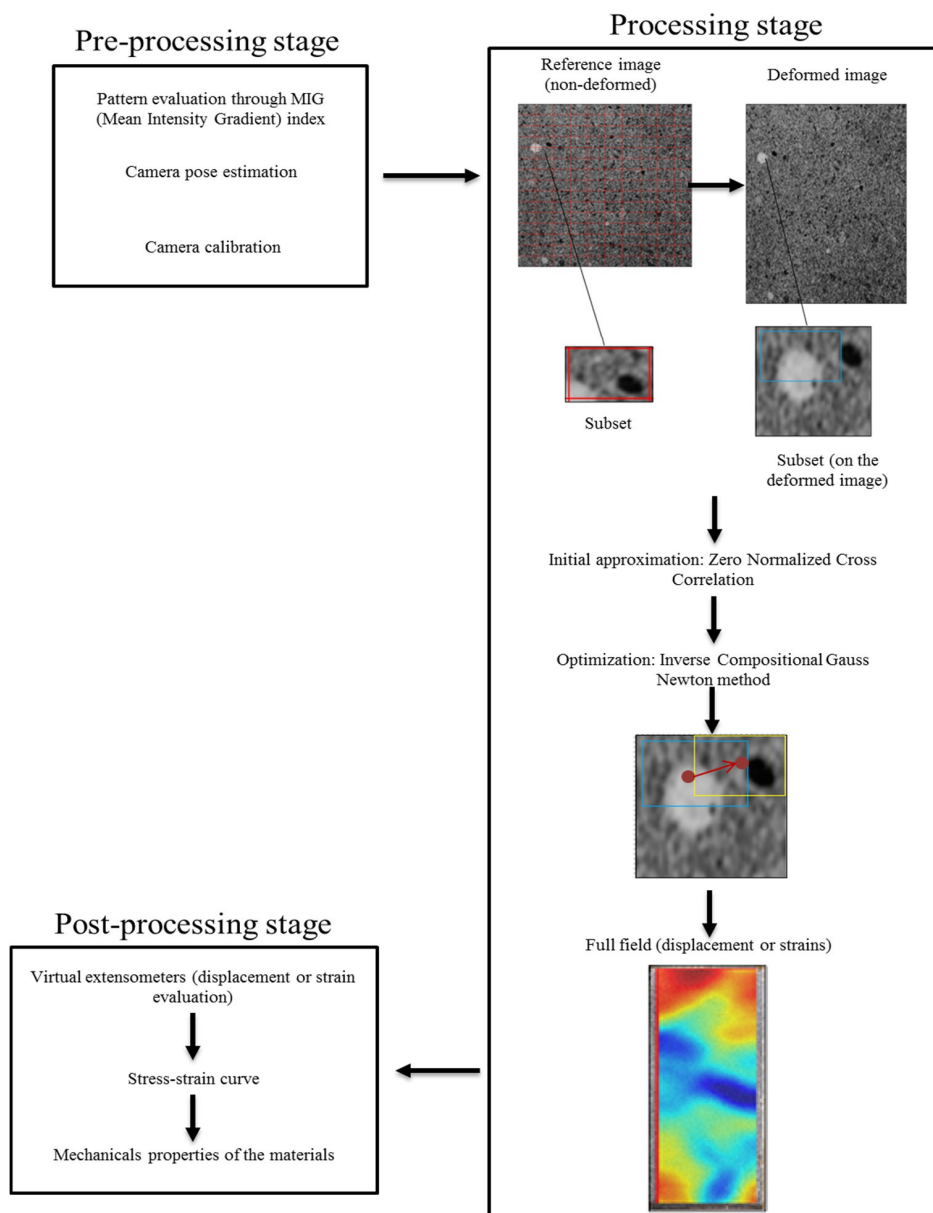


Figure 2. Digital Image Correlation general outline. In red the reference subset, in blue the initial seed, and in yellow, the final location of the subset.

Concerning accuracy, there are different studies [15,21,22] that endorse the DIC’s precision for the assessment of the material’s mechanical properties. For a standard test configuration, the accuracy may range from values of 0.01–0.04 pixels. Considering a conservative threshold at 0.1 pixels, and an acceptable accuracy for the test of 0.01 mm (from which the critical pixel size is set at 0.1 mm), the test’s configuration is shown in (Table 1).

Table 1. Summary of the different properties set during the Digital Image Correlation (DIC) test carried out with a Canon EOS 500D and a macrolens system 70–300 mm.

Values Adopted during the Digital Image Correlation (DIC) Test	
Aperture	7.1
Focal length (mm)	200
Working distance (mm)	2700
Pixel size (mm)	0.063
Acquisition frequency (Hz)	0.33

Once the stress-strain curve has been obtained (by a relationship between the stress applied by the compression press and the strains obtained by DIC) (Figure 3b), it is possible to extract the mechanical properties of the materials as follows (Table 2): (i) the Young Modulus was considered as the ratio between one third of the maximum force achieved and the mean strain provided by the longitudinal extensometers (A-A’ and B-B’); (ii) for the Poisson ratio, the relationship between the strains provided by the longitudinal extensometers and those obtained by the transversal extensometer (C-C’) was taken into account; and (iii) the compression strength was considered as the maximum pressure supported by the specimen.

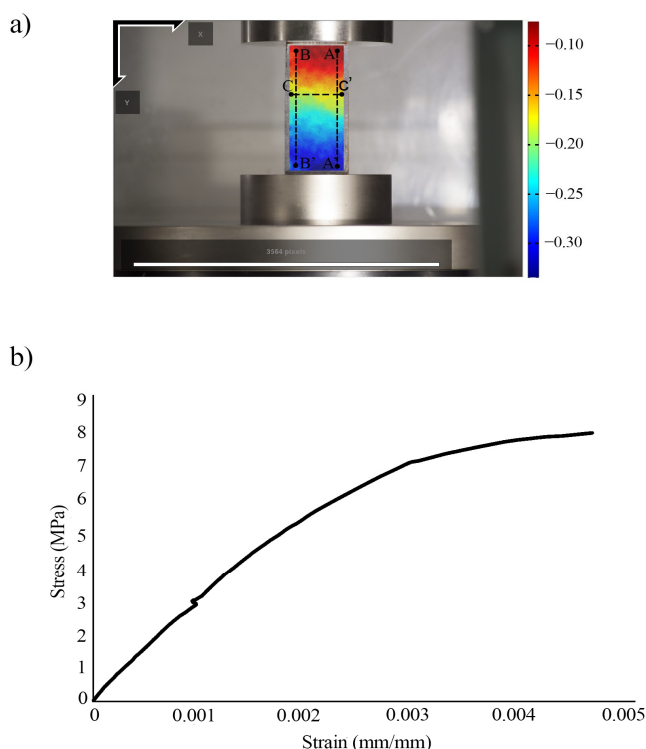


Figure 3. Results after the experimental campaign (2D DIC). (a) Deformation measurement, expressed in pixels, between two captures and positioning of the virtual extensometers; (b) Stress-strain curve obtained with the virtual extensometer A-A’.

Table 2. Mechanical properties obtained by the performed DIC test.

Mechanical Properties Obtained by the DIC Test		
	Clay brick	Gypsum mortar
E (GPa)	3.10 ± 0.30	1.15 ± 0.06
ν (-)	0.22 ± 0.05	0.23 ± 0.02
f_c (MPa)	7.80 ± 0.90	2.12 ± 0.10

To assess the accuracy of the previously mentioned procedure, a comparative study was carried out, between the strain rate applied by the compression press (with an average value of $-1.77 \times 10^{-6} \text{ s}^{-1}$), and the one obtained by the different performed DIC tests and the different virtual extensometers used (with an average value of $-1.93 \times 10^{-6} \text{ s}^{-1}$). The results obtained demonstrate the accuracy and suitability of the applied configuration and algorithms, with an estimated precision of 0.056 pixels (which correspond to an approximate value of $3.53 \mu\text{m}$). This value proves to be lower than the previously shown critical value.

2.2. Image-Based Modelling: Structure from Motion

In recent years the image-based modelling strategy, called Structure from Motion (SfM), has positioned itself as an attractive alternative to laser scanning systems. Its flexibility—as it can be integrated into different types of platforms (e.g., UAV [9])—low-cost, and qualities of the point cloud (high density, photorealistic texture, and accuracy) place the solution at a vantage position in the evaluation of historical buildings [23].

This technique integrates within its operating structure the advantages of computer vision (automation and flexibility) and photogrammetry (accuracy and reliability) [23] to obtain high density three dimensional models whose accuracy can compete with those of the laser scanner system [24,25].

For this case study, a standard SfM strategy is applied, comprising the following stages: (i) automatic extraction and keypoint matching by applying the Affine-Scale Invariant Feature Transform (ASIFT) algorithm [26]; (ii) automatic hierarchical orientation of images; and (iii) dense model generation through the MicMac algorithm. For further details on this methodology see [12]. Concerning the photogrammetric network a convergent protocol was used, combining a total of 32 cameras with high overlap (around 90%) and throwing a mean GSD (Ground Sample Distance) of 1.61 mm. Complementary to these, different circular targets (along the lower part of the pendentive) were used to scale the model (this measurement were taken by a total station using a radiation approach).

As a result of the implementation of the above-mentioned methodology it is possible to obtain a dense and photorealistic texture point cloud (Figure 4a). Afterwards, applying CAD conversion techniques (meshing, surface parameterization, extrusions, revolutions, etc.), or even generating true-ortho-images, increase further the applicability of the obtained product. More precisely, they help to accurately build CAD models suitable for subsequent numerical simulations, as well as complementary products, which analyze patterns of deformation and cracking for the pathological characterization of the structure [9] (Figure 4b).

Concerning the total error, associated with this point cloud, a quadratic error propagation was used Equation (1). Into this approach, two sources were considered: (i) the error coming from the bundle adjustment of the photogrammetric network; and (ii) the error corresponding to the scaling process Equation (2).

$$\varepsilon_t = \sqrt{\varepsilon_p^2 + \varepsilon_s^2} \quad (1)$$

$$\varepsilon_s = \sqrt{2\varepsilon_i^2 + \varepsilon_m^2} \quad (2)$$

where ϵ_t represents the total error; ϵ_s the scale error; ϵ_p the error associated with the photogrammetric network; ϵ_i the origin error established as $\sqrt{2} * (\frac{pixelsize}{\gamma})$, where γ is the subpixel accuracy of the target detection algorithm (estimated in 0.5); and ϵ_m the error associated with the total station.

As a result a budget error of $\epsilon_t = 4.38$ mm was obtained (with values of $\epsilon_p = 3.22$ mm, $\epsilon_i = 1.14$ mm, $\epsilon_m = 2.50$ mm, and $\epsilon_s = 2.97$ mm).

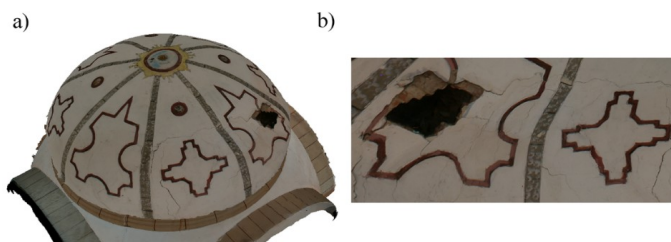


Figure 4. (a) 3D model obtained by the proposed methodology; (b) Detail view of the most damaged section through the texture model.

3. Structural Evaluation of San Lorenzo's Dome

3.1. San Lorenzo Church

The church is built with irregular masonry walls (slabs of slate) fixed with lime mortar and at the corners finished with granite masonry. The parish church of San Lorenzo in Sejas de Aliste is located in the region of Aliste, Zamora province (Spain), 32 m long and 17 m wide, it belongs to the family of temples with transept crossing, Latin cross-shaped floor plan, and transept and nave at different heights (Figure 5).

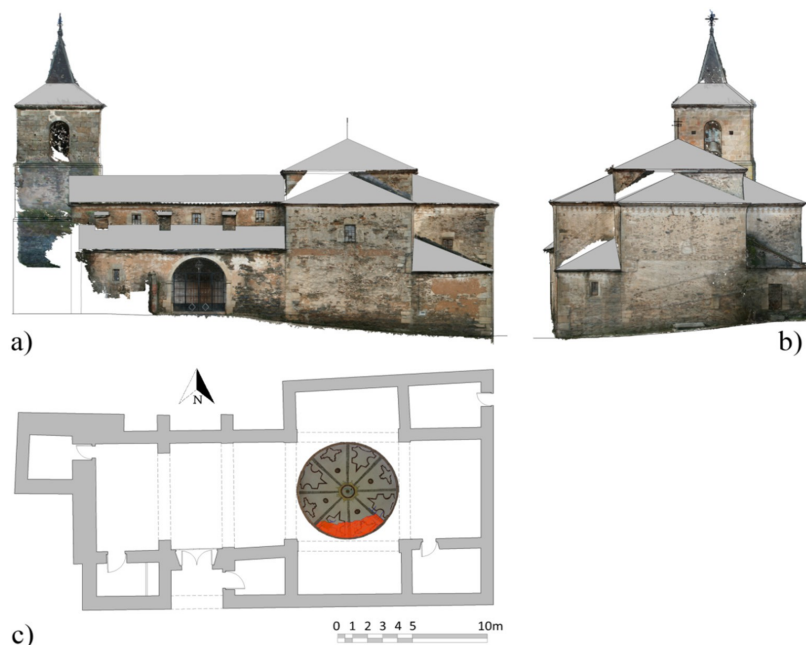


Figure 5. San Lorenzo church: (a) Orthophoto of the main façade through the methodology proposed; (b) Orthophoto of the west façade (chancel) of the construction; (c) Floor plan-view of the church, red color indicates the damaged area of the dome.

The transept crossing is the most representative element of this temple. Its importance in the building is highlighted in the interior through the semi-elliptical dome that shelters the whole crossing. Its eight ribs marked with bands stand out. The transept is highlighted in the outside as well, covering the dome with a hipped roof that rises above the nave and transept height. This roof is built with a pavilion-shaped chestnut-timber framing, with regularly placed rafters that lean on the main beams and bear the load of the roof, made up of curved tiles and wooden roof boards (Figure 6a). Overall stability is obtained by use of tie beams at the top of the bearing walls, which collect the loads of the rafters and the hip rafters or main beams. Angle-ties, placed at 45° in each corner under the hip rafters prevent the transversal deformation of the tie beams (Figure 6a).

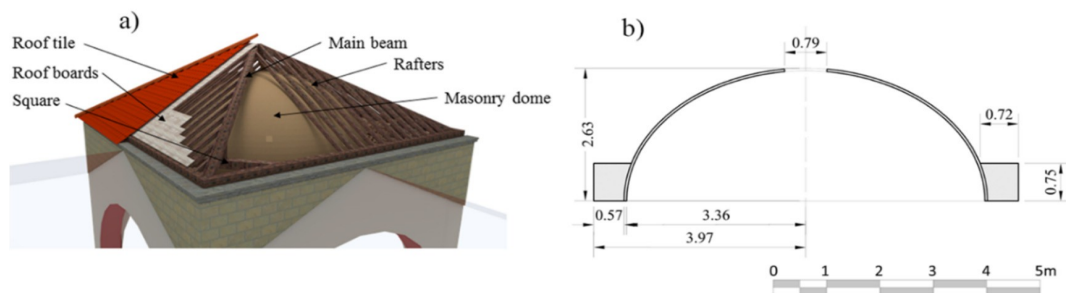


Figure 6. (a) Constructive section of the church's transept; (b) Transversal section of the dome geometry (initial state estimated by the Structure from Motion (SfM) point cloud) with dimensions in meters.

Concerning the dome, the construction has an estimated diameter of 6.72 m and a total height (measured from the pendentive) of 2.63 m. This structure was built with traditional tile brick and gypsum mortar, reaching a total thickness of 5.00 cm. It resembles, from a construction point of view, a Catalan vault (Figure 6b). It is also worth mentioning the presence of an infill (basically composed of a mixture of sand, clay and fragments of bricks with a medium compaction) at the support of the dome. This infill reaches a total height of 0.75 m and an average thickness of 0.65 m, and its presence contributes to the stability of the construction.

3.2. Present Damage and Deformation

The characterization of both, deformations and cracking patterns, is key to understanding the structure in terms of stability and safety. The high density, accuracy, and photorealistic texture of the point cloud obtained by the proposed methodology (Section 2.2) can address this task foregoing any need of physical contact with the structure. Through evaluation of the obtained product, it is possible to obtain a hypothesis for the origin of the damage.

It is worth noting that there is widespread damage in the area enclosed by three ribs (corresponding to the southern part of the dome). This area has two main cracks, in the parallel direction, which are interconnected through the presence of two plastic hinges. At its maximum, there is a deflection of 19.70 cm (compared to the initial estimated model) (Figure 7).

These structural pathologies seem to be related to the presence of asymmetric loads acting on part of the dome's shell (Figure 7a). More specifically the current damages, which are located under the south wing, can be attributed to a failure of the timber structure.

On one hand, the evaluation of photogrammetric products (which are the result of the previously defined SfM strategy) allows an estimation of the possible causes of the dome's damage. However, it is required to have numerical strategies to verify these assumptions and assess the current state of the construction. For the present case study, and considering the hypothesis of failure of the timber structure several numerical analyses were performed: (i) numerical evaluation of the timber structure for the worst load case: snow; (ii) evaluation of the dome's stability under self-weight; and (iii) numerical evaluation of the interaction timber-dome as a result of a timber failure.

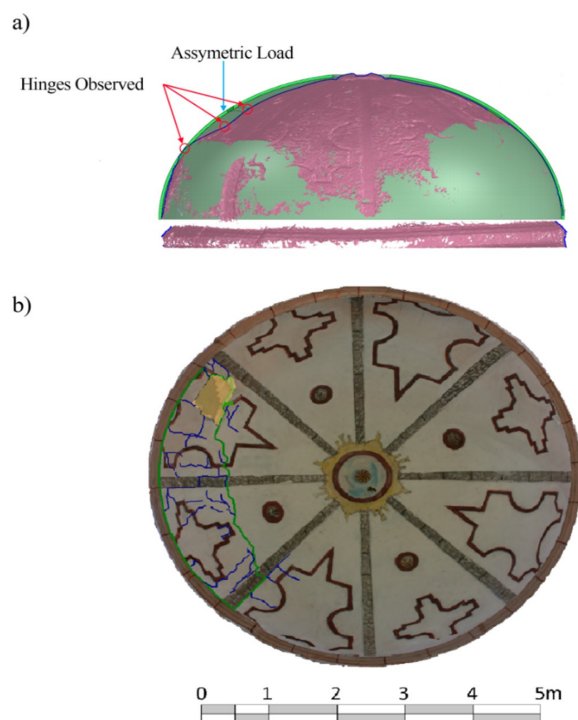


Figure 7. Results of the visual inspection over the different photogrammetric products: (a) Surface comparison between the initial proposed model and the most deformed one estimated by the SfM point cloud; (b) Damage inspection in the orthophoto, in green the main observed cracks, in blue the secondary cracks, in yellow the material removal.

Previous investigations carried out by [16], verified the stability of the timber structure for the most adverse load case: the presence of snow. Yielding a maximum deflection of 2.35 cm, it proves to be insufficient in order to interact with the dome. Considering these results, it is possible to conclude that the interaction between the cover and the dome seems to be linked with the presence of pathological agents (mainly moisture and biological organisms) which reduce the bearing capacity of the timber structure until it fails and rests on the dome.

3.3. Numerical Simulation of the Initial State of the Dome: Self-Weight and South Wing Support

Understanding the degradation mechanisms present in the construction requires a geometrical model of its initial state, a material characterization, as well as its boundary conditions, and load assessment. According to these, several numerical simulations (through non-linear static analysis) were performed in order to understand the causes and the construction's initial conditions. Several improvements, regarding the geometric and mechanical aspects, are introduced in comparison to the previous investigations performed by [16]: (i) consideration and modelization of the infill-dome interaction; and (ii) account of gypsum as union material.

Regarding the mechanical aspect, a macromodelling strategy of the masonry was followed. This technique blends the bricks, mortar joints as well as the brick-mortar interface into one continuum assuming homogeneous material properties (Table 3). Also, the recommendations exposed by reference [6,27] were considered. An initial estimation of the masonry's Young modulus was estimated using the formulas displayed in [28], setting the initial Young modulus at 2.54 GPa. However, further visual inspections showed the presence of an erratic masonry with low overlap between units. In accordance with this, a reduction of the initial Young modulus was considered for subsequent

simulations (half of the initial estimated), yielding a final value of 1.22 GPa, analogous to those used in similar studies [7,29].

Table 3. Mechanical properties adopted for the macromodelling of the masonry.

Mechanical Properties for the Masonry Structure		
E_m (GPa)	Young Modulus	1.22
δ_m (kg/m ³)	Density	1800.00
ν_m (-)	Poisson coefficient	0.25
$f_{t,m}$ (MPa)	Tensile strength	0.16
$f_{c,m}$ (MPa)	Compressive strength	1.60
$d_{t,m}$ (mm)	Ductility index in tensile	0.093
$d_{c,m}$ (mm)	Ductility index in compression	1.6
$\beta_{c,m}$ (-)	Shear retention	0.2

For the numerical simulation of the infill, a Mohr-Coulomb failure criterion was considered, with its mechanical properties set according to the visual inspection (medium compaction) and the recommendations shown by [7,29,30] (Table 4).

Table 4. Mechanical properties adopted for the infill simulation.

Infill Mechanical Properties		
E_i (GPa)	Infill Young Modulus	0.80
δ_i (kg/m ³)	Infill density	1800.00
G (GPa)	Infill shear modulus	$E_i/2$
f_i (MPa)	Cut-off tension	0.02
Φ_i (deg)	Infill friction angle	39
c_i (MPa)	Infill cohesion	$1 \times f_i$

Concerning the load (for the numerical evaluation of the interaction between timber structure and the dome), a value of 8000 N was considered, resulting from the combination of different loads: (i) 650 N/m² for the arabic tiles and wooden board; and (ii) 400 N/m² for the snow load. Finally, the numerical model (for both simulations), had a total of 46,181 high order solid elements (CTE30) [31] (Figure 8a).

It is possible to observe that in the absence of external loads acting on the dome, the structure seems to be stable under its own weight (Figure 8b). In spite of this, considering the support of the south wing (roof tile, boards, and rafters), the dome begins to present damage (cracking) and its deformation tendency (Figure 8c) seems to be similar to the one shown in the photogrammetric model (Figure 7a).

However, in terms of deformation, considering for this purpose six control nodes along the damage area (Figure 8a), the model exhibits high rigidity. This suggests that the initial mechanical conditions are inadequate to reproduce the damage and deformation presented in the dome (Table 5).

Table 5. Comparison between the obtained and expected displacement of the control nodes in the numerical model (initial considerations).

Control Node	Displacement Obtained (mm)	Displacement Expected (mm)
54	1.95	148.00
20256	0.48	46.00
56	1.57	198.00
21125	0.54	52.00
443	2.12	196.00
64123	0.57	25.00

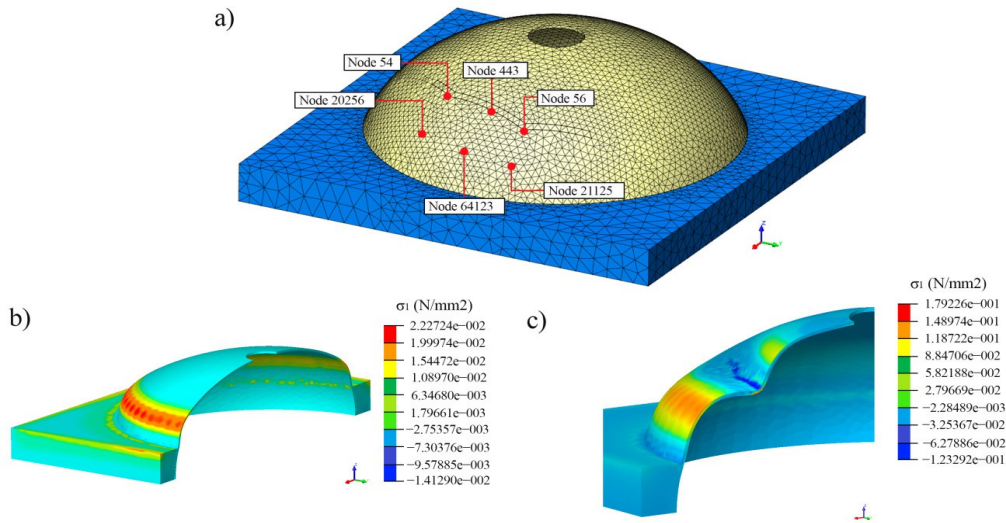


Figure 8. (a) Isometric view of the mesh and the control points (nodes) used for the numerical simulations; (b) First principal stress distribution, expressed in N/mm² for the self-weight case; (c) First principal stress distribution, expressed in N/mm², for the numerical model which considers the asymmetric load.

The high discrepancies shown in the previous numerical simulation suggest the need for an optimization of the mechanical properties. However, performing such an optimization requires inevitably having robustness indices to quantify the level of improvement/worsening introduced by the different variable’s variations.

Exploiting the advantages offered by the SfM or laser scanner systems, two novel robustness parameters (based on geometric discrepancies) are proposed: (i) a global parameter, based on the similarity between the numerical and real model; and (ii) a local index which provides data about the geometrical variations introduced by the new variables considered in different areas of the construction.

4. SfM, NURBS Modelling, Global and Local Hausdorff Metrics: Geometrical Strategies to Improve the Knowledge about the Initial and Current State of the Constructions

4.1. Global and Local Hausdorff Metrics as Geometric Accuracy Indices

The Hausdorff distance or Hausdorff metric is used in a wide range of fields, such as point cloud [32] and meshes [33] comparison, object recognition [34], and image comparison and matching [35]. This metric proves to be a robust strategy for the similarity evaluation of two compact and non-empty sub-sets within a metric space. It is formulated as follows Equations (3) and (4):

$$d(y, X) = \min_{x \in X} \|y - x\|_2 \quad (3)$$

$$d_H(Y, X) = \max_{y \in Y} d(y, X) \quad (4)$$

where $\| \cdot \|_2$ stands for the Euclidean norm; *min* the minimum value (distance); *max* the maximum distance; *X* and *Y* are the two compact sub-sets defined by the numerical and photogrammetric nodes; and *x* and *y* the considered points inside these sub-sets.

It is worth mentioning that, considering the previously defined concept of Hausdorff distance, the value of the norm does not have a symmetrical nature; it is therefore different in each direction ($d_H(X, Y) \neq d_H(Y, X)$). For that reason, the symmetrical Hausdorff distance d_{SH} Equation (5) is used as metric comparison to avoid potential errors of geometrical similarity. This way a more robust solution is provided for geometry comparison.

$$d_{SHi} = \max \{d_H(y, X), d_H(x, Y)\} \tag{5}$$

where d_{SHi} is the symmetrical Hausdorff distance; of sub-set i , between models (numerical and photogrammetric); and x and y are two points that respectively belong to sub-sets X and Y .

On the other hand, understanding the global structural behavior of the analyzed construction inevitably requires several numerical analyses in order to adapt the simulated behavior to the real one. It is necessary to take into account the consideration that new conditions or new values of variables may worsen or improve the global and/or local result of the structure. It is therefore possible to define, out of the previously shown comparison metric Equation (3), two novel geometrical indices of robustness that represent improvements or worsening in the new numerical simulations in comparison to a reference model, considering the different variations of the variables or conditions: Global Hausdorff metric Equation (6); and Local Hausdorff metric Equation (7).

$$GHm_s = \left(\frac{\sum_{i=1}^n d_{SH}(i) - \sum_{i=1}^n d_{SH_b}(i)}{\sum_{i=1}^n d_{SH_b}(i)} \right) \times 100 \tag{6}$$

$$LHm_s(i) = \frac{d_{SH}(i)}{d_{SH_{ref}}(i)} \tag{7}$$

where GHm_s represent the Global Hausdorff metric index and LHm_s the Local Hausdorff metric index, $d_{SH}(i)$ the symmetrical Hausdorff distance to cluster i considered for the model; $d_{SH_b}(i)$ the symmetrical Hausdorff distance for cluster i of the base model (the model that results from the geometrical discrepancies between the initial model and the photogrammetric one); and $d_{SH_{ref}}(i)$ the symmetrical Hausdorff distance from cluster i to the reference one (which may be the base model).

On one hand, GHm_s is able to provide a global value, expressed in percentage, for the improvement/worsening of the numerical simulation model in comparison to the model that was considered as base model. On the other hand, LHm_s provides a comparison of the variations between the numerical model and the reference model at a local level (values lower than one indicates a local improvement and values higher than one, a worsening).

For this case study, the reference model was considered to be the base model, obtained by the application of Equation (3) between the photogrammetric model and the non-deformed numerical model (Figure 9).

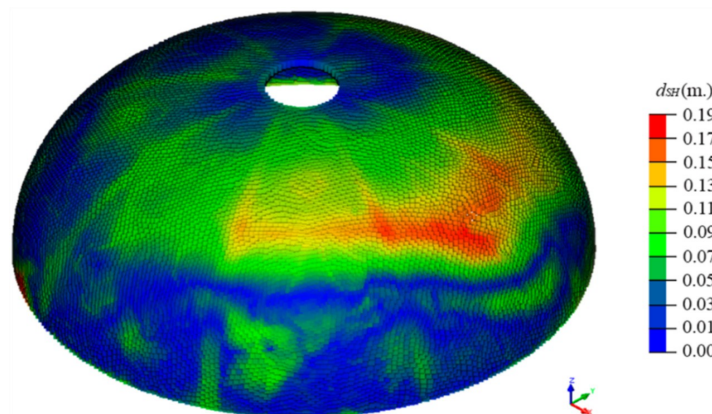


Figure 9. Graphical distribution of the different considered symmetrical Hausdorff distance (d_{SH}) (expressed in m) for the base model.

Finally, and considering GHm_s and LHm_s as the robustness indexes, a manual calibration was carried out, according to the established lower and upper bounds (Table 6) (Figure 10). According to [36], which provides a range of mechanical properties for historical masonry constructions, the upper and lower bounds were established with a safety factor of 1.35, since nowadays only visual inspection and geometrical survey are available (without an extensive experimental campaign).

Table 6. Parameters and variables considered during the manual calibration stage.

	Variable	Initial Value	Upper Bound	Lower Bound	Update Value
f_{tj} (MPa)	Masonry tensile strength	0.16	0.20	0.05	0.13
E_i (GPa)	Infill Young Modulus	0.80	1.00	0.05	0.50
E_m (GPa)	Masonry Young Modulus	1.22	0.89	1.33	0.90
β (-)	Shear retention factor	0.20	0.01	0.20	0.15

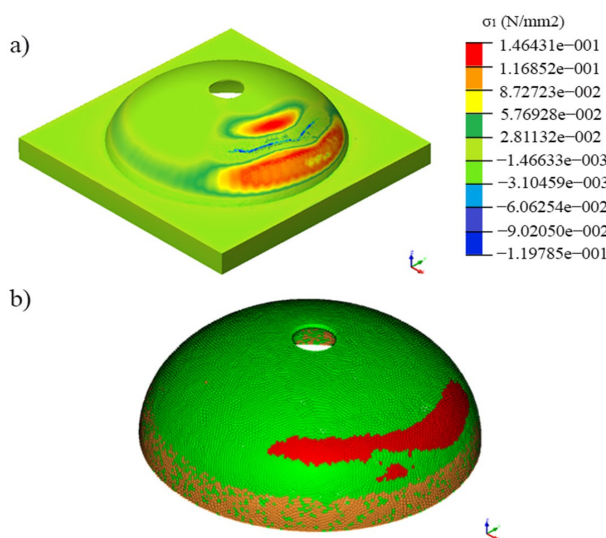


Figure 10. (a) First principal stress distribution, expressed in N/mm2 of the updated model; (b) Geometrical accuracy, in terms of Local Hausdorff metric (LHm_s) of the updated model; in green, values where the geometrical model improves the results, in orange values where no improvements are carried out and in red, areas where the updated numerical model displays worse behavior.

Noteworthy is the presence of a red area (Figure 10). The said phenomenon is associated with the presence of an offset in the spatial distribution of the plastic hinge in comparison to the photogrammetric one. Considering the results provided by the GHm_s and LHm_s indices (Figure 10b) (Table 7), a mild improvement in the geometrical similarity between the photogrammetric and numerical model (Figure 9b) is observable compared with the initial conditions (Figure 10a) and previous studies carried out on the dome [16] (presence of an infill, independent oculus, and manual calibration of the mechanical properties).

On one hand, the obtained numerical results, with a value of GHm_s of 7.40%, are insufficient to study the current stability of the dome based on an initial state model. The discrepancies, derived from the large number of currently unknown variables, call for the use of additional sensors as well as additional experimental campaigns (in laboratory and in field tests).

On the other hand, the causes of the current damage and deformation correspond to the initial one: a local failure of the timber structure (south wing) could be the cause of pathological agents acting on the wood (moisture and biological agents).

In order to understand the current stability of the construction it is required to evaluate it with the actual deformation and damage (cracks). Motivated by this, and given the geometrical and radiometric properties provided by the SfM systems, a geometric strategy is defined below.

Table 7. Comparison between expected and predicted displacement of the considered control nodes.

Control Node	Displacement Obtained (mm)	Displacement Expected (mm)
54	16.56	148.00
20256	22.80	46.00
56	26.10	198.00
21125	31.52	52.00
443	46.19	196.00
64123	38.92	25.00

4.2. Analysis of the Current Stability of the Construction Based on a SfM and NURBs Approach

It should be stressed that the structural evaluation of historical constructions not only implies the assessment of the damage’s causes, but also requires a thorough understanding of the current stability (considering the actual deformation and damage), in order to take efficient restoration actions on the construction and to predict its integrity in case of different events (e.g., earthquakes). With the aim of improving the knowledge of the current stability, with respect to previous studies (Section 3.3 and [16]), a new approach is needed.

Although the point clouds obtained by the previously defined SfM approach, rich in geometric (density and accuracy) and radiometric (photorealistic texture) features, accurately represent the actual state of the construction, it is required to have additional strategies capable of exporting these properties into a numerical environment. The resulting mesh (triangulation of the SfM point cloud) has significant shortcomings to be considered as a suitable CAD/CAM model. Among its deficiencies, the following stand out [37]: (i) High density/resolution, which implies a large number of triangles and (ii) inadequate shapes.

Under the said framework, a methodology able to exploit these features based on the Non-Uniform Rational B-Splines (NURBs) and enhanced by the integration of structural pathologies (such as cracks and lack of material) is proposed. It follows the workflow shown below (Figure 11).

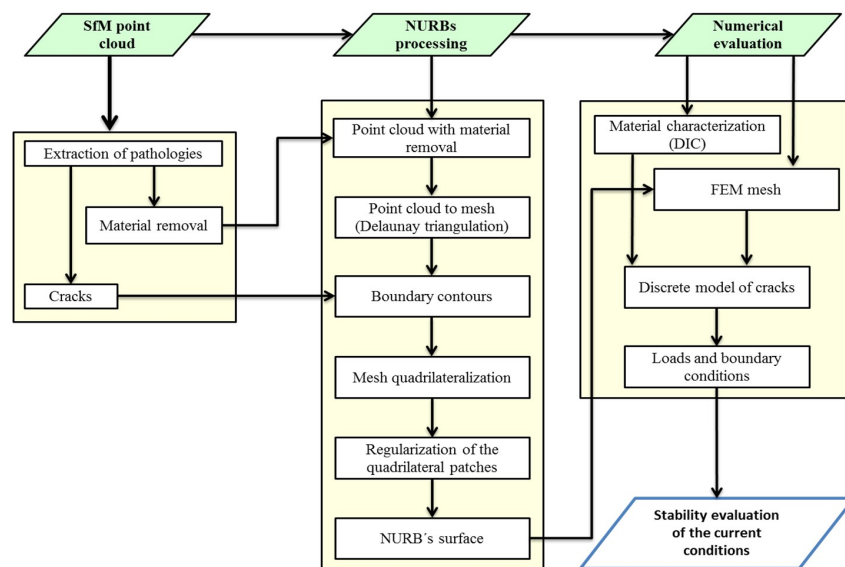


Figure 11. Proposed workflow for the study of the current stability of the construction.

Considering the point cloud as the starting point, this product is firstly meshed by a standard Delaunay triangulation. Usually, these meshes present a non-manifold structure, which implies a low quality product with non-natural triangles which hinder the NURBs' generation. In order to minimize this drawback we use a topological reconstruction, which generates a manifold mesh, based on the approach defined by [38].

Once the mesh has been correctly defined, a region clustering (boundary contours) was carried out, comprising two critical stages. In a first stage the boundary vertex (limits of the construction, lack of material and the absence of an oculus piece) of the mesh are extracted. Later, in a second stage, the cracks are integrated into these boundary contours, through a projection of the observed crack path on the SfM point cloud, as established [9].

After that, a correct representation of these regions by means of NURBS patches is required. For this purpose and in order to build a regular base on which to correctly estimate the parameters of the different regions, a quadrilateralization of the mesh is carried out. This procedure is based on the combination of Morse theory and Spectral mesh analysis according to [37]. This methodology guarantees a complete quadrilateral description of the mesh, with a C^1 (tangential continuity) between neighboring patches, ensuring a continuity along the edges.

Since the construction's surface needs to be fitted using different NURBS regions (quadrilateral patches), a regularization process of these regions is necessary. This procedure comprises several steps [37]: (i) selection of one random border in the considered path and its opposite; (ii) border's regularization using B-Splines with a lambda density; and (iii) matching between points by means of the Fast Marching Method.

Finally, the points obtained by the regularization procedure are used as control points to fit each quadrilateral path to a NURBS' surface. It is worth mentioning, that, in construction elements such as arches, vaults or domes, the acquisition of its extrados (as a point cloud) is not possible in most of the cases, due to the presence of several setbacks (e.g., presence of infill, poor lighting conditions or lack of accessibility). Therefore, this previously shown strategy restricted the analysis of such constructions with the membrane theory (Mindlin-Reissner or Kirchhoff-Love theories). These theories limit the geometry of the numerical model's different elements to a minimum recommended size of ten times the construction's thickness. It implies as well the waste of the geometrical potentialities offered by the previously shown methodology.

Based on what is remarked above, a complementary strategy is proposed; able to estimate the construction's extrados based on its intrados geometry. This methodology is made up of the following stages: (i) decorative elements removal; (ii) normal estimation of the points by means of eigenvalue analysis of the covariance matrix [39]; (iii) translation of each point along the normal direction (with a value equivalent to the construction's thickness); (iv) point cloud meshing based on the Poisson approach and (v) projection of the cracks along its orthogonal direction. As a result, an accurate geometrical model of the construction is obtained with which to evaluate its actual stability (Figure 12).

Regarding the numerical aspect, and for the present case study, an incremental static non-linear FEM was carried out [40]. The material properties and the modelling strategy remain the same as those estimated for the initial model (considering the most appropriate ones) in Section 3.3, including a discrete model of the cracks.

For the present case study, this cracking is modelled considering the residual transversal stiffness (shear strength) through Equation (8). Concerning the normal stiffness, only a contribution in compression was considered, dismissing any contribution to the tensile regime according to Equation (9) (Table 8).

$$K_{t,c} = \frac{G_b G_m}{h_m (G_b - G_m)} \beta_{crack} \quad (8)$$

$$K_{n,c} = \frac{E_b E_m}{h_m (E_b - E_m)} \quad (9)$$

where $K_{t,c}$ and $K_{n,c}$ represent the tangential and normal stiffness respectively; G_b and G_m the shear modulus of brick and mortar, respectively; E_b and E_m the Young modulus of brick and mortar, respectively; h_m the mortar thickness; and β_{crack} the shear retention factor.

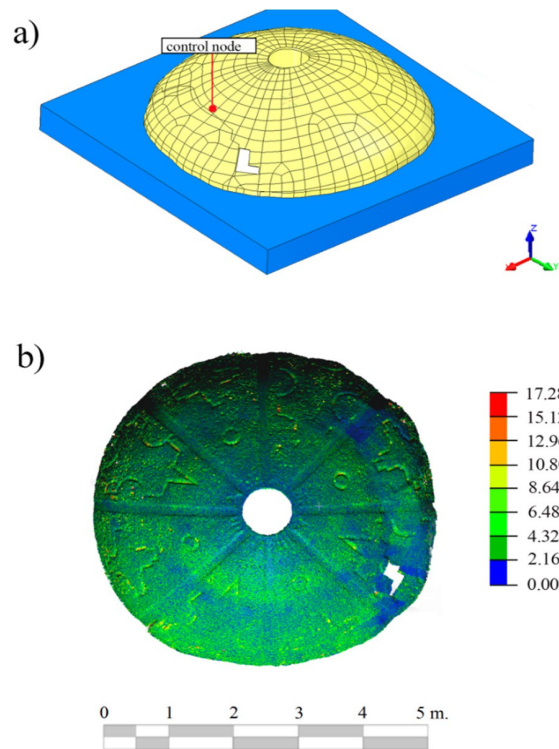


Figure 12. (a) Isometric view of the considered mesh model; (b) Discrepancies, expressed in mm, between the Non-Uniform Rational B-Splines (NURBs) and the photogrammetric models.

Table 8. Mechanical properties considered for the interaction between macroblocks (cracks).

Mechanical Properties of the Cracks		
h_m (mm)	Mortar thickness	15.00
G_b (N/mm ²)	Brick's shear modulus	1.27
G_m (N/mm ²)	Mortar's shear modulus	0.47
β_{crack}	Shear retention factor	$\beta_{c,m}$
$K_{t,c}$ (N/mm ³)	Tangential stiffness	121.88
$K_{n,c}$ (N/mm ³)	Normal stiffness (compression)	49.74

Finally a mesh for the numerical simulation is provided, with a total of 45,350 elements, clustered in: 45,196 high order solid elements and 154 high order interface elements.

For the stability analysis, all the loads acting on the dome (self-weight, infill pressure and asymmetric load) were considered. Afterwards, the estimated safety factor was established as the ratio between the current load and the collapse load obtained in the numerical simulation (Figure 13).

According to the study carried out in the Section 4.1 and the inspection of the SfM point cloud, the collapse mechanisms are mainly due to the formation of plastic hinges in the tensile regime.

The complexity of the model and the uncertainties associated with the variables (e.g., soil properties) require the study of the influence of different mechanical variables in the global stability of the construction, through parametrics analysis.

For these analyses, only the most important mechanical properties (to the tensile regime) were considered, namely: (i) Young modulus; (ii) tensile strength; and (iii) shear retention factor.

It can be observed, that the stability of the dome is mainly conditioned by the mechanical properties of the masonry, rather than the mechanical properties of the infill. Therefore, a safety factor (considering the initial mechanical properties) of 1.23 was established (Figure 13c).

However, it is worth mentioning that only the most important cracks were taken into account. By following a discrete strategy, minor and diffuse cracks were not considered. For this reason further investigation, integrating complementary approaches is necessary in order to obtain a better estimation of the actual stability.

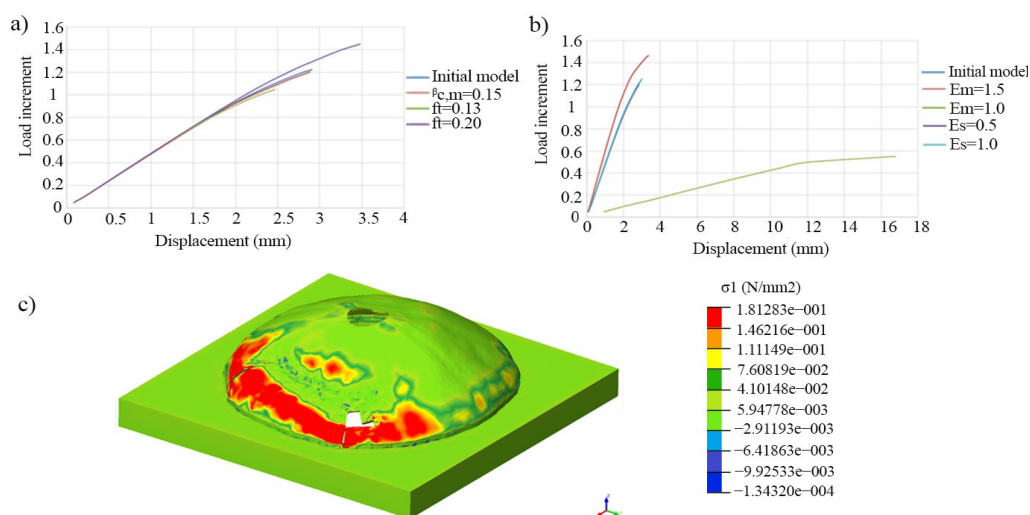


Figure 13. (a) Parametric analysis of different tensile strengths and shear retention factors; (b) Parametric analysis of different masonry and infill's Young modulus; (c) Maximum principal stress (σ_1), expressed in N/mm², at collapse of the initial considered model.

5. Conclusions

Based in the already established photogrammetric techniques of Digital Image Correlation (DIC) and image-based modelling (SfM), and complemented with geometrical (NURBs modelling and Hausdorff distance) and numerical methodologies (FEM), the strategies defined and used in the article allow the needs of structural evaluation of historical constructions to be met.

On one hand, two novel geometric quality indices are introduced and defined, called Global Hausdorff metric or GHm_s and Local Hausdorff metric or LHm_s . They allow to assess globally (GHm_s) and locally (LHm_s) the robustness, in geometric terms, of the obtained numerical model in comparison to the point cloud (deformed shape) of the construction. These indices can calibrate the different variables, based on the geometrical similarity between models acting on the numerical simulation.

On the other hand, with the aim of evaluating the actual stability of the construction and exploiting the geometrical and radiometric components of the obtained products (SfM point clouds), a modelling strategy based on NURBs is proposed. This strategy is able to profit from these properties to obtain an accurate geometrical model (with the actual deformation and damage), that serves as a basis for subsequent numerical analysis.

In order to validate these parameters and modelling methodology, it was applied to a real case study: the dome of the church of San Lorenzo in Sejas de Aliste (Zamora, Spain). Several simulations were carried out to understand the degradation process between the initial and the current state, and to corroborate the viability of the defined robustness parameters with a value of 7.40%, for the GHm_s .

When studying the current construction's stability, through the modelling strategy defined in the article, the results reveal a damaged construction with an estimate safety factor of 1.23.

However, the complexity of the model, the initial state, the absence of comprehensive knowledge of the different construction stages and the need of more experimental campaigns hinder the numerical results and the correct estimation of the safety factor. Taking this into account, further research will focus on the following aspects: (i) dynamical tests; and (ii) a robust calibration procedure (e.g., Non-Linear Square Minimization) based on the geometrical indices defined to enhance the numerical simulation of the dome.

Complementary to this, concerning the used image-based procedures, their potential includes: (i) flexibility (these may be used in the evaluation of mechanical properties of materials as well as geometrical models); (ii) wide range of applications, its use may be extended to other types of constructions such as tunnels or bridges; (iii) non-contact and non-destructive techniques; (iv) low associated cost; and (v) abundance of geometric and radiometric data. However, the methodology has some limitations: (i) the lack of geometrical information in non-visible areas, requiring complementary sensors such as electric tomography or ground penetration radar; and (ii) the model's accuracy, with several millimeters of error, restricting this strategy to constructions with large deformations.

Acknowledgments: Authors would like to thank Remote Sensing and the anonymous reviewers. Also the assistance provided by the University of Vigo and Minho. Authors would also like to thank architect Jose Luis Bordell for his valuable comments.

Author Contributions: All of the authors conceived and designed the study. Luis Javier Sánchez-Aparicio implemented the geometrical methodologies defined in the article. He also evaluated the structural behavior of the construction and carried out the experimental campaigns with the support of Alberto Villarino. Jesús García-Gago investigated the construction, its materials and constructive solutions, and also contributed to the experimental campaign. Luis Javier Sánchez-Aparicio, Alberto Villarino, Jesús García-Gago and Diego González-Aguilera wrote the manuscript.

Conflicts of Interest: The authors declare no conflict of interest.

References

1. Saloustros, S.; Pelà, L.; Roca, P.; Portal, J. Numerical analysis of structural damage in the church of the poblet monastery. *Eng. Fail. Anal.* **2015**, *48*, 41–61. [[CrossRef](#)]
2. Huerta, S. The analysis of masonry architecture: A historical approach: To the memory of professor Henry J. Cowan. *Arch. Sci. Rev.* **2008**, *51*, 297–328. [[CrossRef](#)]
3. Riveiro, B.; Solla, M.; de Arteaga, I.; Arias, P.; Morer, P. A novel approach to evaluate masonry arch stability on the basis of limit analysis theory and non-destructive geometric characterization. *Autom. Constr.* **2013**, *31*, 140–148. [[CrossRef](#)]
4. Heyman, J. *The Stone Skeleton: Structural Engineering of Masonry Architecture*; Cambridge University Press: Cambridge, UK, 1997.
5. Ramos, L.F.; Aguilar, R.; Lourenço, P.B.; Moreira, S. Dynamic structural health monitoring of Saint Torcato Church. *Mech. Syst. Signal Process.* **2013**, *35*, 1–15. [[CrossRef](#)]
6. Lourenço, P.B. Recent advances in masonry modelling: Micromodelling and homogenisation. *Multiscale Model. Solid Mech. Comput. Approaches* **2009**, *3*, 251–294.
7. Milani, G.; Simoni, M.; Tralli, A. Advanced numerical models for the analysis of masonry cross vaults: A case-study in Italy. *Eng. Struct.* **2014**, *76*, 339–358. [[CrossRef](#)]
8. Del Pozo, S.; Herrero-Pascual, J.; Felipe-García, B.; Hernández-López, D.; Rodríguez-González, P.; González-Aguilera, D. Multi-sensor radiometric study to detect pathologies in historical buildings. *Int. Arch. Photogramm. Remote Sens. Spat. Inf. Sci.* **2015**. [[CrossRef](#)]
9. Sánchez-Aparicio, L.J.; Riveiro, B.; González-Aguilera, D.; Ramos, L.F. The combination of geomatic approaches and operational modal analysis to improve calibration of finite element models: A case of study in Saint Torcato Church (Guimarães, Portugal). *Constr. Build. Mater.* **2014**, *70*, 118–129. [[CrossRef](#)]
10. Villarino, A.; Riveiro, B.; Gonzalez-Aguilera, D.; Sánchez-Aparicio, L. The integration of geotechnologies in the evaluation of a wine cellar structure through the finite element method. *Remote Sens.* **2014**, *6*, 11107–11126. [[CrossRef](#)]

11. Hausdorff, F. *Felix Hausdorff-gesammelte Werke Band III: Mengenlehre (1927, 1935) Deskripte Mengenlehre und Topologie*; Springer-Verlag: Berlin, Germany, 2008; Volume 3.
12. García-Gago, J.; González-Aguilera, D.; Gómez-Lahoz, J.; san José-Alonso, J.I. A photogrammetric and computer vision-based approach for automated 3D architectural modeling and its typological analysis. *Remote Sens.* **2014**, *6*, 5671–5691. [[CrossRef](#)]
13. Rodríguez-Martín, M.; Lagüela, S.; González-Aguilera, D.; Rodríguez-González, P. Procedure for quality inspection of welds based on macro-photogrammetric three-dimensional reconstruction. *Opt. Laser Technol.* **2015**, *73*, 54–62. [[CrossRef](#)]
14. Ghorbani, R.; Matta, F.; Sutton, M. Full-field displacement measurement and crack mapping on masonry walls using digital image correlation. In *Advancement of Optical Methods in Experimental Mechanics*; Jin, H., Sciammarella, C., Yoshida, S., Lamberti, L., Eds.; Springer International Publishing: New York, NY, USA, 2014; Volume 3, pp. 187–196.
15. Salmanpour, A.; Mojsilovic, N. Application of digital image correlation for strain measurements of large masonry walls. In *Proceedings of the 5th Asia Pacific Congress on Computational Mechanics*, Queens Town, Singapore, 11–14 December 2013; pp. 11–14.
16. Sánchez-Aparicio, L.; Villarino, A.; García-Gago, J.; González-Aguilera, D. Non-contact photogrammetric methodology to evaluate the structural health of historical constructions. *Int. Arch. Photogramm. Remote Sens. Spat. Inf. Sci.* **2015**. [[CrossRef](#)]
17. Pan, B.; Lu, Z.; Xie, H. Mean intensity gradient: An effective global parameter for quality assessment of the speckle patterns used in digital image correlation. *Opt. Lasers Eng.* **2010**, *48*, 469–477. [[CrossRef](#)]
18. Schweighofer, G.; Pinz, A. Robust pose estimation from a planar target. *IEEE Trans. Pattern Anal. Mach. Intell.* **2006**, *28*, 2024–2030. [[CrossRef](#)] [[PubMed](#)]
19. Bouguet, J.-Y. Camera Calibration Toolbox for Matlab. 2004. Available online: http://www.vision.caltech.edu/bouguetj/calib_doc/ (accessed on 7 August 2015).
20. Pan, B.; Quian, K.; Xie, H.; Asundi, A. Two-dimensional digital image correlation for in-plane displacement and strain measurement: A review. *Meas. Sci. Technol.* **2009**, *20*, 062001. [[CrossRef](#)]
21. Xavier, J.; Fernandes, J.R.A.; Frazão, O.; Morais, J.J.L. Measuring mode I cohesive law of wood bonded joints based on digital image correlation and fibre Bragg grating sensors. *Compos. Struct.* **2015**, *121*, 83–89. [[CrossRef](#)]
22. Pan, B. Bias error reduction of digital image correlation using gaussian pre-filtering. *Opt. Lasers Eng.* **2013**, *51*, 1161–1167. [[CrossRef](#)]
23. Barazzetti, L.; Binda, L.; Scaioni, M.; Taranto, P. Photogrammetric survey of complex geometries with low-cost software: Application to the “G1” temple in Myson, Vietnam. *J. C Herit.* **2011**, *12*, 253–262. [[CrossRef](#)]
24. Pierrot-Deseilligny, M.; de Luca, L.; Remondino, F. Automated image-based procedures for accurate artifacts 3D modeling and orthoimage generation. *Geoinform. FCE CTU* **2011**, *6*, 291–299. [[CrossRef](#)]
25. Rodríguez-González, P.; García-Gago, J.; Gómez-Lahoz, J.; González-Aguilera, D. Confronting passive and active sensors with non-gaussian statistics. *Sensors* **2014**, *14*, 13759–13777. [[CrossRef](#)] [[PubMed](#)]
26. Morel, J.-M.; Yu, G. Asift: A new framework for fully affine invariant image comparison. *SIAM J. Imaging Sci.* **2009**, *2*, 438–469. [[CrossRef](#)]
27. Selby, R.G.; Vecchio, F. *Three-dimensional Constitutive Relations for Reinforced Concrete*; Department of Civil Engineering, University of Toronto: Toronto, ON, Canada, 1993.
28. Freeda Christy, C.; Tensing, D.; Mercy Shanthi, R. Experimental study on axial compressive strength and elastic modulus of the clay and fly ash brick masonry. *J. Civil Eng.* **2013**, *4*, 134–141.
29. Atamturktur, S.; Li, T.; Ramage, M.H.; Farajpour, I. Load carrying capacity assessment of a scaled masonry dome: Simulations validated with non-destructive and destructive measurements. *Constr. Build. Mater.* **2012**, *34*, 418–429. [[CrossRef](#)]
30. Recommendations, Maritime Works. *Geotechnical Recommendations for the Design of Maritime and Harbour Works (ROM 0.5-94)*; Puertos del Estado: Madrid, Spain, 1995.
31. Manie, J.; Kikstra, W.P. *Finite Element Analysis User’s Manual-Release 9.4.4*; TNO DIANA BV: Delft, The Netherlands, 2011.
32. Girardeau-Montaut, D.; Roux, M.; Marc, R.; Thibault, G. Change detection on points cloud data acquired with a ground laser scanner. *Int. Arch. Photogramm. Remote Sens. Spat. Inf. Sci.* **2005**, *36*, W19.

33. Aspert, N.; Santa Cruz, D.; Ebrahimi, T. MESH: Measuring errors between surfaces using the Hausdorff distance. In Proceedings of the IEEE International Conference in Multimedia and Expo (ICME), Lausanne, Switzerland, 26–29 August 2002; Volume 1, pp. 705–708.
34. Alexandre, L.A. Set distance functions for 3D object recognition. In *Progress in Pattern Recognition, Image Analysis, Computer Vision, and Applications*; Ruiz-Shulcloper, J., di Baja, G.S., Eds.; Springer: Berlin, Germany, 2013; pp. 57–64.
35. Wu, J.-M.; Jing, Z.; Wu, Z.; Feng, Y.; Xiao, G. Study on an improved Hausdorff distance for multi-sensor image matching. *Commun. Nonlinear Sci. Numer. Simul.* **2012**, *17*, 513–520. [[CrossRef](#)]
36. Ministero delle Infrastrutture. *Ntc (Nuove Norme Tecniche per le Costruzioni)*; Ministero delle Infrastrutture: Rome, Italy, 2008.
37. Branch, J.W.; Prieto, F.; Boulanger, P. Automatic extraction of quadrilateral patches from triangulated surfaces using morse theory. In Proceedings of the 16th International Meshing Roundtable; Brewer, M.L., Marcum, D., Eds.; Springer: Berlin, Germany, 2008; pp. 199–212.
38. Attene, M. A lightweight approach to repairing digitized polygon meshes. *Vis. Comput.* **2010**, *26*, 1393–1406. [[CrossRef](#)]
39. Schaer, P.; Skaloud, J.; Landtwing, S.; Legat, K. Accuracy estimation for laser point cloud including scanning geometry. In Proceedings of the 5th International Symposium on Mobile Mapping Technology, Padova, Italy, 29–31 May 2007.
40. Milani, G.; Valente, M. Comparative pushover and limit analyses on seven masonry churches damaged by the 2012 Emilia-Romagna (Italy) seismic events: Possibilities of non-linear finite elements compared with pre-assigned failure mechanisms. *Eng. Fail. Anal.* **2015**, *47*, 129–161. [[CrossRef](#)]



© 2016 by the authors; licensee MDPI, Basel, Switzerland. This article is an open access article distributed under the terms and conditions of the Creative Commons by Attribution (CC-BY) license (<http://creativecommons.org/licenses/by/4.0/>).

CAPÍTULO IV

PRACTICAL USE OF MULTISPECTRAL TECHNIQUES FOR THE DETECTION OF PATHOLOGIES IN CONSTRUCTIONS.

RESUMEN: Evaluadas las patologías de carácter geométrico (tales como los agrietamientos y deformaciones), el presente Capítulo trata de ampliar el campo de actuación tratado. Moviéndose hacia enfoques capaces de explotar el carácter radiométrico de los sensores geomáticos y ampliar así la caracterización patológica.

Si bien tradicionalmente el concepto de análisis multiespectral está ligado a un análisis de un único sensor que opera en diferentes longitudes de onda. El presente capítulo tratara de explotar los datos provistos por varios sensores. Para ello y tras una correcta toma de datos (considerando una red previamente planificada), se procederá a la segmentación, ortorectificación y registro de los datos radiométricos. Tras dicho registro, diversos clasificadores (Fuzzy k-medias y Máxima Vecindad) son empleados para agrupar los píxeles en diferentes clases informacionales. Por último, se emplearán diversos índices estadísticos (e.j. Kappa de Cohen, matriz de confusión, etc.) para evaluar la robustez de los resultados obtenidos.

Resultado de la actividad investigadora ejecutada en el presente capítulo, diferentes conclusiones pueden ser extraídas: (i) los sistemas de clasificación multiespectral permiten detectar y cuantificar patologías no cuantificables por procedimientos geométricos; (ii) una correcta planificación y pre-procesado de imágenes y nubes de puntos son aspectos críticos a considerar; (iii) aunque ha sido posible detectar humedades, algas, mohos, etc. se requiere de una mayor variedad de sensores para aumentar la separabilidad de las clases informacionales a extraer.

Palabras clave: Kapa de Cohen, Precisión global, Separabilidad, Clasificación supervisada, Clasificación no-supervisada, Corrosión por cloruros, Caracterización de material, Acción biológica, Construcción histórica, Infraestructura civil de hormigón armado.

Chapter 13

Practical Use of Multispectral Techniques for the Detection of Pathologies in Constructions

*L.J. Sánchez-Aparicio, S. Del Pozo, P. Rodríguez-Gonzálvez,
J. Herrero-Pascual, A. Muñoz-Nieto and D. González-Aguilera*

*Department of Cartographic and Land Engineering, High School of Ávila,
University of Salamanca, Ávila, Spain*

D. Hernández-López

*Regional Development Institute-IDR, University of Castilla-La Mancha,
Albacete, Spain*

Abstract

Our approach to multispectral remote sensing assessment of constructive pathologies has been organized in two different parts. The first one ([Chapter 7](#)) dealt with equipment and methods. The second one, developed in this chapter, will be related to the application to real cases, encompassing relevant aspects such as: data acquisition (sensor type choice and field works planning), processing (filtering and segmentation), sensor registration, true orthophoto generation, orthophoto classifications (through supervised and unsupervised techniques) and the qualitative and quantitative analysis of results (by means of confusion matrix, spectral separability, overall accuracy, reliability and agreement of informational classes). Based on these premises three case studies have been addressed. On the one hand, two historical stone masonry constructions and on the other hand one modern reinforced concrete construction. These three case studies will be used as examples of best practices in multispectral dataset management and processing, and will serve to evaluate the flexibility of the methodology proposed for detecting and classifying accurately a wide range of constructive pathologies.

13.1 Introduction

[Chapter 7](#) addressed, from a theoretical point of view, a study of instrumentation and methods to process multispectral datasets of different building elements. This chapter will describe and analyze a selected group of experiences resulting from the application of such methodologies in two of the most significant civil engineering fields such as cultural heritage constructions and buildings and civil infrastructures.

Safeguarding and enhancement of the built heritage can be considered a fundamental feature for modern developed societies. Sometimes by its own intrinsic value, and also for its artistic or cultural value, preservation of these types of constructions becomes extremely important. Due to their unique nature or their fragility it is necessary to know thoroughly their geometric and structural characteristics and, where appropriate,

254 NDT for the Evaluation of Structures and Infrastructure

provide information to establish intervention plans based on a comprehensive diagnosis and assessment of their pathologies. Experience in conservation and restoration projects highlights the need to use non-destructive techniques to acquire required datasets. This fact restricts the use of some techniques and sensors.

The exposure to chemically aggressive environments, moisture or biological organisms produces deteriorations that usually worsen over time. This situation is especially pronounced in constructions and old buildings. However, modern buildings and civil infrastructures that use different materials and construction techniques also suffer different types of deterioration.

The case studies submitted below have been selected within a broader set of experiences developed by the research group TIDOP (Armesto-González et al. 2010, Crespo et al. 2010, Del Pozo et al. 2015, González-Jorge et al. 2012, Rodríguez-González et al. 2013), which belongs to the University of Salamanca (<http://tidop.usal.es>), in order to offer a wide casuistry applying multispectral data in diagnosis and assessment of pathologies in constructions.

Following a common structure, the next items will be addressed in each case study:

- Description and building materials: after a brief introduction of the case study, a broad description of materials and construction technics will be done.
- Pathological assessment: as a result of the constructive elements analyzed, a brief description of the expected pathologies will be assessed.
- Sensors and methods: under these paragraphs the characteristics of the used sensors and the methodology applied in the data process will be explained.
- Experimental results: these paragraphs will show, by means of graphics and statistical analysis, an objective assessment of the followed methodology. The main issues to be considered in the analysis of multispectral images are: (i) Separability; (ii) Cohen's Kappa coefficient; (iii) Overall accuracy; and (iv) Comparative study between supervised and non-supervised classifications.

The following table (Table 13.1) synthesizes the technical specifications of the sensors that have been used. The next figure (Fig. 13.1) shows, schematically, the workflow applied to data processing, which is common for most cases.

To complete this chapter, a best practices guide, derived from case studies, will be presented in the conclusion section.

13.2 First Case Study: Ribeiriño Bridge (Ourense, Spain)

13.2.1 Description and Building Materials of the Ribeiriño Bridge

Located in Ourense county (northern Spain), Ribeiriño bridge (Fig. 13.2) is a key to the communication network between the cities of Santiago of Compostela and Madrid (capital and largest city of Spain). Predominantly built in reinforced and pre-stressed concrete (arc, abutments, bearings and piers) following the Spanish standard EH-68 (Ministerio de Fomento 1968). The construction entered in service in 1971.

Set in an environment with high level of humidity and under an average rainfall of 880 mm/yr, the bridge is 147 m long and it is supported by several piers along its structure. In the central span, these constructive elements are supported by a parabolic

Practical Use of Multispectral Techniques for the Detection of Pathologies 255

Table 13.1 Technical specifications of the sensors used in the case studies.

		Trimble GX200	FARO Photon 80	Riegl LMS z390i
Active sensors	Measuring principle	Time of flight	Phase shift	Time of flight
	Wavelength	534 nm (green)	785 nm (VNIR)	1,550 nm (SWIR)
	Radiometric resolution	8 bits	11 bits	8 bits
	Deflection system	Oscillating flat mirror	Rotating mirror	Rotating mirror
	Field of view	360° H 60° V	360° H 320° V	360° H 80° V
	Standard deviation	1.4 mm for $D \leq 50$ m	2 mm for $D = 25$ m	6 mm for $D \leq 50$ m
	Range of measurement	2–350 m	0.60–76 m	1.50–400 m
	Angular resolution	Azimuth: 12" Zenith: 14"	Azimuth and Zenith: 33"	Azimuth and Zenith: 3.6"
	Beam divergence	3 mm to 5 m	0.16 mrad	0.3 mrad
	Scan speed (p/s)	5,000	120,000	11,000
		Nikon D200	Nikon Coolpix L11	
Passive sensors	Camera type	Single-lens reflex camera	Compact digital camera	
	Sensor type	CCD	CCD	
	Sensor size	23.60 × 15.80 mm	5.76 × 4.29 mm	
	Pixels	2872 × 2592	2816 × 2112	
	Radiometric resolution	12 bits	8 bits	
	Focal length	18 mm	6.2 mm	
	Max aperture	3.5	2.8	

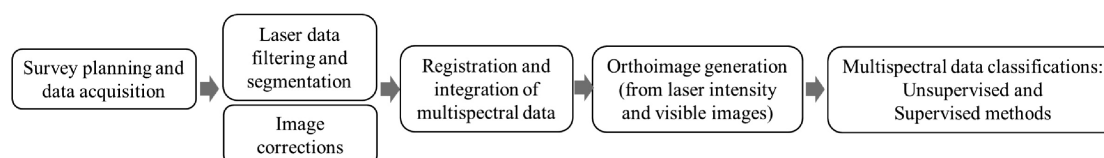


Figure 13.1 Workflow of the methodology proposed.

concrete arch. While the lateral spans (with a rectangular shape) are supported on several piers.

13.2.2 Pathologies of the Structure

Considering the environmental conditions previously defined: (i) High humidity on a cyclic basis; (ii) Concrete exposed to water contact; (iii) Presence of carbon dioxide; (iv) Possible attack of melting salts, the main pathological agent to be expected was the carbonation corrosion. It can be also considered, to a lesser extent, to be chloride corrosion given the presence of a marine environment.

Although they have different origins, both corrosive processes, cause similar degrading result in concrete. For a better understanding, the concept of the steel passivation process should be reviewed.



Figure 13.2 Pier of the Ribeiriño bridge.

Passivation involves the formation of an inert film with a high pH (12.6–14) as a result of the hydration of Portland cement, in particular the calcium hydroxide component, forming the passive layer (physical protection against chemical aggressions).

Although this layer masks the steel against the action of external agents, the corrosion (presence of carbon dioxide and chloride) can promote the removal of this protective layer. As a consequence of its removal, a low pH environment is created and the steel is exposed to oxidation, causing a volume increase. This increase leads to the detachment of concrete areas and loss of mechanical adherence between steel and concrete. Complementarily, the presence of high levels of moisture, oxygen and a suitable temperature facilitates the growth of biological organisms on the bridge.

As a result of the different chemical attacks (mainly corrosion), the concrete durability is conditioned by the penetration of the several agents and the speed at which is attacked. Causing a decomposition of the elements and a loss of mechanical adherence between the steel and concrete.

To sum up two different pathologies will be expected:

- Biological colonization
- Moistures that can lead to corrosion by carbonation and chloride.

13.2.3 Materials and Methods

Considering the two pathologies mentioned above, it was decided to make a comparative multispectral study. To do this, we worked both with the radiometric results provided by the terrestrial laser scanner Riegl LMS z390i, in the SWIR range of the electromagnetic spectrum, and the photographs taken with a Nikon D200 camera built into the scanner (see Table 13.1).

The joint use of the laser scanner and the built in camera not only gives us an ideal 3D scene reconstruction. After a proper parallax-baseline correction, we can get a

true orthoimage with four multispectral channels (R, G, B and SWIR) increasing the spectral resolution of the study with the consequent enrichment in the pathological surveying of the bridge's pier.

The proposed methodology, which consists of several stages as shown in [Figure 13.1](#), focuses on automation as a basic guideline to detect pathologies. Next, the procedures followed and its main characteristics are explained:

Planning and data acquisition. To carry out a proper data acquisition and to facilitate subsequent data process and orthoimage creation, the laser scanner was placed and leveled just once, 9 to 17 m far from the bridge. The spatial resolution achieved at this distance was 10 mm. Data acquisition was managed by Riscan Pro software, taking first data from laser intensity and then photographs in the selected area.

Filtering and segmentation. The first step of data processing consisted of point cloud filtering and segmentation of a selected area in which a great number of pathologies are presented, excluding all other irrelevant areas in the case study.

Data corrections. The separation of each RGB image in three different images (coming from red, green and blue channels), was performed through the free software DCRaw (Coffin 2011) by means of the Bayer demosaicing filter. As a result three images (1436×1296 pixels) were obtained.

Orthoimages generation. Once we have three separated images as mentioned above, and the SWIR one, coming from laser scanner, we obtained four orthoimages with Riscan Pro. Firstly, the orthoimage from the point cloud data, which incorporates intensity values in the SWIR range, was generated by the orthogonal projection of points in a plane parallel to the bridge structure. Then, to generate orthoimages in R, G and B channels the external camera orientation parameters with respect to the coordinate system of the laser model were obtained (registration). This step involves identifying and pointing out singular points in the images and the laser model. For this purpose we used external targets previously attached to the bridge. Finally, the projection of the points was performed using the collinearity condition (see [Chapter 7](#)). The final resolution of the orthoimages was 30 mm.

Multispectral data classification. The classification of these two groups (SWIR and SWIR+RGB) of orthoimages encloses a first *fuzzy k-means* unsupervised classification and a second *maximum likelihood* supervised classification:

- Unsupervised classification: the unsupervised classification algorithms based on the k-means approach is the most commonly used. It classifies a given data set in a certain number of clusters that are previously fixed. Within k-means algorithms, *fuzzy k-means* is one of the most frequently used. *Fuzzy k-means* give a specific weighting to each data associated with the inverse distance to the cluster's center.
- Supervised classification: the *maximum likelihood* classifier is the most complex, robust and reliable supervised algorithm, as it is closely based on the original data distribution. It considers that the radiometry (digital levels) of each category follows a normal distribution. It allows describing each category by a probability function from the mean vector and variance-covariance matrix. In this way, it is possible to calculate the probability that a given pixel belongs to a category.

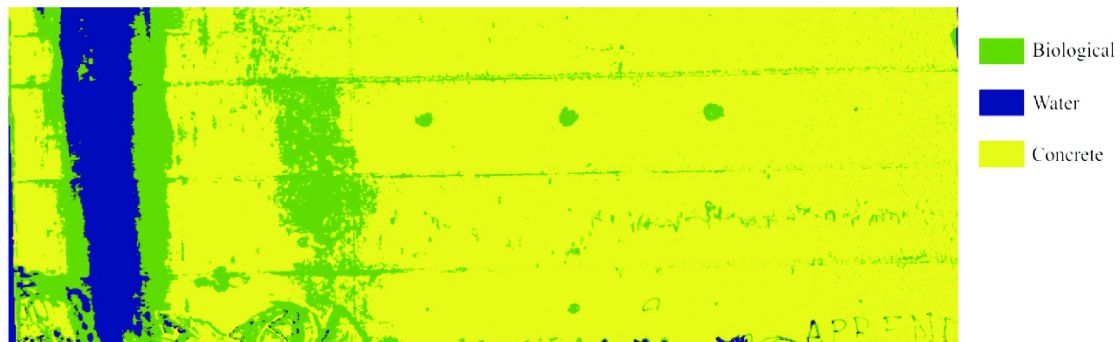


Figure 13.3 Supervised classification based on fuzzy *k-means* algorithm: SWIR (Laser) + RGB (Camera).

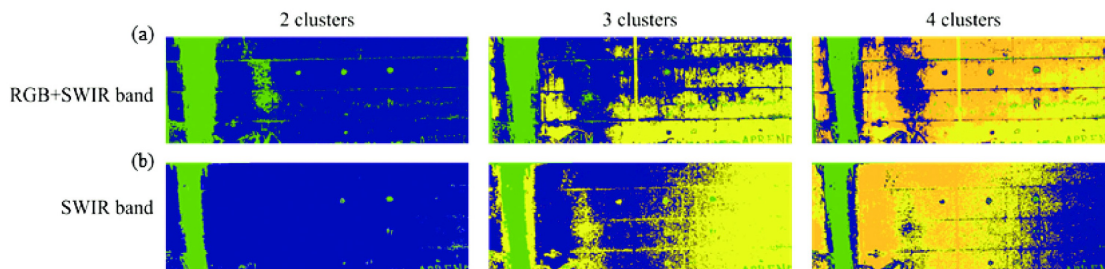


Figure 13.4 Unsupervised classification: (a) RGB + SWIR channels. (b) SWIR channel.

13.2.4 Experimental Results

At this point we must remember that the aim is to achieve an automatic process. This aim implies that the classification methodology should be a non-supervised classification one, which should be as close as possible to the ideal of a supervised process (which will act as a reference).

The supervised classification process, where user intervention to define training areas is required, was performed using the *maximum likelihood* algorithm (Fig. 13.3). For this purpose three informational classes were used, generating a Cohen's Kappa coefficient (Cohen 1968) of 0.97787.

The high value of Cohen's Kappa coefficient suggests good results in the classification process, but as seen in Figure 13.3, there are informational errors arising from classes not taken into account such as graffiti or drain pipes, where the presence of shadows generates several confusions. This fact reveals the limitations of the workflow based on the use of four channels, workflow applied in the discretization of informational classes that were not considered in the initial study.

Looking for the maximum possible automation, application of an unsupervised mono-channel classification (*fuzzy k-means*) (Fig. 13.4b) gives a biased result where clusters have no direct equivalence to informational classes (Fig. 13.3).

A four channels unsupervised *fuzzy k-means* classification (SWIR + RGB) gives better results (Fig. 13.4a). Using four clusters and applying an aggregation process to

guarantee the equivalence between clusters and informational classes, results are closer to the reality.

The quality assessment of the latest automated (non-supervised classification) results, contrasted with supervised process, shows an overall accuracy of 90.89%. The major errors come from the wrong assignment of concrete to biological class, and biological to water class. This second error has less effect because both classes represent aggressive pathologies for concrete, revealing the presence of moisture on it.

We can conclude that in a practical approach, when a general detection of pathologies is required, and the speed of data acquisition becomes important, a strategy based on the use of two sensors (active and passive) provides valid results in a completely automatic process. Moreover, from data acquired we can manage a metric 3D model of the construction.

13.3 Second Case Study: Santo Domingo Ruins (Pontevedra, Spain)

13.3.1 Description and Building Materials of the Santo Domingo Ruins

Popularly known as the “Ruins of Santo Domingo”, which was once a Dominican monastery, is one of the most interesting historical-artistic properties of the Spanish north. The presence of tombs, heraldic shields and altarpieces rich in detail, unique and fragile, increases the value of the construction (Porto 1993). Built in granite, the beginning of its works dates from the first third of the XIV century. During its construction period, the monastery suffered different reforms, with the expansion of monastic stays. Nevertheless, the current building retains the main characteristics of the local Dominicans monasteries (Fig. 13.5).

Nowadays, the poor state of conservation of the different construction elements, together with the existence of biological colonization, loss of material, cracking and continuous leaks on the apses, expose this construction to a continued degradation process.

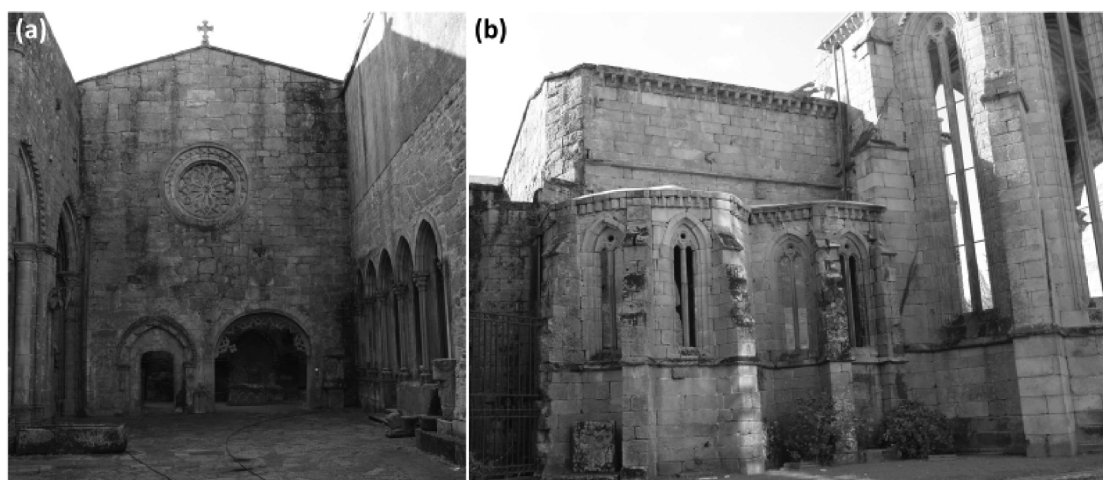


Figure 13.5 Santo Domingo ruins: (a) Front view of the façade. (b) Lateral view of the ruins.

260 NDT for the Evaluation of Structures and Infrastructure

The main construction material is the two-mica granite (at least in the area of the monastery ruins) (Montejo Santos et al. 2014). Such material was used to form the different masonry elements along the monastery. The different blocks were joined by lime mortar and complemented by underpinning rubbles.

For the artistic elements, the high level of biological colonization hinders the identification of the granite. It should be noted that the presence of accumulations of dark minerals (biotite and turmalita), with oxidation strips (iron oxide-hydroxides) gives a characteristic brown-rusty tone (Fig. 13.5).

13.3.2 Pathologies of the Structure

Subject to a wide variety of biological, atmospheric and structural degradation agents, the Santo Domingo ruins are an artistic-cultural property in an advanced state of degradation. Within the wide range of pathologies present in the building, the following degradation processes are expected to be detected:

- Efflorescence (white layer): given the presence of soluble salts, due to environmental conditions, mortars used in the restoration process, decorative materials employed in the different constructive elements or by capillary rise from the ground. This pathological effect starts with the crystallization of the salts, outside or into the material, causing a wedge effect (expansion) which degraded the material properties.
- Biological activity: materialized with the presence of moss, lichens, algae, plants with stem and remains of metabolic activity on the construction. This pathology causes a degradation of the mortar and rocks present on the different constructive elements (chemical erosion and fracture).
- Damp spots: on the pavement and walls, caused mostly by capillary rise. They are also visible on the ledges of the construction as a result of different runoffs.
- Crusts (black color): they appear throughout the building, their origin can be attributed to: (i) Biological colonization; and (ii) Contamination from urban activity. Both causes create dark color crusts with different grip levels on the affected area.

13.3.3 Materials and Methods

Although there are several tests capable of detecting damage, caused by different pathological agents, in the construction (e.g. X-ray diffraction, microscopes or chemical assays) (Montejo Santos et al. 2014), it is required to provide a quantification procedure, as was explained in the previous case study. Due to the characteristic of the construction, and the needed of a geometrical monitoring, the terrestrial laser scanner was the a priori best solution. Complementary to the geometrical data captured by this sensor, the radiometric information was employed, in order to carry out a multispectral image classification procedure.

Since the main goal of the present chapter is focused on the pathological detection by the radiometry captured by the different sensors used, the geometrical processing was omitted. For the present case study, and given the variety of pathologies presented, four sensors (three terrestrial laser scanners and a visible camera) were used. On the one hand, and in order to capture the visible spectrum, a time of flight

Trimble GX200 laser scanner (Green-534 nm) and a Nikon D200 digital camera were utilized. On the other hand and with the purpose of acquiring the near (NIR) and medium (SWIR) infrared spectrum, a FARO Photon (785 nm) and Riegl LMS z390i (1,550 nm) laser scanners were used (to see more about its technical specifications see [Table 13.1](#)).

As shown [Figure 13.1](#), the methodology followed for the acquisition and evaluation of the results comprise a total of five stages, as explained below:

Planning and data acquisition. Prior to data collection, a visual inspection was performed to evaluate the different pathologies presented in the construction. Also it was to assess the accessibility and restrictions in the area. Additionally to the localization and the value of the construction, the environmental conditions were considered (e.g. high probability of rain and high humidity).

During the data acquisition process, the different laser scanners used were placed according to a plan previously prepared and at a distance from the façade between 5–10 m getting thirty one point clouds with a 10 mm of spatial resolution. This process was assisted by different software: Realworks Survey for Trimble, Scene 3D for Faro Photon 80 and Riscan Pro for Riegl LMS z390i. The number of scan stations was selected according to the different technical specifications provided by the manufacturer ([Table 13.1](#)).

Filtering and segmentation. Applied after data gathering, this stage comprises the filtering (denoising) and registration of the different point clouds. For the point clouds the alignment was considered the ICP (Iterative Closest Point) strategy.

Data corrections. Encloses the images demosaicking, since the camera used in this work utilizes a Bayer filter. For more details about this process consult the previous case study.

Orthoimages generation. For each point cloud registered, an orthoimage was generated providing a total of six channels: Four orthoimages in the visible range (R, G1, G2_{Trimble} and B) and two in the infrared (NIR and SWIR) one. Taking the advantage of the registration performed in the previous step (with the different point clouds captured) the orthoimages were generated (see previous case study). As result 10 mm resolution images were obtained.

Multispectral data classification. The multispectral dataset, evaluated in the present case study, enclose a total of six orthoimages. A *fuzzy k-means* algorithm was used in the unsupervised classification (for more details see the previous case of study). Also a supervised classification was required with the aim of improving the results, by the addition of informational classes introduced by an expert.

13.3.4 Experimental Results

Starting from the geometrical base, provided by the orthoimage previously defined (with 10 mm of spatial resolution), the main goal now is the pathological clustering identification (in contrast to the material classification which is not considered). For this purpose an initial analysis (non-supervised) classification was carried out. Six informational classes were considered and a *fuzzy k-means* algorithm was used. The results of this process are shown in [Figure 13.6](#), considering the following classes: (i) Granite without pathological affections; (ii) Pathologies arising from water (dampness) and

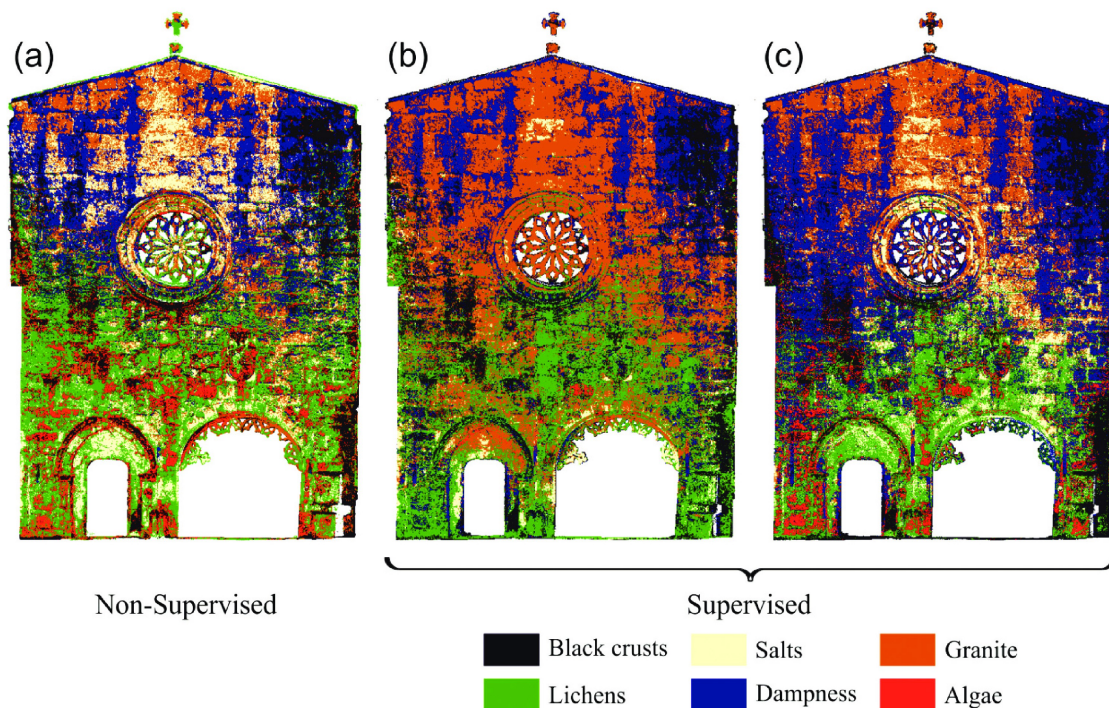


Figure 13.6 (a) Non supervised classification with merged classes. (b) Supervised classification with six channels. (c) Supervised classification with three channels (only active sensors).

salts; (iii) Two types of biological elements (lichens and algae); and (iv) Pathologies of decay (black crusts). Despite this initial study, the unsupervised classification, with six clusters and the employment of *fuzzy k-means* algorithm, fails to yield results close to real ones, even using all available channels.

Given the large variety of pathological processes presented in this construction, and some of them with similar origin (algae-lichen), the resulting analysis shows a radiometric overlap. Therefore it was required to increase the number of clusters to improve the separability between classes.

In order to enhance the unsupervised classification performance, it was necessary to establish an aggregation process (merge phase) attended by the user. The main goal of this process is to approximate the new clusters to the informational class showed in Figure 13.6a. This process is applied to the Biological colonization, moss and lichen classes, shown in Section 13.3.2.

Despite the aggregation process, classification results are far from optimal, with an overestimation of the affected areas by the pathological processes. The greatest variations were shown between biological agents. In view of the obvious errors occurring in the non-supervised process, it was necessary to use a supervised approach based on a *maximum likelihood* algorithm. Six classes, from the initial hypothesis and the six channels available, were considered in this classification process (Fig. 13.6b). Results (Table 13.2) show an overall accuracy of 0.8844 and a Cohen's Kappa coefficient of 0.8157 (excluding the null class).

Practical Use of Multispectral Techniques for the Detection of Pathologies 263

Table 13.2 Supervised classification: confusion matrix with six channels.

	Black crusts	Lichens	Salts	Dampness	Granite	Algae
Black crusts	15.16%	0.18%	0.00%	1.73%	0.02%	0.02%
Lichens	0.02%	4.03%	0.02%	0.00%	0.02%	0.02%
Salts	0.00%	0.00%	1.44%	0.00%	0.02%	0.00%
Dampness	1.17%	0.25%	0.00%	17.29%	1.97%	0.04%
Granite	0.08%	1.52%	0.25%	4.17%	50.17%	0.06%
Algae	0.00%	0.00%	0.00%	0.00%	0.00%	0.35%

Table 13.3 Supervised classification: confusion matrix with five channels.

	Black crusts	Lichens	Salts	Dampness	Granite	Algae
Black crusts	15.01%	0.37%	0.00%	1.70%	0.00%	0.02%
Lichens	0.10%	3.98%	0.00%	0.02%	0.02%	0.02%
Salts	0.00%	0.02%	1.44%	0.00%	0.00%	0.00%
Dampness	1.13%	0.74%	0.00%	16.65%	2.18%	0.04%
Granite	0.14%	1.95%	0.31%	4.33%	49.41%	0.06%
Algae	0.00%	0.00%	0.00%	0.00%	0.00%	0.35%

Since the black crusts were associated to the granite decay caused by a granular disintegration due to the presence of dampness and/or soiling, there was a class overlap as shown in Table 13.3. In a similar way, the high level of deterioration of the façade (approx. half of it is affected by some kind of pathology) hindered the granite discretization for the different wavelengths.

Regarding the wavelengths and the overlap between green channels (Trimble GX200 and visible camera), the results provided by classifications carried out with five (excluding passive green channel) and six channels had a similar efficiency (Table 13.2 and Table 13.3).

Evaluating the statistical results, it is possible to observe a slight decline. The overall accuracy and Kappa coefficient go down to 0.8684 and 0.7916 respectively. This decline hardly has a negative effect on the final result, from a qualitative point of view. This change has its origin in the slight variations (during the classification) between lichens-dampness and lichens-granite classes. For the algae class any variation was observed given its spectral signature, with high variations in the visible zone (manifested through red/orange tonalities).

Classification results derived from the independent use of the active channels, three in total (Fig. 13.6c) corresponding with the different laser scanner used, seem to be insufficient. With an overall accuracy of 0.7526 and a Cohen's Kappa coefficient of 0.6367 (Table 13.4) this classification cannot be considered as the best one. It may lead to the wrong considerations for later restoration actions.

For these purposes, sensor hybridization was applied considering two classifications: (i) Five channels classification (three from the active sensors and two from the red and blue channel of the camera) and (ii) Six channels classification (adding to the previous channels clustering the green channel of the camera). As a result of this hybridization the classification improved (Table 13.2 and Table 13.3).

264 NDT for the Evaluation of Structures and Infrastructure

Table 13.4 Supervised classification: confusion matrix with three channels.

	Black crusts	Lichens	Salts	Dampness	Granite	Algae
Black crusts	14.92%	0.31%	0.00%	1.71%	0.00%	0.16%
Lichens	0.14%	2.84%	0.10%	0.02%	0.02%	0.97%
Salts	0.00%	0.27%	1.01%	0.00%	0.18%	0.00%
Dampness	0.95%	0.88%	0.08%	16.15%	2.32%	0.39%
Granite	0.08%	3.74%	6.55%	5.10%	40.02%	0.76%
Algae	0.00%	0.00%	0.00%	0.00%	0.00%	0.33%

Also there is a remarkable worsening in the unaffected material classification, since the granite used in this construction presents a heterogeneous texture, with large variations in the grain size and mineral distribution, requiring for instance an expansion in the number of channels used or the use of an additional algorithm based on spatio-contextual classification techniques (Li et al. 2014), in order to have an optimal result.

As shown in the results (Table 13.2 and Table 13.3), the addition of redundant channels, with overlapping (in terms of spectral signatures) areas, did not generate significant improvements. Regarding the use of channels from the cameras, despite having a bad radiometric resolution, they achieve better classification results in areas with several classes (that need to be classified), even without the presence of large pathologies on it.

13.4 Church of San Pedro Case Study (Avila, Spain)

13.4.1 Description and Building Materials of the San Pedro Church

The historical and cultural heritage of the city of Ávila is famous mainly due to its variety of medieval constructions both religious and civil in origin. Within this wide range of buildings the predominant use of granite masonry is certainly highlighted.

It is worth to noting that the construction material depended on its availability close to the working area. The presence of a granite deposit in the village of “La Colilla”, just a few kilometers from the city, served as a quarry for the extraction of this construction material for buildings.

Much of the appeal of this heritage architecture lies in the wide variety of types of granites present in this quarry. A total of 5 granite varieties can be recognized and all of them have been used as building material in historical constructions in Ávila (Molina Ballesteros 1993): (i) Unaltered grey coarse-grained granite; (ii) Unaltered grey fine-grained granite; (iii) Ochre granite; (iv) Red granite and (v) White granite. Each of the three latter granite types is the result of several alterations produced during the Iberian Hercynian Base and presents its own physical and mechanical properties that were considered in the multispectral analysis.

The church of San Pedro is located in the old big market square devoted to Santa Teresa, facing the medieval door of the Alcazar, and is one of the most characteristic monuments of Romanesque architecture in the city. With a cross-shaped layout, it consists of three naves with five sections topped by three apses. It has a recognized dome base and a tower in the northern arm of the transept.

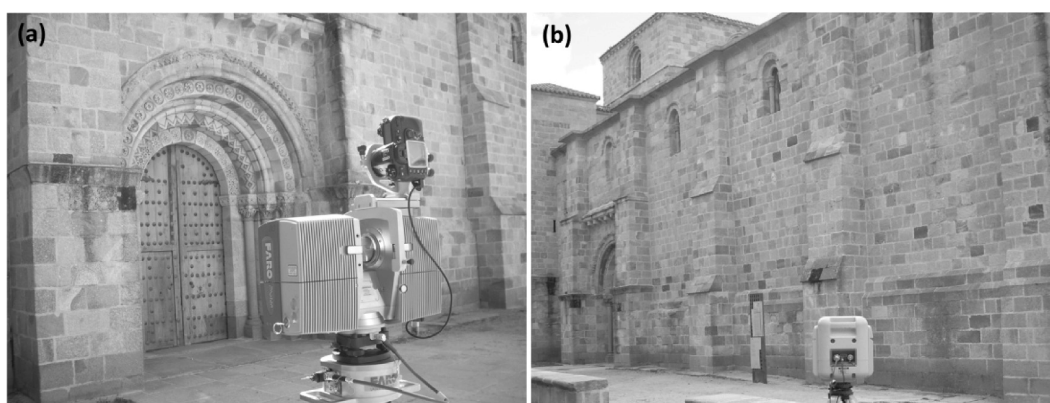


Figure 13.7 Church of San Pedro: (a) Detail view of the north entrance. (b) General view of the north façade (Flórez García, 2009).

Here, the different granite types of masonry combined on the façade are generally assessed (Fig. 13.7):

- The main façade (westward orientation): consists of a plinth and buttress of grey granite blocks. The use of this constructive solution in the upper archivolts and the pinnacles should be highlighted. The rest of the façade is built with ochre and red granite blocks.
- The eastern façade: consisting, similarly to the main façade, of a grey granite plinth (variable in height) and walls with ochre and red granite blocks.
- The north façade: slightly different from the rest, presents a red granite plinth and the rest of the elements are erected with ochre granite as predominant construction material.
- The southern façade: similarly to the western façade has a buttress fully erected in grey granite.
- The inside of the church: consists of a combination of ochre and grey granite. The grey granite was used for the pillars, since ochre granite was used for the rest of the structural elements (walls, arches, vaults, etc.).

13.4.2 Pathologies of the Structure

While white, ochre and red granites present better properties to be hewed and become part of the façade ornamentation: their physical-mechanical properties, such as water absorption, frost resistance, bending strength, shock and compression resistance, are worse than those of the grey granite from bedrock (García-Talegón et al. 1993). That is why a complete pathological evaluation with a comprehensive knowledge of the structure (finite element analysis, limit analysis, etc.) may yield not only a correct identification of the different construction materials but also detect possible pathologies of such materials as listed below:

- Grey granite: mainly composed of quartz, feldspar, mica and chlorite.
- Ochre granite: altered granite without chlorites, biotites and plagioclases. Its mineralogical composition consists of iron oxyhydroxides and phyllosilicates.

266 NDT for the Evaluation of Structures and Infrastructure

- Granite of reddish color: weathered granite that has undergone a kaolinization process with long periods of water saturation. It has a greater content of iron oxides.
- Degree of moisture: as a result of filtration and capillarity processes.
- Biological colonization: the effects of specific atmospheric conditions such as high humidity and temperature and the presence of oxygen lead to the proliferation and persistence of certain organisms on the rock.
- Color changes: as patinas of dirt, a damage due to environmental pollution.

13.4.3 Materials and Methods

In this case study, technologies such as terrestrial laser scanning and close range photogrammetry were again applied to analyze and diagnose the diseases presented in the different construction materials of the north façade of the church, because this façade is the most affected of the church.

A pathological assessment of the constructions was undertaken in response to the damage caused by external factors in the previous case studies. However, in this case the variability of different types of granites was examined as an intrinsic factor of the origin of pathologies. Thus it was decided to work in the visible and near infrared range to analyze the potential of these two spectral ranges in order to distinguish building materials. For the visible range and as an active sensor the laser scanner Trimble GX200 was used, whereas the compact camera Nikon Coolpix L11 was applied as passive sensor. For the near infrared range, the laser scanner FARO Photon 80 was selected (the technical characteristics of each sensor are listed in Table 13.1).

The methodology for the data analysis and the workflow followed are proposed in Figure 13.1: planning and data acquisition, filtering and segmentation, some data corrections, orthoimages generation and multispectral data classification.

Planning and data acquisition. An initial assessment and inspection of the area under study were essential to plan the multisensory data acquisition. Some possible limitations during data capture and the accessibility to the area depend on the time of day, number of stations and the distance established to the structure, among other factors. Therefore, the success in the fieldwork depends largely on the previous inspection. In this particular study various problems were observed: hidden areas caused by the projected shadows by two nearby buildings, inability to station the sensors in the desired position and frequent pedestrian traffic. Finally, the ideal moment was selected to achieve a homogeneous lighting to ensure uniformity in the radiometric values of the field campaign.

With laser scanners leveled properly, a total of 2 stations at a distance to the façade that varied between 6 and 3 m were performed. The final spatial resolution of the point cloud was 8 mm. As in previous cases, Trimble Realworks Survey and Scene 3D software were used for the data acquisition. Meanwhile, the Nikon Coolpix L11 was integrated into the FARO Photon 80 to take pictures simultaneously from the same point of view.

Filtering and segmentation. As has been mentioned, since the church was located in a city center and surrounded by some buildings, the multispectral study was very interrupted by pedestrian traffic and affected by the shadows projected by neighboring

buildings. Therefore, the first step of data processing was the segmentation of the point clouds leaving only data belonging to the façade of interest.

Data corrections. Some data required corrections such as carry out a proper registration and alignment of all stations belonging to each sensor. The targets disposed on the walls were used to perform the alignments, and therefore these targets should appear in each laser scan.

Orthoimages generation. After getting all the scans aligned and registered in the same coordinate system, the three orthoimages (from: RGB, G_{Trimble} , and NIR) were created. The orthoimage generation was carried out with the Trimble Realworks Survey software. Firstly, orthoimages from both laser scanners point clouds in the green and NIR ranges respectively were created and orthoimages from the RGB afterwards (similarly as in the previous case). The spatial resolution reached for the orthoimages was 20 mm.

Multispectral data classification. Finally, the set of three orthoimages arranged in a three-channels multispectral image was initially classified in an unsupervised way and subsequently in a supervised way. For the unsupervised classification the *fuzzy k-means* algorithm was used.

13.4.4 Experimental Results

The methodology required to ensure a right pathological classification of the structural materials involved performing a supervised classification. To this end, it was necessary to establish the suitable number of a priori informational classes and their connection with the data collected by all the sensors.

The initial hypothesis was set based on: (i) Three classes for construction materials (granites); (ii) Three classes for pathologies (two classes for moisture and one for biological factors); (iii) wood structures; and (iv) null class.

The study of mortar between blocks was not possible since its thickness was less than the GSD achieved with all sensors. This building material was perceptible only in the joints with a widest thickness of 3 cm while the spatial resolution of the orthoimages was 2 cm. Therefore, it was decided to dismiss it from the classification process.

Regarding the *fuzzy k-means* unsupervised classification, where the aforementioned hypothesis of clusters was established, provided results were not comparable even with the visual inspection. Therefore, it was necessary to fix other informational classes (a total of seven) including artificial elements of the guttering system, excluding wooden class present in the door and the union of the two types of unaltered granites in one class. This was necessary since the spectral resolution of the five-channels images generated was not enough.

The overall accuracy achieved in the classification shown in [Figure 13.8](#) was 0.8835 with a Cohen's Kappa coefficient of 0.8328 for six informational classes ([Table 13.5](#)).

After the unsupervised classification by setting seven clusters, the roof gutters and metal rivets of the door were classified within the same class. Regarding the detection of pathologies on the façade, the confusion between moisture and biological factors should be noted ([Table 13.6](#)). This fact occurs because both pathologies are usually interrelated.

Moreover, the classes for which the worst value of separability (1.735/2.000) was obtained were “unaltered granite” and “penetrating damp”, as shown in [Table 13.6](#).

268 NDT for the Evaluation of Structures and Infrastructure

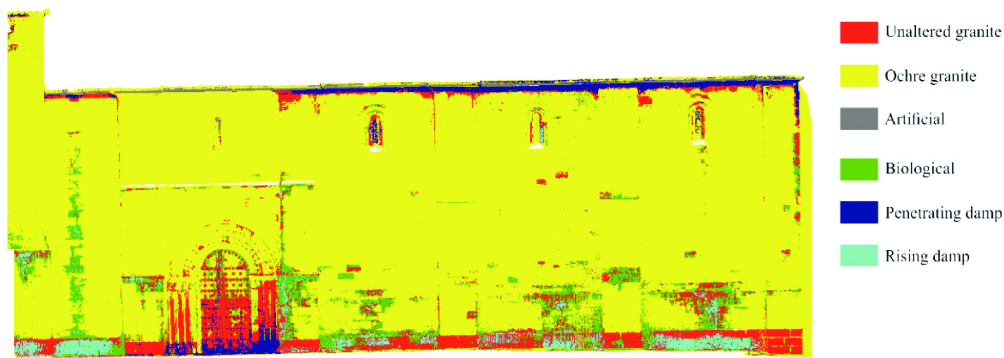


Figure 13.8 Orthoimage classification result after the supervised classification.

Table 13.5 Supervised classification: confusion matrix with six channels.

	Unaltered granite	Ochre granite	Artificial elements (e.g. gutter)	Biological colonization	Penetrating damp	Rising damp
Unaltered granite	82.28%	0.96%	0.00%	1.26%	15.48%	0.02%
Ochre granite	0.73%	98.70%	0.00%	0.57%	0.00%	0.00%
Artificial elements	0.00%	0.00%	100.00%	0.00%	0.00%	0.00%
Biological colonization	1.90%	1.33%	0.00%	84.30%	12.46%	0.00%
Penetrating damp	2.53%	0.00%	0.00%	6.41%	91.05%	0.00%
Rising damp	3.36%	0.00%	0.00%	0.00%	0.00%	96.64%

Table 13.6 Separability between classes.

	Unaltered granite	Ochre granite	Artificial elements	Biological colonization	Penetrating damp	Rising damp
Unaltered granite	–					
Ochre granite	1.99642	–				
Artificial elements	2.00000	2.00000	–			
Biological colonization	1.83363	1.98558	2.00000	–		
Penetrating damp	1.73514	2.00000	2.00000	1.87890	–	
Rising damp	1.98978	2.00000	2.00000	2.00000	1.99994	–

The main reason is the similar radiometric response of the unaltered granite and slightly damp unaltered granite and due to unaltered granite is only part of the façade plinth and this part of the structure is likely to be affected by rising damp.

As a general conclusion, it is important to highlight that limitations in robust discrimination potential of pathologies after the classification process is not only due to the radiometric resolution, which depends on the available sensors for each case study, but also depends on the smallest element that it is possible to discriminate, i.e. the spatial resolution of the orthoimages.

An approximate knowledge of the spectral signatures of the materials studied, although they come from laboratory tests, would help in the selection of the optimal wavelengths for the definition of effective informational classes.

13.5 Conclusions

Although the described methodology based on multispectral dataset management allows detecting and classifying accurately a variety of constructive pathologies, certain aspects such as peelings, cracks or disaggregation processes (abundant in masonry elements) are not completely explained. Given the flexibility of this methodology, which allows the analysis of data obtained by laser scanning and photogrammetry techniques, such degradation processes can be completely characterized through a geometric analysis of the construction. Also, the possibility of a large scale evaluation (large evaluated areas) and pathologies quantification are the strong points of photogrammetry and laser systems, making them valuable resources within the buildings' pathological assessment. However, as noted above, certain geometric aspects are not fully defined, as well as qualitative data on the material affected by pathological processes (which can be obtained by in-situ or laboratory test).

In order to make a full pathological assessment it is recommended to perform the following stages: (i) Geometric analysis (measuring deformations, settlements, kaolinization, etc.); (ii) Multispectral classification (using the described methodology); and (iii) Complementary qualitative in-situ and laboratory tests (use of reagents to assess biological colonization, mineralogical analysis, mechanical analysis, etc.).

Also essential is planning periodic field campaigns which will allow monitoring and assessing the pathological condition and the effectiveness of the applied restoration techniques.

Regarding the field campaigns, a series of particular best practices have been covered in the previous subsections. However, the optimal data acquisition protocol changes for the different spectral regions. When the discretization of the textural differences is required, the visible region is advisable, so the acquisition should be done with uniform light conditions. However, for a more detailed analysis of moisture (different degree of moisture) it is recommended to add a thermal infrared channel, which requires a light absence (mainly the solar effects) for an optimal data gathering. Although it is possible a priori knowledge of the material spectral signature, this information comes from laboratory test where not only the light conditions are controlled, but also specimens are optimal. In the field campaign, the constructive materials may have a heterogeneous appearance due to the textural differences which hinder their correct classification. In this regard, the use of additional SWIR channels, despite its worst geometric resolution, will improve their classification. Finally, the 3D spatial characterization of the study object is a strong point when the quantitative metric analysis associated to the areas affected is required. As additional advantage, the quantification of the prevention measures and their associated cost is directly drawn. When only a qualitative analysis is required, a pure 2D approach could be applied, supported by a projective transformation. However, the results and the resultant conclusions will be valid, only if the error budget is admissible and has been taken into account.

The current emergence of BIM (Building Information Modeling) and HBIM (Historical Building Information Modeling) multilayer models can be the perfect complement

270 NDT for the Evaluation of Structures and Infrastructure

to the methodology presented. As a result, it would be possible to create a complete information model including in it an exhaustive material characterization and pathological evaluation through time. As a result, analyses based on predictive models allow us to anticipate possible events, allowing to safeguard the integrity of the construction. It is in this field where the methodology presented could play a crucial role and provide added value.

References

- Armesto-González, J., Riveiro-Rodríguez, B., González-Aguilera, D., & Rivas-Brea, M. T. (2010). Terrestrial laser scanning intensity data applied to damage detection for historical buildings. *Journal of Archaeological Science*, 37(12): 3037–3047. doi: <http://dx.doi.org/10.1016/j.jas.2010.06.031>.
- Coffin, D. (2011). Raw digital photo decoding. Retrieved January 24, 2015.
- Cohen, J. (1968). Weighted kappa: Nominal scale agreement provision for scaled disagreement or partial credit. *Psychological bulletin*, 70(4): 213.
- Crespo, C., Armesto, J., González-Aguilera, D., & Arias, P. (2010). Damage Detection on Historical Buildings Using Unsupervised Classification Techniques. *ISPRS-International Archives of the Photogrammetry, Remote Sensing and Spatial Information Sciences*, XXXVIII, 184–188.
- Del Pozo, S., Herrero-Pascual, J., Felipe-García, B., Hernández-López, D., Rodríguez-Gonzálvez, P., & González-Aguilera, D. (2015). Multi-Sensor Radiometric Study to Detect Pathologies in Historical Buildings. *ISPRS-International Archives of the Photogrammetry, Remote Sensing and Spatial Information Sciences*, XL-5/W4, 193–200.
- Flórez García, E. (2009). *Aplicación de técnicas geomáticas al análisis y diagnóstico de patologías en edificios del patrimonio histórico*. Departamento de Ingeniería Cartográfica y del Terreno. Politécnica Superior de Ávila. Ávila.
- García-Talegón, J., García del Amo, D., Iñigo, A., Mendiña, J., Molina Ballesteros, E., & Hernández, V. (1993). Propiedades físico mecánicas de los granitos empleados en la catedral de Avila procedentes del yacimiento de “La Colilla” (Avila).
- González-Jorge, H., Gonzalez-Aguilera, D., Rodriguez-Gonzalvez, P., & Arias, P. (2012). Monitoring biological crusts in civil engineering structures using intensity data from terrestrial laser scanners. *Construction and Building Materials*, 31(0): 119–128. doi: <http://dx.doi.org/10.1016/j.conbuildmat.2011.12.053>.
- Instrucción del Hormigón Estructural, E. (2008). EHE-08. Madrid, Ministerio de Fomento, Secretaría General Técnica.
- Li, M., Zang, S., Zhang, B., Li, S., & Wu, C. (2014). A Review of Remote Sensing Image Classification Techniques: the Role of Spatio-contextual Information. *European Journal of Remote Sensing*, 47, 389–411.
- Lu, W., & Tan, Y.-P. (2003). Color filter array demosaicking: new method and performance measures. *IEEE Transactions on Image Processing*, 12(10), 1194–1210.
- Ministerio de Fomento (1968). Instrucción para el proyecto y ejecución del obras de hormigón en masa o armado. Madrid.
- Molina Ballesteros, E. (1993). *Incidencia de las alteraciones del zocalo hercinico iberico en las características de las rocas afectadas, empleadas como materiales de construccion. Los granitos de “La Colilla” (Ávila)*. Paper presented at the Alteracion de granitos y rocas afines, empleados como materiales de construccion: deterioro de monumentos historicos. Actas del workshop, Consejo Superior de Investigaciones Científicas, Avila, Spain, 1993.
- Montejo Santos, C., López de Silanes Vázquez, M., Álvarez Andrés, J., Sánchez-Biezma Serrano, M. J., Prieto Lamas, B., Silva Hermo, B. M., & López Díaz, A. J. (2014). Las ruinas de Santo Domingo de Pontevedra.

- Porto, C. M. (1993). Arte gótico en Galicia: los dominicos I.
- Rodríguez-González, P., Pascual, J. H., Aguilera, D. G., Nieto, Á. L. M., Mancera-Taboada, J., Martín, N. S., & Hidalgo, M. Á. M. (2013). Aplicación de técnicas geomáticas al análisis y diagnóstico de patologías en el Patrimonio Arquitectónico. *Mapping* (161), 4–19.
- Sánchez-Aparicio, L. J., Riveiro, B., González-Aguilera, D., & Ramos, L. F. (2014). The combination of geomatic approaches and operational modal analysis to improve calibration of finite element models: A case of study in Saint Torcato Church (Guimarães, Portugal). *Construction and Building Materials*, 70(0): 118–129. doi: <http://dx.doi.org/10.1016/j.conbuildmat.2014.07.106>.

CAPÍTULO V

CONCLUSIONES Y FUTURAS INVESTIGACIONES

La presente Tesis Doctoral centra sus esfuerzos en uno de los campos de mayor peso en la ingeniería civil, la detección y cuantificación de daños en infraestructuras y su influencia en el comportamiento estructural de estas. A continuación son expuestas las conclusiones y contribuciones aportadas por el presente documento, en relación a los objetivos previamente marcados:

- I. **Evaluación de la aplicabilidad de los sensores geomáticos (sistemas láser escáner terrestre y cámara digitales) en construcciones con daños estructurales.**
 - a) Los componentes geométricos y radiométricos de las nubes de puntos, obtenidas a través de los sistemas láser escáner y fotogramétricos muestran grandes potencialidades como sistemas para la monitorización de la salud estructural de la construcción.
 - b) La Correlación Digital de Imágenes ha probado ser una técnica de amplia potencialidad en la evaluación mecánica de materiales. Posicionándose como una estrategia no destructiva, sin contacto y bajo coste capaz de competir con los sistemas tradicionales tales como las galgas extensiométricas o extensómetros.
 - c) El empleo de plataformas VANT, junto a cámaras digitales ofrece una solución de amplia potencialidad para la reconstrucción de zonas de difícil acceso.
 - d) La combinación de los sistemas Structure from Motion, y los láser escáner permiten la caracterización geométrica de la construcción y la creación de modelos CAD.
 - e) Aunque las grietas son fenómenos geométricos, estos pueden ser evaluados a través de componentes radiométricos (como los detectores de bordes).
- II. **Desarrollo de estrategias de modelización y construcción de modelos CAD en estructuras con procesos patológicos con un claro componente geométrico (deformaciones y grietas), aptos para posteriores simulaciones numéricas.**
 - a) Las segmentaciones basadas en curvatura mantienen todos los detalles relevantes de la nube de puntos. Diezmando las zonas planas.

- b) Para una correcta conversión de la nube de puntos al modelo CAD, una malla manifold es requerida. Las mallas manifold presentan formas naturales y reales.
- c) El enfoque basado en la Descomposición Funcional (basados en la teoría de Morse) ha provado ser una estrategia capaz de segmentar mallas en regiones de topología similar.
- d) Las superficies paramétricas (planos, cilindros, etc.) y no-paramétricas (*NURBs*) pueden ser empeladas dentro de modelos CAD para análisis numérico.
- e) Las metodologías de representación mediante *NURBs*, que emplean la cuadrilaterización de la malla (basada en la teoría de Morse y el análisis Espectral de la malla) y la regularización de esta, muestran buenos resultados para la modelización CAD.
- f) La consideración de patologías estructurales (como agrietamientos o falta de material) pueden ser integradas dentro de superficies *NURBs* a través de contornos.

III. Evaluación de los procedimientos de dinámica de estructuras basados en el enfoque del Análisis Modal Operacional en la evaluación de daños.

- a) El Análisis Modal Operacional ha provado ser una herramienta efectiva para diferentes tipos de construcciones.
- b) La Identificación de los Subespacios Estocásticos (*SSI*) y el Método Mejorado de la Descomposición en el Dominio de la Frecuencia (*EFDD*) requieren de excitaciones aleatorias, con ruido ambiental, que permiten una identificación simple y efectiva de los parámetros modales.
- c) La detección de daños (con influencia en el comportamiento global de la estructura) pueden ser determinados por cambios en las frecuencias de la estructura.
- d) Los daños locales presentan una importante relación con los modos de vibración. Por tanto, carecer de un número suficiente de puntos de medida pueden limitar la capacidad de localización de daños a través de los índices *MAC* y *COMAC*.

IV. Aplicación y desarrollo de metodologías robustas para la calibración de modelos numéricos. Capaces de localizar e interpretar los daños presentes en las construcciones.

- a) Las variables estáticas y dinámicas de una estructura (deformaciones, frecuencias, modos de vibración, etc.) pueden ser empleadas para calibrar la respuesta estructural de una construcción.
- b) Las características geométricas de la nube de puntos pueden ser empleadas para la calibración de modelos numéricos.
- c) La métrica Global Hausdorff (GHm_s) y Local Hausdorff (GHm_s) parece mostrar potencialidad en la evaluación de la similitud geométrica entre un modelo numérico y su estado deformado real.
- d) El Método de los Elementos Finitos muestra grandes capacidades. Sin embargo, la diversidad de variables actuante requieren de la calibración de las mismas a fin de obtener resultados adecuados.
- e) El método de Douglas-Reid y los enfoques Determinísticos pueden ser empleados para calibrar complejos sistemas estructurales por Elementos Finitos
- f) Las funciones de daño (discretas o sistemas de subestructuras) pueden ser empleadas para detectar y cuantificar agrietamientos en construcciones dañadas.
- g) Las funciones de daño pueden emplearse en conjunción con las simulaciones numéricas por Elementos Finitos para mejorar la respuesta obtenidas.

V. Aplicación del análisis multiespectral de imágenes en la detección de patologías con un componente eminentemente radiométrico (e.j. caracterización de materiales, humedad en hormigones, acciones biológicas, etc.) y con una estrecha relación con la estabilidad y la vida útil de la construcción.

- a) Los sistemas láser escáner y fotogramétrico proveen de información de amplia utilidad (componente radiométrico) sobre el estado patológico de la construcción.

- b) Los sistemas de clasificación Supervisados y No-supervisados (e.j. Fuzzy k-medias o Máxima Probabilidad) han probado ser potenciales herramientas en la detección de una amplia variedad de patologías (e.j. algas, líquenes o humedades en hormigones).
- c) La respuesta espectral de los materiales y patologías presentes es un requisito a considerar en la correcta evaluación de las clases informacionales.
- d) La hibridación de sensores (láser escáner y cámaras digitales) se ha llevado a cabo con éxito, mejorando así los resultados arrojados por la clasificación multiespectral.
- e) Las nubes de puntos láser escáner y fotogramétricas pueden emplearse como un soporte métrico sobre el cual evaluar y cuantificar los daños presentes en la construcción.

En términos más prácticos, y en lo concerniente a la actividad de investigación desarrollada, diferentes tipos de construcción han sido evaluadas: desde construcciones históricas o vernáculas, hasta construcciones erigidas en hormigón armado o en fase experimental.

El trabajo desarrollado durante la elaboración de la presente Tesis Doctoral trata de dar respuesta a los procesos patológicos más comunes presentes en las construcciones. Permitiendo la evaluación de la estabilidad de la vida útil remanente de estas. Sin embargo, parte de dichos procedimientos requieren de desarrollos futuros que mejoren los resultados y aplicabilidad de estos:

I. Hibridación de sensores.

- a) Empleo de cámaras termográficas y la dinámica de estructuras a fin de evaluar la influencia de la temperatura en el comportamiento dinámico de la estructura.

II. Estrategias de modelado CAD para simulación numéricas.

- a) Desarrollar sistemas de interconexión entre modelos CAD y estrategias numéricas avanzadas como el análisis isogeométrico o en análisis *Nurbs-Enhanced Finite Element Method* (método NEFEM) capaces de aprovechar la riqueza geométrica aportada por los sistemas láser y fotogramétricos.

-
- b) Mejorar los procesos de segmentación basados en curvatura con estrategias *mean-shifting*.
 - c) Avanzar en la clasificación de zonas segmentadas y la conexión de estas a través de superficies paramétricas y no-paramétricas.
 - d) Mejorar la segmentación de mallas a través de sistemas entrenados y clasificadores expertos. Permitiendo la clasificación de los diferentes componentes estructurales y sus posibles patologías.

III. Estrategias de daños basadas o no basadas en modelos:

- a) Desarrollar procedimientos de detección de daños basados en modelos a través de una mejora de las funciones de daño (e.j. considerar la dirección y profundidad de las grietas).
- b) Usar las metodologías de detección de daños no basadas en modelos para delimitar espacialmente el daño presente y permitir la posterior aplicación de funciones de daño.
- c) Continuar la validación de los parámetros de calidad geométrica propuestos, GHm_s and LHm_s , para la calibración de modelos numéricos.

IV. Clasificación multiespectral.

- a) Mejorar el emparejamiento de sensores a través de estrategias de emparejamiento multimodal.
- b) Emplear cámaras multiespectrales o hiperespectrales en la evaluación de procesos patológicos.
- c) Extender la clasificación multiespectral a un entorno multiespectral a fin de integrar materiales y patologías en modelos CAD aptos para análisis numéricos o incluso en sistemas avanzados de información (sistemas BIM).

- d) Complementar la clasificación multispectral a través de sistemas de Redes Neuronales que permitan mejorar el reconocimiento y clasificación de materiales y patologías.

REFERENCIAS

A

Adewole, K. K., & Bull, S. J. (2013). Prediction of the fracture performance of defect-free steel bars for civil engineering applications using finite element simulation. *Construction and Building Materials*, 41, 9-14. doi: <http://dx.doi.org/10.1016/j.conbuildmat.2012.11.089>

Akca, D., & Grün, A. (2007). *Least Squares 3D surface matching*: Inst. für Geodäsie und Photogrammetrie.

Armesto-González, J., Riveiro-Rodríguez, B., González-Aguilera, D., & Rivas-Brea, M. T. (2010). Terrestrial laser scanning intensity data applied to damage detection for historical buildings. *Journal of Archaeological Science*, 37(12), 3037-3047. doi: <http://dx.doi.org/10.1016/j.jas.2010.06.031>

Armesto, J., Roca-Pardiñas, J., Lorenzo, H., & Arias, P. (2010). Modelling masonry arches shape using terrestrial laser scanning data and nonparametric methods. *Engineering Structures*, 32(2), 607-615. doi: <http://dx.doi.org/10.1016/j.engstruct.2009.11.007>

Attene, M. (2010). A lightweight approach to repairing digitized polygon meshes. *The Visual Computer*, 26(11), 1393-1406.

B

Barazzetti, L., Binda, L., Scaioni, M., & Taranto, P. (2011). Photogrammetric survey of complex geometries with low-cost software: Application to the 'G1' temple in Myson, Vietnam. *Journal of cultural heritage*, 12(3), 253-262.

Besl, P. J., & McKay, N. D. (1992). *Method for registration of 3-D shapes*. Paper presented at the Robotics-DL tentative.

Branch, J. W., Prieto, F., & Boulanger, P. (2008). *Automatic Extraction of Quadrilateral Patches from Triangulated Surfaces Using Morse Theory*. Paper presented at the Proceedings of the 16th International Meshing Roundtable.

C

Cabaleiro, M., Riveiro, B., Arias, P., Caamaño, J., & Vilán, J. (2014). Automatic 3D modelling of metal frame connections from LiDAR data for structural engineering purposes. *ISPRS Journal of Photogrammetry and Remote Sensing*, 96, 47-56.

Campbell, J. B. (2002). *Introduction to remote sensing*: CRC Press.

Castellazzi, G., D'Altri, A. M., Bitelli, G., Selvaggi, I., & Lambertini, A. (2015). From laser scanning to finite element analysis of complex buildings by using a semi-automatic procedure. *Sensors*, *15*(8), 18360-18380.

Conde, B., Villarino, A., Cabaleiro, M., & Gonzalez-Aguilera, D. (2015). Geometrical Issues on the Structural Analysis of Transmission Electricity Towers Thanks to Laser Scanning Technology and Finite Element Method. *Remote Sensing*, *7*(9), 11551-11569.

D

De Borst, R., Remmers, J. J., Needleman, A., & Abellan, M.-A. (2004). Discrete vs smeared crack models for concrete fracture: bridging the gap. *International Journal for Numerical and Analytical Methods in Geomechanics*(28), 583-607.

Del Pozo, S., Lindenbergh, R., Rodríguez-González, P., Blom, J. K., & González-Aguilera, D. (2015). Discrimination between Sedimentary Rocks from Close-Range Visible and Very-Near-Infrared Images. *PloS one*, *10*(7), e0132471.

Del Pozo, S., Rodríguez-González, P., Hernández-López, D., & Felipe-García, B. (2014). Vicarious radiometric calibration of a multispectral camera on board an unmanned aerial system. *Remote Sensing*, *6*(3), 1918-1937.

Dong, C., Zhang, P., Feng, W., & Huang, T. (1994). *The sensitivity study of the modal parameters of a cracked beam*. Paper presented at the Proceedings of the 12th International Modal Analysis.

Douglas, B. M., & Reid, W. H. (1982). Dynamic tests and system identification of bridges. *Journal of the Structural Division*, *108*(ST10).

F

Farrar, C. R. (2003). *Damage prognosis: current status and future needs*: Los Alamos National Laboratory.

Farrar, C. R., & Worden, K. (2007). An introduction to structural health monitoring. *Philosophical Transactions of the Royal Society of London A: Mathematical, Physical and Engineering Sciences*, *365*(1851), 303-315.

G

García-Talegón, J., García del Amo, D., Iñigo, A., Menduiña, J., Molina Ballesteros, E., & Hernández, V. (1993). Propiedades físico mecánicas de los granitos empleados en la catedral de Avila procedentes del yacimiento de "La Colilla"(Avila).

Gentile, C., & Saisi, A. (2007). Ambient vibration testing of historic masonry towers for structural identification and damage assessment. *Construction and Building Materials*, *21*(6), 1311-1321.

Gonilha, J. A., Barros, J., Correia, J. R., Sena-Cruz, J., Branco, F. A., Ramos, L. F., . . . Santos, T. (2014). Static, dynamic and creep behaviour of a full-scale GFRP-SFRSCC hybrid footbridge. *Composite Structures*, 118, 496-509. doi: <http://dx.doi.org/10.1016/j.compstruct.2014.08.009>

H

Haque, M., Zain, M., Hannan, M., Jamil, M., & Johari, H. (2012). Recent application of structural civil health monitoring using WSN and FBG. *World Applied Sciences Journal*, 20(4), 585-590.

Hausdorff, F. (2008). *Felix Hausdorff-Gesammelte Werke Band III: Mengenlehre (1927, 1935) Deskripte Mengenlehre und Topologie* (Vol. 3): Springer-Verlag.

Heyman, J. (1997). *The stone skeleton: structural engineering of masonry architecture*: Cambridge University Press.

Housner, G. W., Bergman, L. A., Caughey, T., Chassiakos, A., Claus, R., Masri, S., . . . Yao, J. T. (1997). Structural control: past, present, and future. *Journal of Engineering Mechanics*, 123(9), 897-971.

Huerta, S. (2008). The Analysis of Masonry Architecture: A Historical Approach: To the memory of Professor Henry J. Cowan. *Architectural Science Review*, 51(4), 297-328.

L

Li, M., Zang, S., Zhang, B., Li, S., & Wu, C. (2014). A Review of Remote Sensing Image Classification Techniques: the Role of Spatio-contextual Information. *European Journal of Remote Sensing*, 47, 389-411.

Liang, D., & Yuan, S. (2015). Structural health monitoring system based on multi-agent coordination and fusion for large structure. *Advances in Engineering Software*, 86, 1-12.

Lorenzoni, F., Casarin, F., Modena, C., Caldon, M., Islami, K., & da Porto, F. (2013). Structural health monitoring of the Roman Arena of Verona, Italy. *Journal of Civil Structural Health Monitoring*, 3(4), 227-246.

M

Milani, G., & Valente, M. (2015). Comparative pushover and limit analyses on seven masonry churches damaged by the 2012 Emilia-Romagna (Italy) seismic events: Possibilities of non-linear finite elements compared with pre-assigned failure mechanisms. *Engineering Failure Analysis*, 47, Part A(0), 129-161. doi: <http://dx.doi.org/10.1016/j.engfailanal.2014.09.016>

Moody, D. I., Brumby, S. P., Rowland, J. C., & Altmann, G. L. (2014). Land cover classification in multispectral imagery using

clustering of sparse approximations over learned feature dictionaries. *Journal of Applied Remote Sensing*, 8(1), 084793-084793.

Mottershead, J., & Friswell, M. (1993). Model updating in structural dynamics: a survey. *Journal of sound and vibration*, 167(2), 347-375.

O

Osmancikli, G., Bayraktar, A., Türker, T., Uçak, Ş., & Mosallam, A. (2015). Finite element model calibration of precast structures using ambient vibrations. *Construction and Building Materials*, 93, 10-21. doi: <http://dx.doi.org/10.1016/j.conbuildmat.2015.05.096>

P

Pandey, A., Biswas, M., & Samman, M. (1991). Damage detection from changes in curvature mode shapes. *Journal of sound and vibration*, 145(2), 321-332.

Peeters, B., & De Roeck, G. (2001). One-year monitoring of the Z 24-Bridge: environmental effects versus damage events. *Earthquake engineering & structural dynamics*, 30(2), 149-171.

Piegl, L., & Tiller, W. (2012). *The NURBS book*: Springer Science & Business Media.

Pope, A., & Rees, W. G. (2014). Impact of spatial, spectral, and radiometric properties of multispectral imagers on glacier surface classification. *Remote sensing of environment*, 141, 1-13.

R

Rainieri, C., & Fabbrocino, G. (2014). *Operational modal analysis of civil engineering structures*: Springer.

Ramos, L. F. (2007). Damage identification on masonry structures based on vibration signatures.

Ramos, L. F., Aguilar, R., Lourenço, P. B., & Moreira, S. (2013). Dynamic structural health monitoring of Saint Torcato church. *Mechanical Systems and Signal Processing*, 35(1-2), 1-15. doi: <http://dx.doi.org/10.1016/j.ymsp.2012.09.007>

Ramos, L. F., Marques, L., Lourenço, P. B., De Roeck, G., Campos-Costa, A., & Roque, J. (2010). Monitoring historical masonry structures with operational modal analysis: Two case studies. *Mechanical Systems and Signal Processing*, 24(5), 1291-1305

Riveiro, B., Morer, P., Arias, P., & de Arteaga, I. (2011). Terrestrial laser scanning and limit analysis of masonry arch bridges. *Construction and Building Materials*, 25(4), 1726-1735. doi: <http://dx.doi.org/10.1016/j.conbuildmat.2010.11.094>

Rytter, A. (1993). *Vibrational based inspection of civil engineering structures*. Unknown.

S

Saloustros, S., Pelà, L., Roca, P., & Portal, J. (2015). Numerical analysis of structural damage in the church of the Poblet Monastery. *Engineering Failure Analysis*, 48(0), 41-61. doi: <http://dx.doi.org/10.1016/j.engfailanal.2014.10.015>

Scaioni, M., Barazzetti, L., Brumana, R., Cuca, B., Fassi, F., & Prandi, F. (2009). *RC-Heli and Structure & Motion techniques for the 3-D reconstruction of a Milan Dome spire*. Paper presented at the Proceedings of the 3rd ISPRS International Workshop 3D-ARCH.

Simoen, E., De Roeck, G., & Lombaert, G. (2015). Dealing with uncertainty in model updating for damage assessment: A review. *Mechanical Systems and Signal Processing*, 56–57(0), 123-149. doi: <http://dx.doi.org/10.1016/j.ymsp.2014.11.001>

Solis, M., He, L., Lombaert, G., & De Roeck, G. (2013). FINITE ELEMENT MODEL UPDATING OF A FOOTBRIDGE BASED ON STATIC AND DYNAMIC MEASUREMENTS. *ECCOMAS*.

Stubbs, N. (1987). A general theory of non-destructive damage detection in structures *Structural Control* (pp. 694-713): Springer.

Stubbs, N., Kim, J., & Topole, K. (1992). *An efficient and robust algorithm for damage localization in offshore platforms*. Paper presented at the Proceedings of the ASCE Tenth Structures Congress.

T

Teughels, A., & De Roeck, G. (2003). *Damage assessment of the Z24 bridge by FE model updating*. Paper presented at the Key engineering materials.

Titurus, B., & Friswell, M. (2008). Regularization in model updating. *International Journal for numerical methods in engineering*, 75(4), 440-478.

Tognaccini, R. (2009). La chiesa di Santa Maria del Mar a Barcellona: dal rilievo tridimensionale all'analisi strutturale.

Toldo, R., Beinat, A., & Crosilla, F. (2010). *Global registration of multiple point clouds embedding the Generalized Procrustes Analysis into an ICP framework*. Paper presented at the 3DPVT 2010 Conference.

Türker, T., & Bayraktar, A. (2014). Structural safety assessment of bowstring type RC arch bridges using ambient vibration testing and finite element model calibration. *Measurement*, 58, 33-45. doi: <http://dx.doi.org/10.1016/j.measurement.2014.08.002>

V

Várady, T., Facello, M. A., & Terék, Z. (2007). Automatic extraction of surface structures in digital shape reconstruction. *Computer-Aided Design*, 39(5), 379-388. doi: <http://dx.doi.org/10.1016/j.cad.2007.02.011>

Villarino, A., Riveiro, B., Gonzalez-Aguilera, D., & Sánchez-Aparicio, L. (2014). The Integration of Geotechnologies in the Evaluation of a Wine Cellar Structure through the Finite Element Method. *Remote Sensing*, 6(11), 11107-11126.

W

Watt, D. S. (1999). *Building pathology: Principles and practice*: Blackwell Science.

Worden, K., & Dulieu-Barton, J. (2004). An overview of intelligent fault detection in systems and structures. *Structural Health Monitoring*, 3(1), 85-98.

Y

Yan, Y., Cheng, L., Wu, Z., & Yam, L. (2007). Development in vibration-based structural damage detection technique. *Mechanical Systems and Signal Processing*, 21(5), 2198-2211.

Z

Zienkiewicz, O., & Taylor, R. (1994). El método de los elementos finitos. Volumen 1: Formulación básica y problemas lineales: CIMNE, Barcelona.

Zordan, T., Briseghella, B., & Liu, T. (2014). Finite element model updating of a tied-arch bridge using Douglas-Reid method and Rosenbrock optimization algorithm. *Journal of Traffic and Transportation Engineering (English Edition)*, 1(4), 280-292.

ANEXO |

ENHANCE YOUR FINITE ELEMENT MODELS SOFTWARE

Desarrollado en Matlab®, Enhance your Finite Element Models (EyFEM) es un add-on no oficial para el software de Elementos Finitos TNO-DIANA® desarrollado durante el transcurso de la presente Tesis Doctoral. EyFEM incluye todos los procedimientos desarrollados y mostrados en los capítulos II y III, y listados a continuación:

- Funciones de daño discreto.
- Sistema de subestructuración de daños.
- Funciones de daño híbridas (funciones discretas y sistemas de subestructuración).
- Procedimientos de calibración robusta, basados en enfoques deterministas (estáticos, dinámicos o combinación de ambos).
- Incidencias de calidad geométrica (GHm_s y LHm_s) basados en la similitud geométrica entre el modelo numérico y el modelo capturado por un sensor geomático (láser escáner o fotogramétrico).

EyFEM ha sido concebido con el propósito de calibrar complejas simulaciones numéricas (dentro del ámbito estático, dinámico o la combinación de ambos) a través del Método de los Elementos Finitos (Fig. 1).

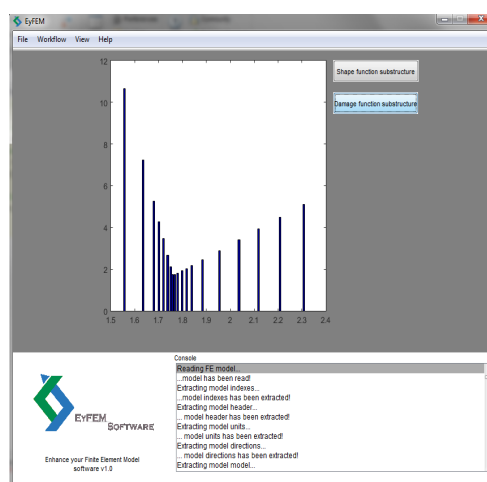


Figure 1. EyFEM interface

Su estructura funcional incluye procedimientos para la identificación y cuantificación de daños, basando su éxito en las funciones de daño (1) (2).

$$X^e = X_o^e(1 - a^e) \quad (1)$$

$$a^e = \sum_{i=1}^n p_i N_i(X^e) \quad (2)$$

Donde X_o^e es el valor físico asociado al daño (e.j. Módulo de Young) en su fase inicial, X^e es el valor calibrado, p_i es un factor multiplicador y N_i es la función de daño considerada (bien sea esta discreta o un sistema de subestructuración).

Todo ello complementado por un sistema Determinístico acotado que asume una relación directa entre los datos experimentales y los valores numéricos arrojados, y que trata de encontrar el valor mínimo de la función objetiva considerada (3) (4).

$$J^{sta} = 1/2 W_\delta \sum_{j=1}^m (\delta_j^{num} - \delta_j^{exp}) / (\delta_j^{exp})^2 \quad (3)$$

$$J^{din} = 1/2 [W_f \sum_{i=1}^m ((f_i^{num} - f_i^{exp}) / (f_i^{exp}))^2 + W_\phi \sum_{i=1}^m (\phi_i^{num} (\phi_i^{exp}) / \phi_{ref}^{exp})^2] \quad (4)$$

Donde W_f , W_ϕ , y W_δ son los pesos considerados para las frecuencias, los modos de vibración y los desplazamientos, f son las frecuencias, ϕ las formas modales δ los desplazamientos estáticos, y ϕ_{ref} el factor de escala (normalización) que permite una comparación entre los valores numéricos y experimentales. En lo que respecta a las funciones dinámicas (J^{din}) el índice i expresa el modo de vibración considerado, mientras que para las funciones estáticas (J^{sta}) el índice j indica el caso de carga (combinación de cargas actuantes en la estructura).

El mínimo de dicha función objetiva es encontrado a través de un sistema de Mínimos Cuadrados (5), complementado con un sistema de optimización por gradientes (Gauss-Newton).

$$r = 1/2 \left\| \begin{matrix} J^{sta} \\ J^{din} \end{matrix} \right\|^2 \quad (5)$$

Donde $\|*\|$ denota la norma Euclidiana, r es el vector de residuales y J^{sta} , J^{din} son las funciones

objetivas estáticas y dinámicas respectivamente.

EyFEM considera, para la resolución del mínimo un sistema de matrices Hessianas (basadas en el concepto de diferencias finitas) que responden a la siguiente formulación (6)(7).

$$\nabla J(\boldsymbol{\theta}) = \sum_{i=1}^m r_i(\boldsymbol{\theta}) \nabla r_i(\boldsymbol{\theta}) = \text{Jacob}(\boldsymbol{\theta})^T r(\boldsymbol{\theta}) \quad (6)$$

$$\nabla^2 J(\boldsymbol{\theta}) = \text{Jacob}(\boldsymbol{\theta})^T \text{Jacob}(\boldsymbol{\theta}) + \sum_{i=1}^n r_i(\boldsymbol{\theta}) \nabla^2 r_i(\boldsymbol{\theta}) \cong \text{Jacob}(\boldsymbol{\theta})^T \text{Jacob}(\boldsymbol{\theta}) \quad (7)$$

Donde *Jacob* es la matriz jacobina, *r* es el vector de residuales, $\boldsymbol{\theta}$ es el vector de variables a minimizar, $\nabla r_i(\boldsymbol{\theta})$ es el gradiente de los residuales, $\nabla J(\boldsymbol{\theta})$ es la derivada primera and $\nabla^2 J(\boldsymbol{\theta})$ la derivada segunda de la función objetiva. Por último, *n* indica el número de variables a considerar durante el proceso de minimización.

De forma adicional, EyFEM incluye un sistema de índices de calidad geométrica, definidos en el Capítulo 3, para la evaluación de la robusted geométrica entre una simulación numérica y su correspondiente estado de deformación obtenido a través de un sistema láser escáner o fotogramétrico (8) (9).

$$GHm_s = \left(\sum_{(a=1)}^n d_{SH}(a) - \sum_{(a=1)}^n d_{SHb}(a) \right) / \left(\sum_{(a=1)}^n d_{SHb}(a) \right) \times 100 \quad (8)$$

$$LHm_s = d_{SH}(a) / d_{SHref}(a) \quad (9)$$

Donde GHm_s representa la métrica Global Hausdorff and LHm_s la métrica Local Hausdorff, $d_{SH}(a)$ la distancia simétrica Hausdorff para un cluster *a* considerado del modelo numérico, $d_{SHb}(a)$ la misma distancia pero para el modelo base y $d_{SHref}(a)$ la distancia simétrica Hausdorff desde el cluster *a* al cluster de referencia.

ANEXO II

DESCRIPTORES DE CALIDAD DE LOS ARTÍCULOS PUBLICADOS

INDICES DE CALIDAD PARA LA PUBLICACIONES:

- **INDICADOR SJR:** Expresa la media ponderada de citas recibidas para el año seleccionado acorde a los documentos publicados en la revista seleccionada en los tres últimos años.
- **INDICE H:** El índice H expresa el número de artículos (h) que han recibido al menos h citas. Cuantifica por tanto la productividad y el impacto científico de la revista considerada.
- **NUMERO TOTAL DE DOCUMENTOS:** Número total de documentos presentes en la revistas.
- **TOTAL DE DOCUMENTOS (3 AÑOS):** Número total de documentos publicados en los tres años previos. Son considerados todo tipo de documentos.
- **NUMERO TOTAL DE REFERENCIAS:** Número total de referencias bibliográficas de una revista. En el periodo considerado.
- **NÚMERO TOTAL DE CITAS (3 AÑOS):** Number of citations received in the selected year by a journal to the document published in the three previous years. All types of documents are considered.
- **DOCUMENTOS CITABLES:** Número de documentos publicados en una revista y que pueden ser citados. Se consideran de forma exclusiva los artículos, revistas y conferencias.
- **CITAS POR DOCUMENTOS (2 AÑOS):** Media de citas por documento en los últimos 2 años. Este valor es obtenido considerando el número de citaciones total recibidas por la revista en los últimos 2 años.
- **CITAS POR DOCUMENTOS (3 AÑOS):** Media de citas por documento en los últimos 3 años. Este valor es obtenido considerando el número de citaciones total recibidas por la revista en los últimos 3 años.
- **CITAS POR DOCUMENTOS (4 AÑOS):** Media de citas por documento en los últimos 4 años. Este valor es obtenido considerando el número de citaciones total recibidas por la revista en los últimos 4 años.
- **REF./DOC.:** Media de citas por documento.
- **AUTO-CITAS:** Número de autocitas recibidas en los tres años previos. Todos los tipos de documentos son considerados.
- **DOCUMENTO NO-CITABLES :** Número de documentos no-citables.
- **DOCUMENTOS NO-CITADOS:** Número de artículos no citados en los tres años previos.

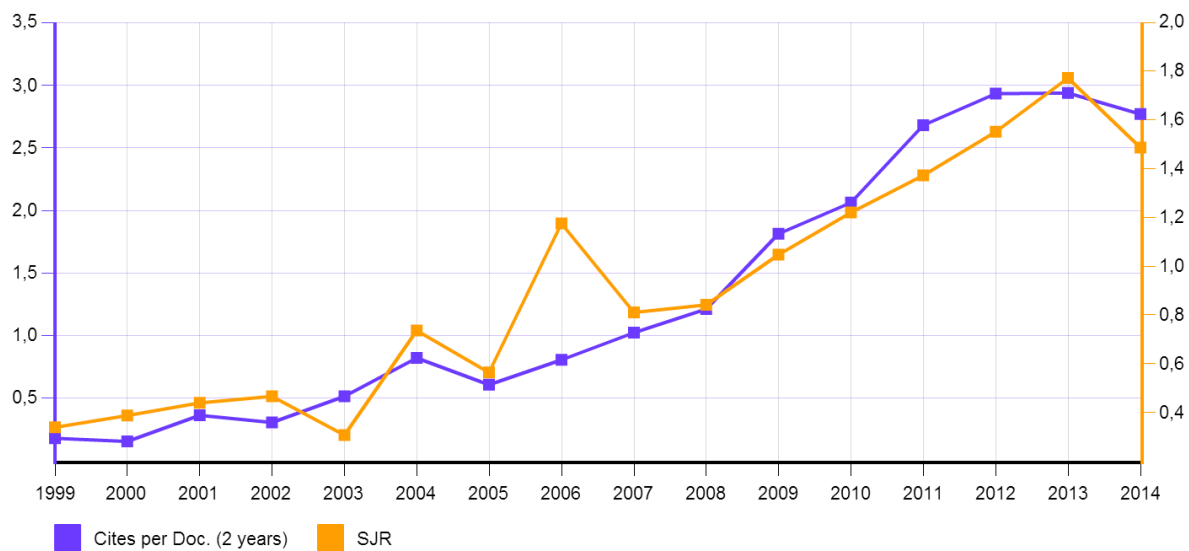
- **% COLABORACIÓN INTERNACIONAL:** Número de publicaciones con autores de diversos países.

ÍNDICES DE CALIDAD PARA LOS CAPÍTULO DE LIBRO:

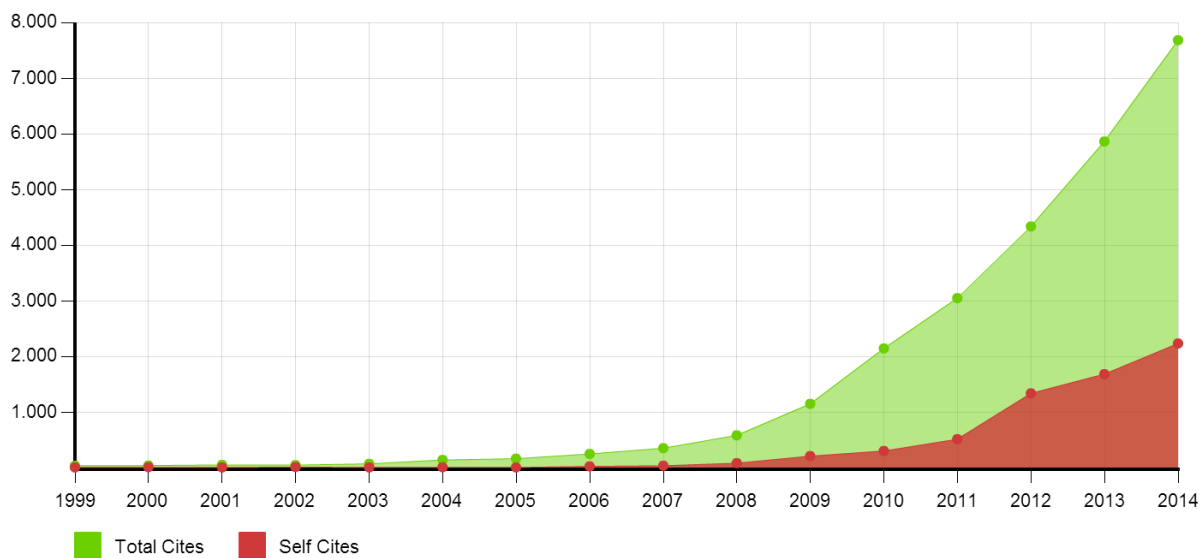
- **PBK:** Número total de libros publicados en un cierto campo o disciplina en los últimos cinco años.
- **PCH:** Número total de capítulos de libros publicados en un cierto campo o disciplina en los últimos cinco años.
- **CIT:** Número total de citas recibidas por una editorial en un cierto campo o disciplina.
- **FNCS:** Citaciones normalizadas recibidas.

REVISTA:	Construction & Building Materials Journal
URL:	http://www.journals.elsevier.com/construction-and-building-materials/
EDITORIAL:	Elsevier
FACTOR DE IMPACTO:	2,29
INDICE H:	70
CUARTIL:	Q1 (PRIMER DECIL)
POSICIÓN:	12(124)

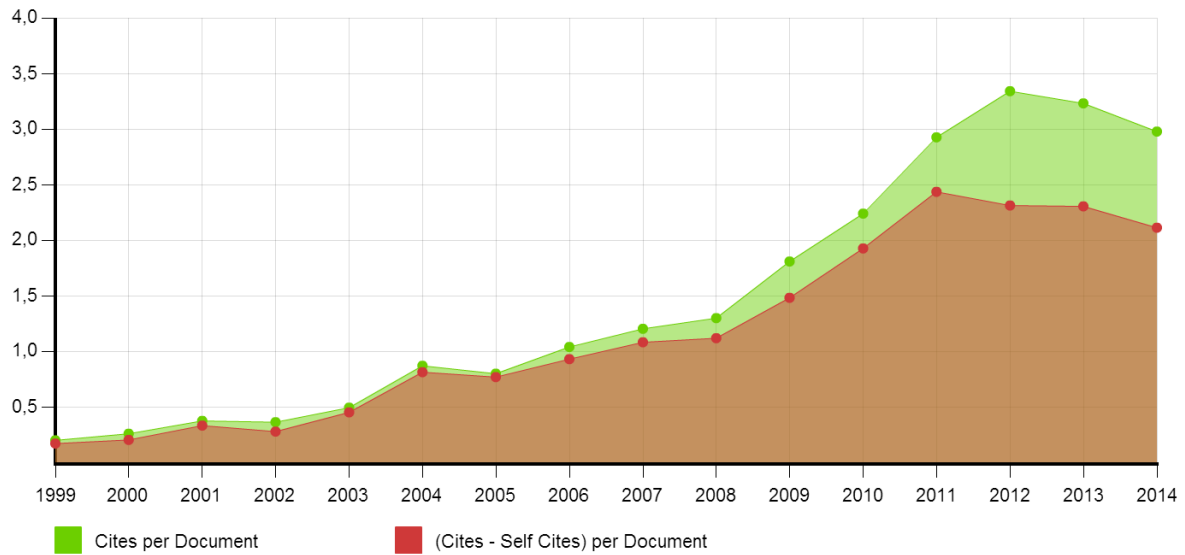
Indicador SJR vs. Citas por documento (2 años)



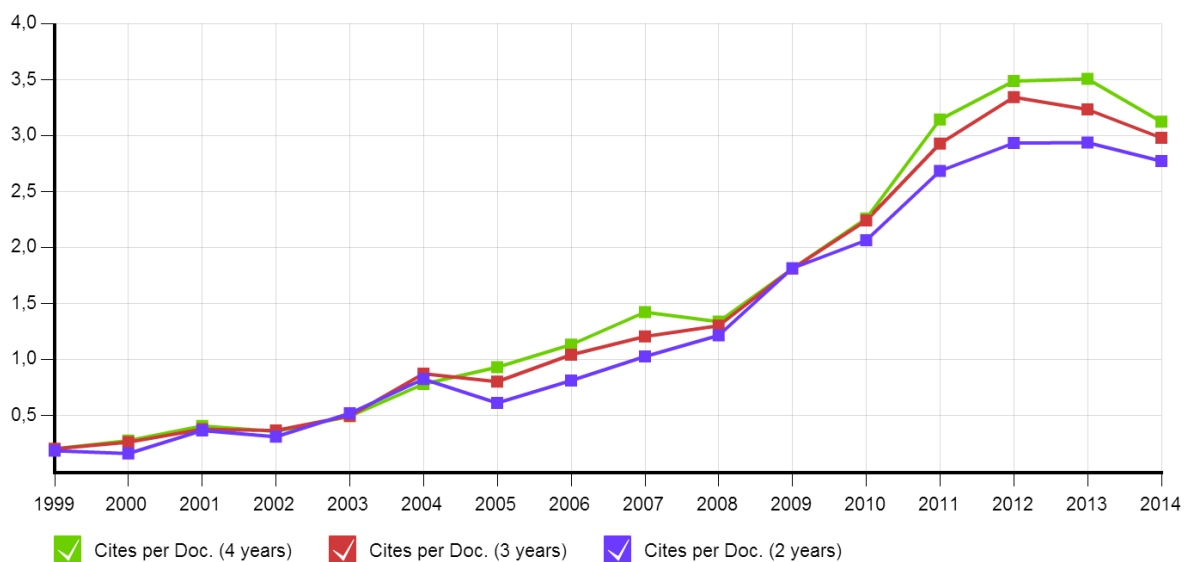
Citas vs. Auto-citas



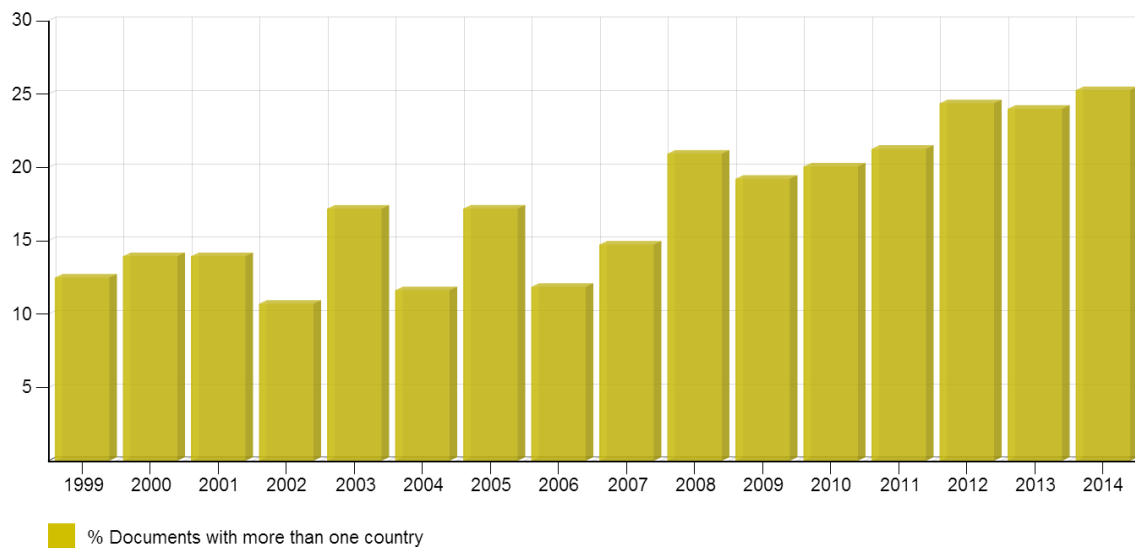
Citas por documento vs. Citas externas por documento



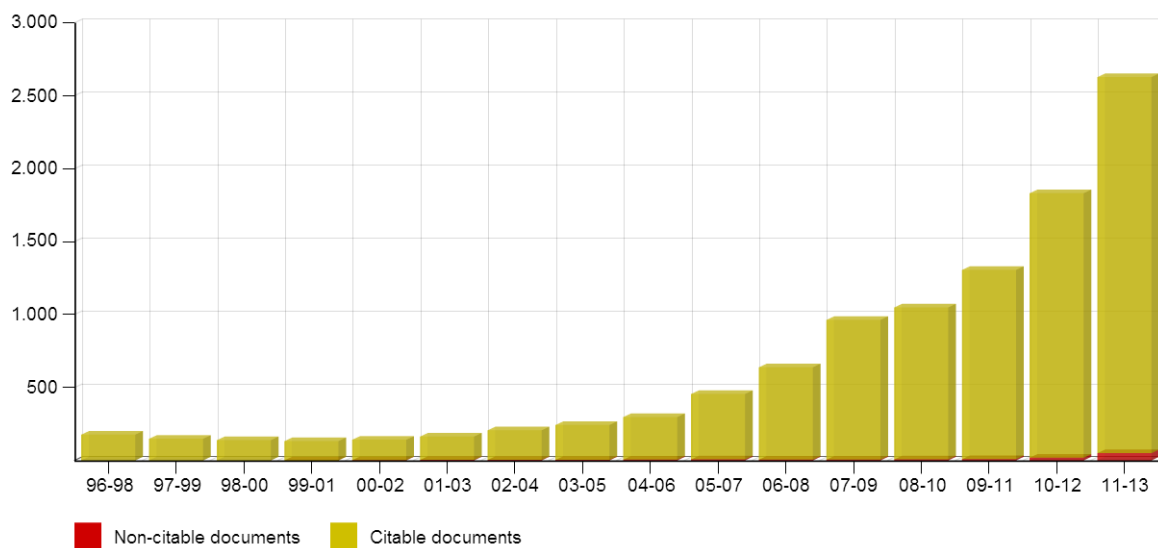
Citas por documento en 2, 3 y 4 años.



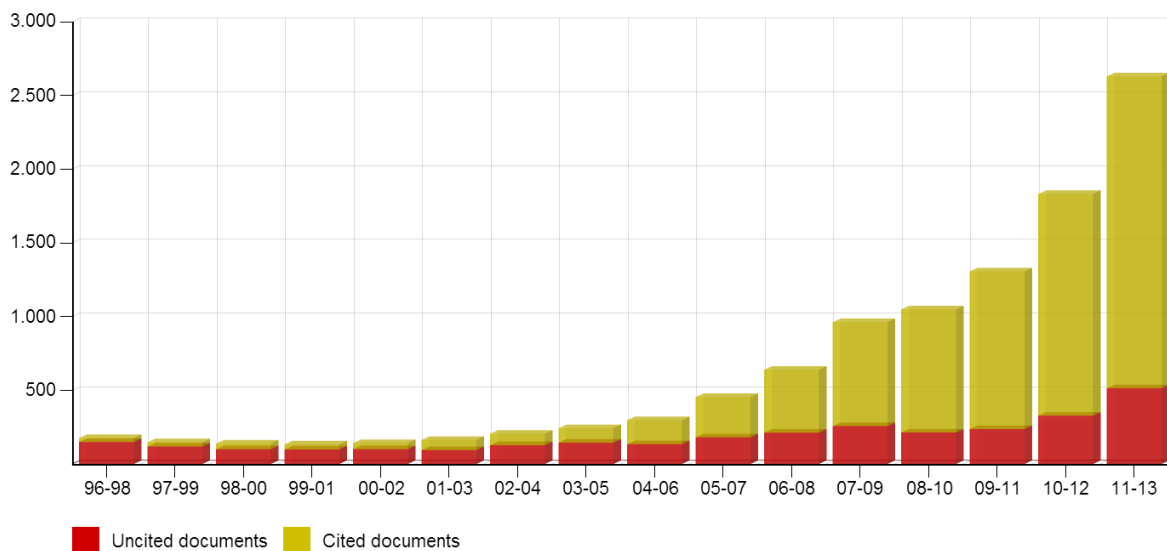
Colaboración internacional



Artículos citables vs. Documentos no-citables

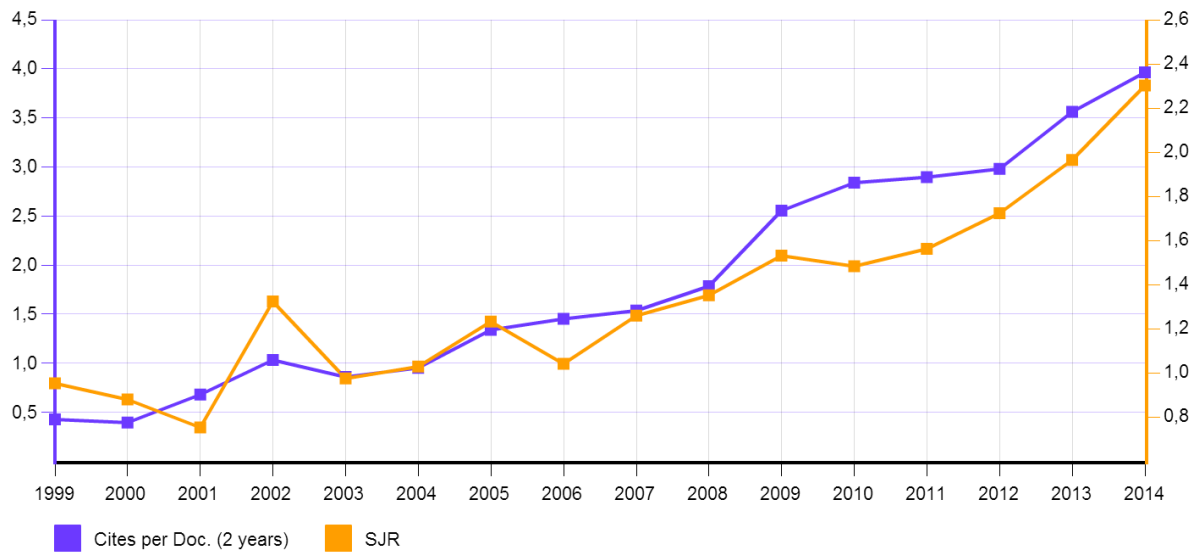


Artículos citables vs. Documentos no citados

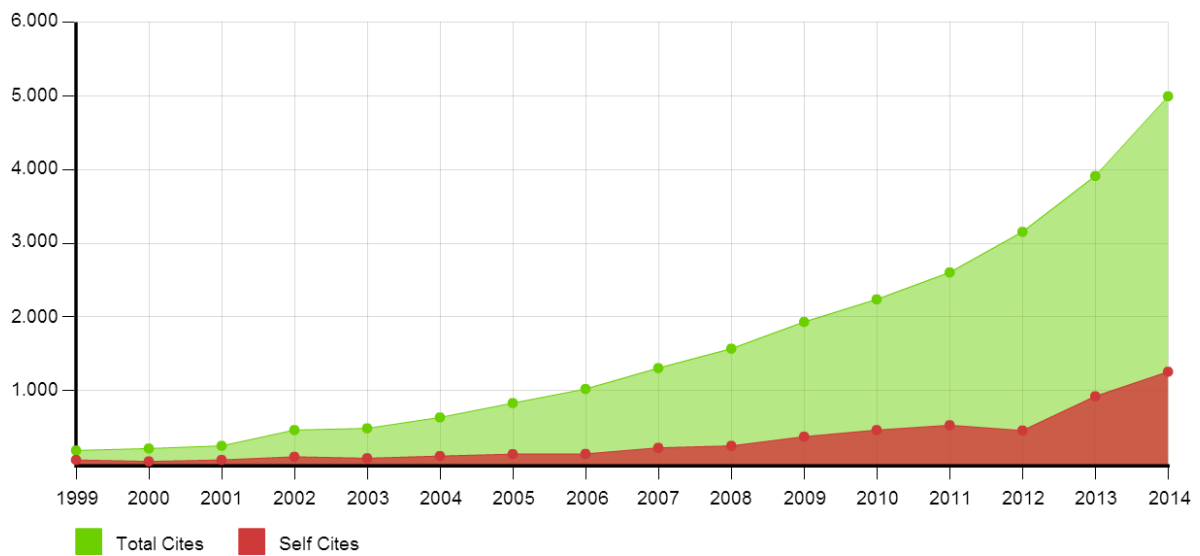


REVISTA:	Composite Structures Journal
URL:	http://www.journals.elsevier.com/composite-structures/
EDITORIAL:	Elsevier
FATOR DE IMPACTO:	3,32
INDICE H:	82
CUARTIL:	Q1
POSICIÓN:	3(24)

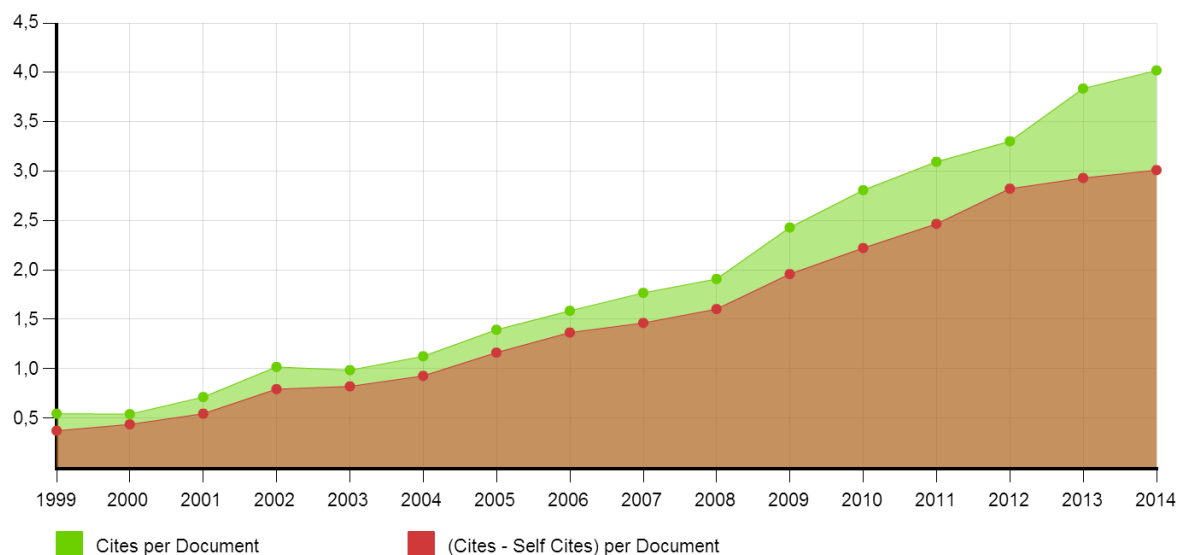
Indicador SJR vs. Citas por documento (2 años)



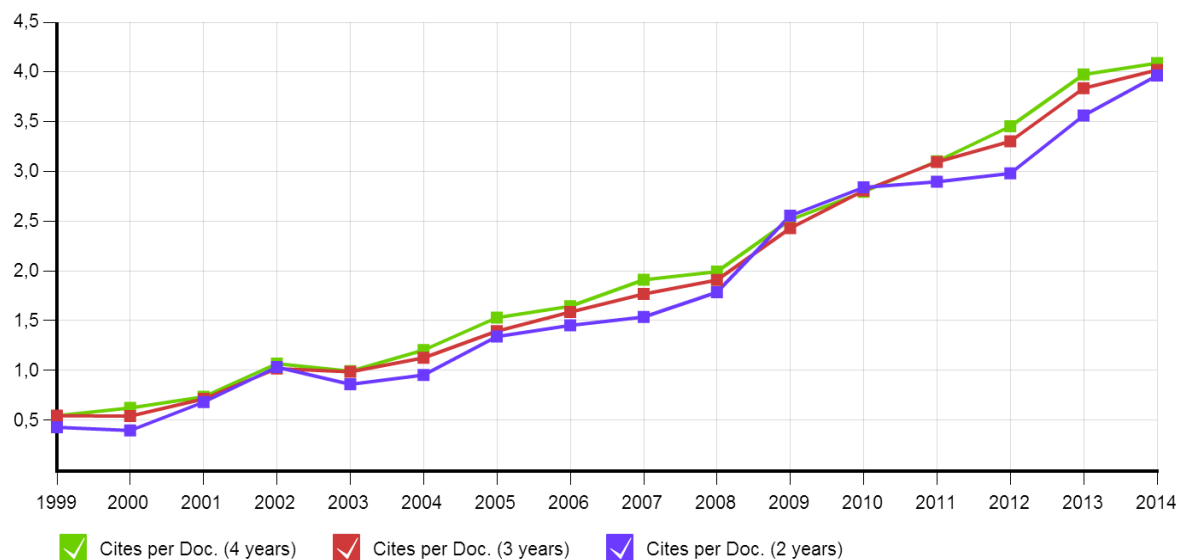
Citas vs. Auto-citas



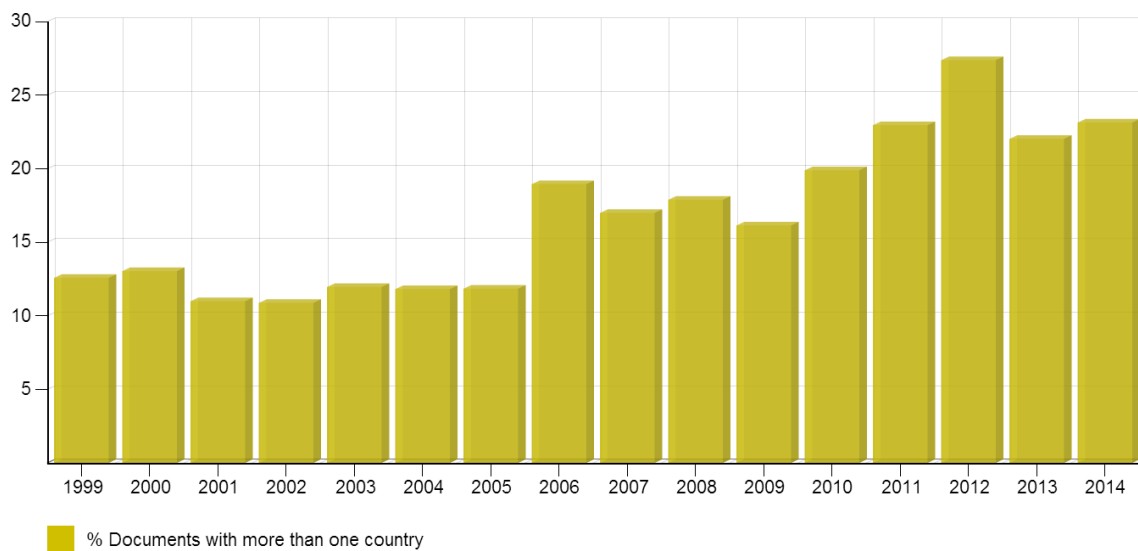
Citas por documento vs. Citas externas por documento



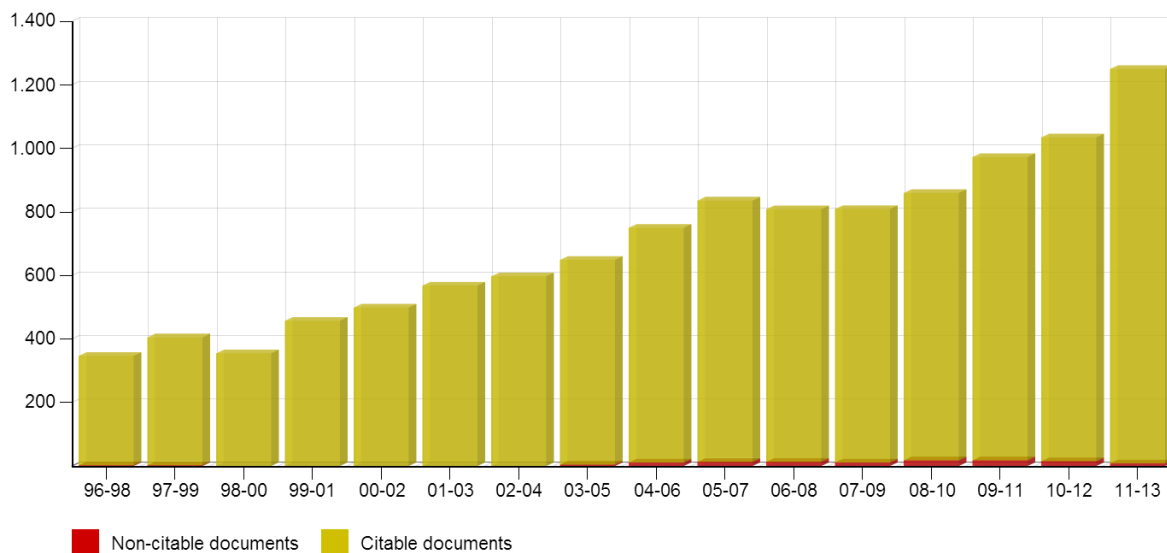
Citas por documento en 2, 3 y 4 años.



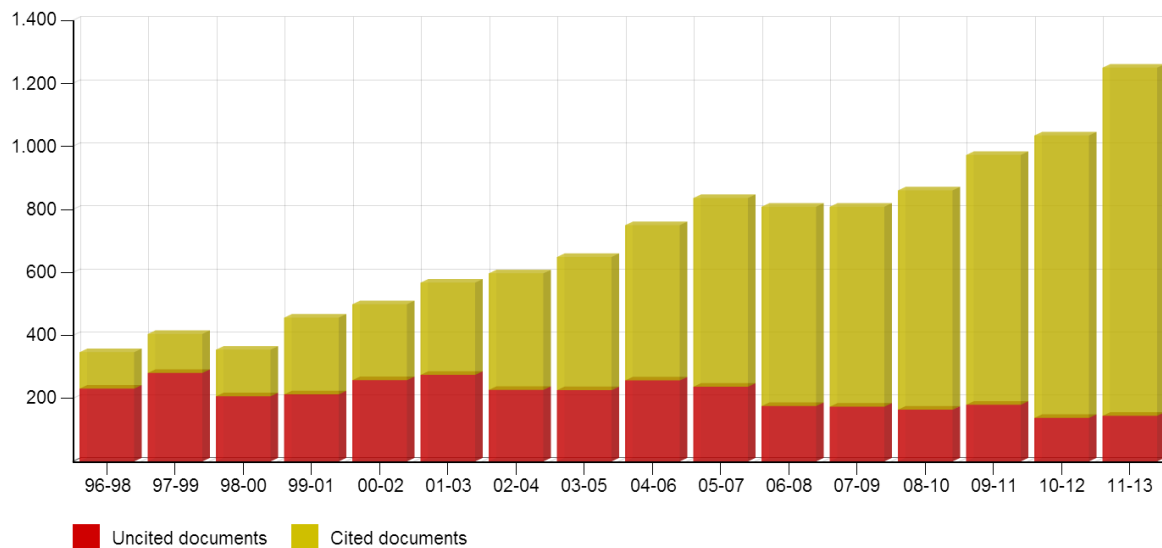
Colaboración internacional



Artículos citables vs. Documentos no-citables

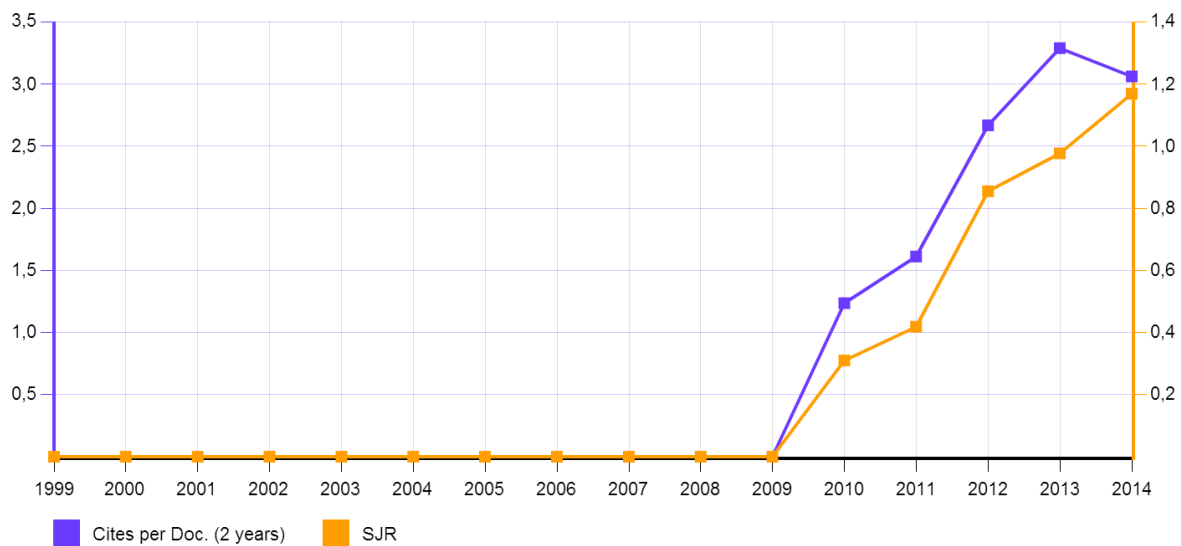


Artículos citables vs. Documentos no citados

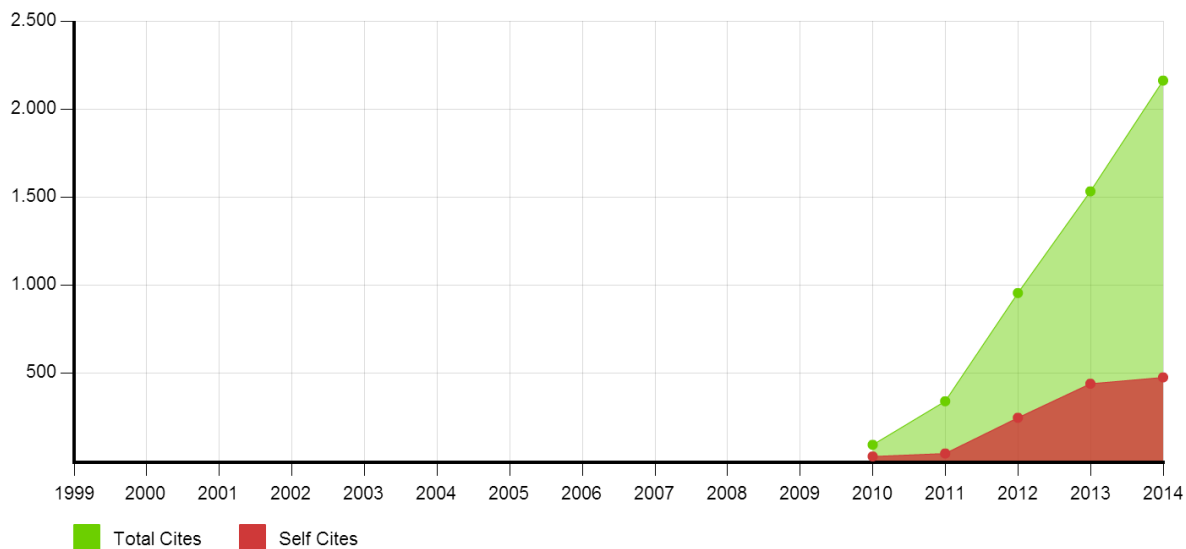


REVISTA:	Remote Sensing
URL:	http://www.mdpi.com/journal/remotesensing
EDITORIAL:	MDPI
FACTOR DE IMPACTO:	3,18
INDICE H:	70
CUARTIL:	Q1
POSICIÓN:	5(28)

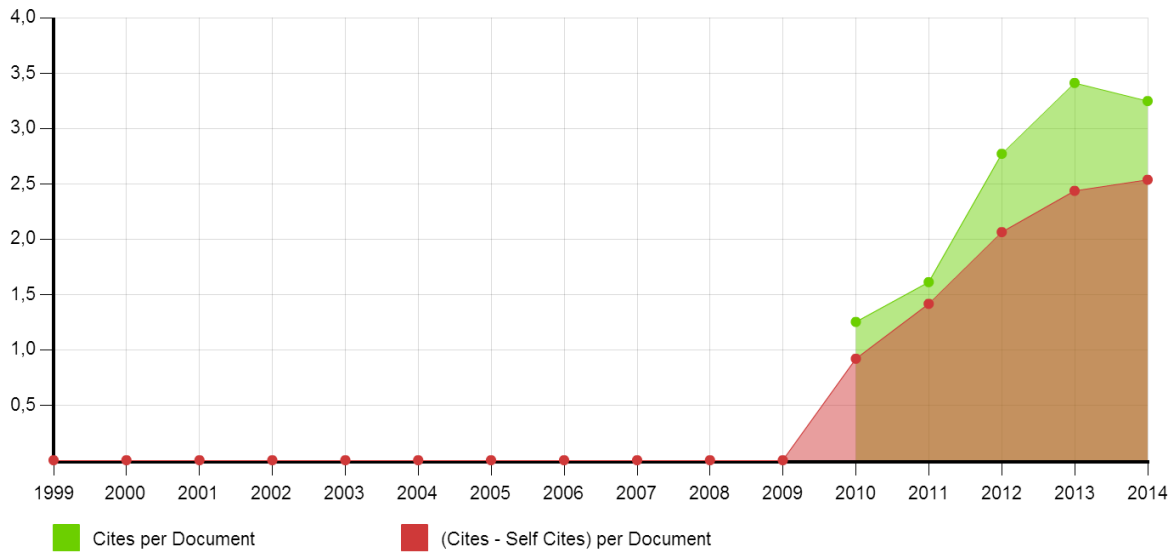
Indicador SJR vs. Citas por documento (2 años)



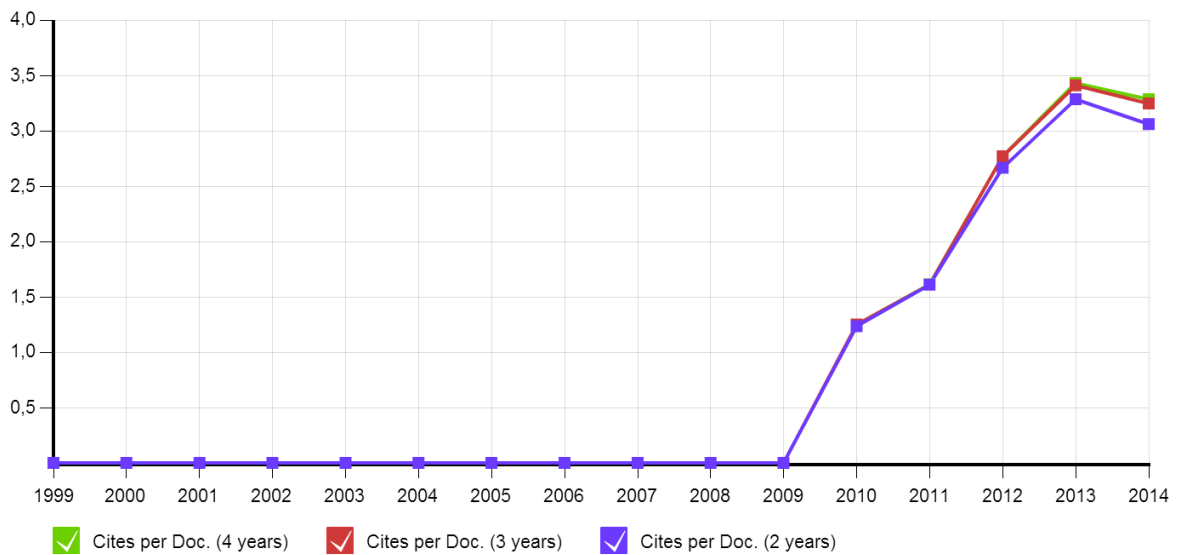
Citas vs. Auto-citas



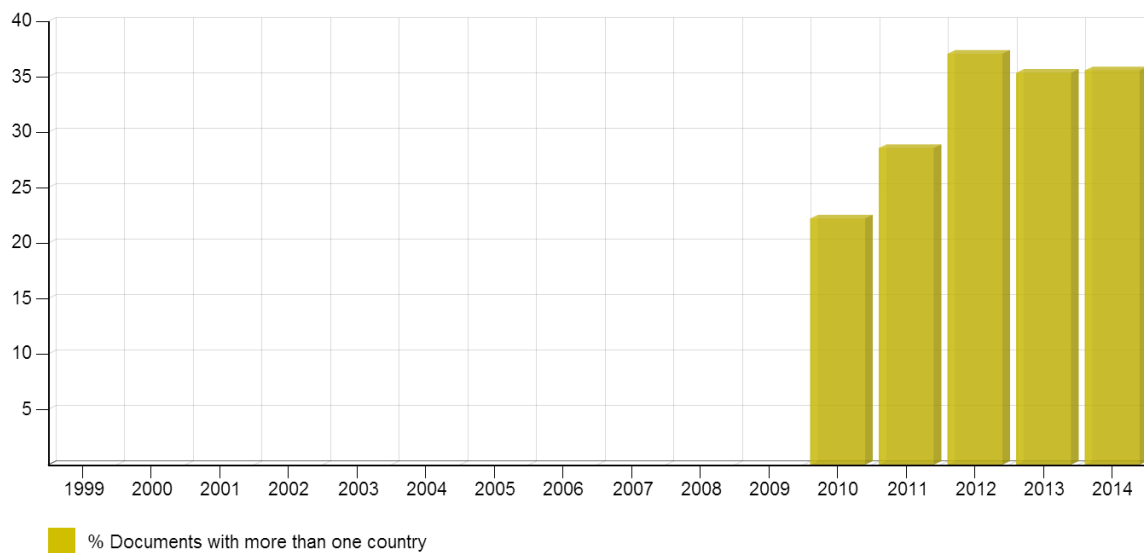
Citas por documento vs. Citas externas por documento



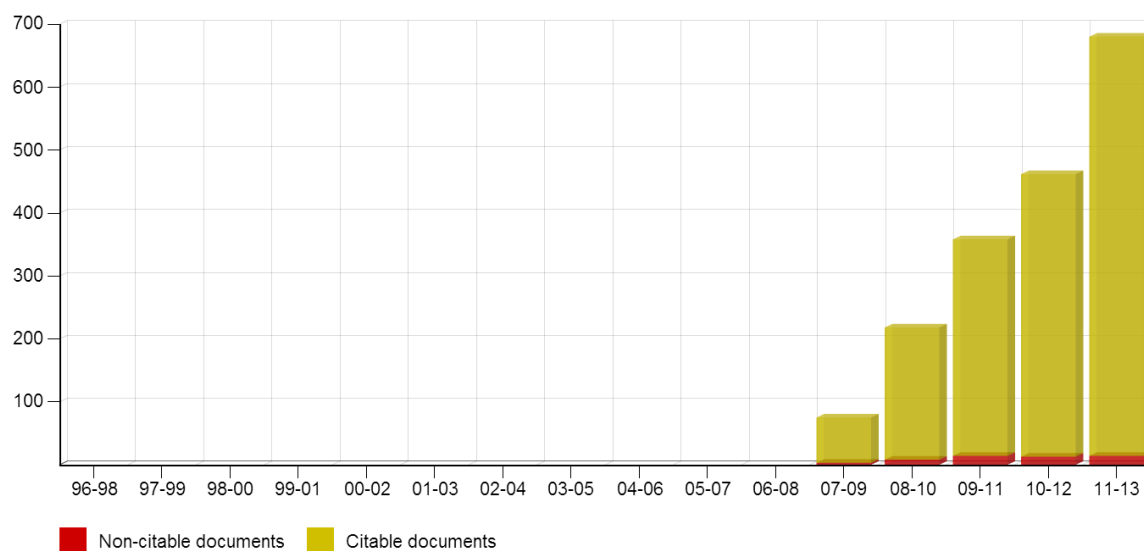
Citas por documento en 2, 3 y 4 años.



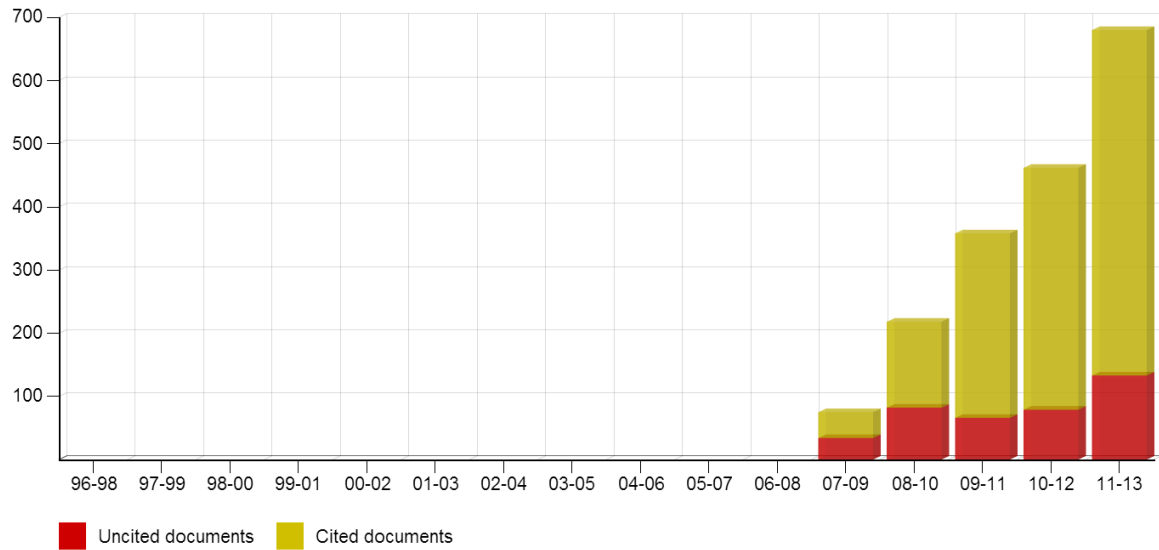
Colaboración internacional



Artículos citables vs. Documentos no-citables



Artículos citables vs. Documentos no citados



REVISTA:	CRC Press Balkema
URL:	http://www.balkema.nl/
EDITORIAL:	Taylor & Francis
PBK:	126
PCH:	1832
CIT:	2400
FNCS:	1,22
POSICION:	6(75)(PRIMER DECL)

	PBK	PCH	CIT	FNCS
SPRINGER	1054	12139	14831	1,29
ELSEVIER	387	5238	3943	1,19
NOVA SCIENCE PUBLISHERS	267	2665	954	0,28
WOODHEAD PUBLISHING	192	2482	878	0,43
ARTECH HOUSE	142	1759	676	0,55
CRC PRESS	126	1832	2400	1,22
CAMBRIDGE UNIVERSITY PRESS	99	966	1543	2,08
PAN-STANFORD	79	845	405	1,12
WILEY-BLACKWELL	49	542	194	1,21
MIT PRESS	47	580	437	1,36
IGI GLOBAL	48	593	92	0,38
WILLIAM ANDREW	35	481	169	0,62
DE GRUYTER	25	296	368	1,08
IWA PUBLISHING	22	249	78	0,89
SAE INTERNATIONAL	16	200	16	0,17
SIAM	16	142	248	1,67
SCIENTIFIC PUBLISHING Co PTE LTD	13	134	80	0,97
EDWARD ELGAR	12	147	81	0,82
TAYLOR & FRANCIS	11	172	73	0,46
ASTM INTERNATIONAL	10	206	9	0,06
ROUTLEDGE	10	143	33	0,45

SPON PRESS	9	85	56	0,93
EDITIONS TECHNIP-TECHNICAL BOOKS	8	114	26	0,88
WIT PRESS	8	84	11	0,15
ISTE LTD	7	76	12	0,21
PALGRAVE MACMILLAN	7	60	35	0,74
AM. SOCIETY OF MECHANICAL ENGINEERS	6	72	20	0,33
IOS PRESS	6	122	35	0,31
WORLD BANK	6	52	22	0,51
AM. INST. AERONAUTICS ASTRONAUTICS	5	73	18	0,21

